

INFORMATION TO USERS

This manuscript has been reproduced from the microfilm master. UMI films the text directly from the original or copy submitted. Thus, some thesis and dissertation copies are in typewriter face, while others may be from any type of computer printer.

The quality of this reproduction is dependent upon the quality of the copy submitted. Broken or indistinct print, colored or poor quality illustrations and photographs, print bleedthrough, substandard margins, and improper alignment can adversely affect reproduction.

In the unlikely event that the author did not send UMI a complete manuscript and there are missing pages, these will be noted. Also, if unauthorized copyright material had to be removed, a note will indicate the deletion.

Oversize materials (e.g., maps, drawings, charts) are reproduced by sectioning the original, beginning at the upper left-hand corner and continuing from left to right in equal sections with small overlaps. Each original is also photographed in one exposure and is included in reduced form at the back of the book.

Photographs included in the original manuscript have been reproduced xerographically in this copy. Higher quality 6" x 9" black and white photographic prints are available for any photographs or illustrations appearing in this copy for an additional charge. Contact UMI directly to order.

UMI

**A Bell & Howell Information Company
300 North Zeeb Road, Ann Arbor MI 48106-1346 USA
313/761-4700 800/521-0600**

Flotation Deinking of Toner-Printed Papers

by

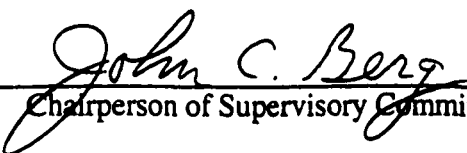
Dale C. Schmidt

A dissertation submitted in partial fulfillment
of the requirements for the degree of

Doctor of Philosophy

University of Washington

1996

Approved by 
Chairperson of Supervisory Committee

Program Authorized
to Offer Degree Department of Chemical Engineering

Date October 4, 1996

In presenting this dissertation in partial fulfillment of the requirements for the Doctoral degree at the University of Washington, I agree that the Library shall make its copies freely available for inspection. I further agree that extensive copying of this dissertation is allowable only for scholarly purposes, consistent with "fair use" as prescribed in the U. S. Copyright Law. Requests for copying or reproduction of this dissertation may be referred to University Microfilms, 1490 Eisenhower Place, P.O. Box 975, Ann Arbor, MI 48106, to whom the author has granted "the right to reproduce and sell (a) copies of the manuscript in microform and/or (b) printed copies of the manuscript made from microform."

Signature Dale C. Schmidt

Date Oct. 4, 1996

University of Washington

Abstract

Flotation Deinking of Toner-Printed Papers

by Dale C. Schmidt

Chairperson of the Supervisory Committee: Professor John C. Berg
Department of Chemical Engineering

The role of electrostatic properties and particle shape on toner flotation is investigated. Toner electrostatic properties, as measured by the zeta potential, are found to have little correlation on floatability due to the strong hydrophobicity of the toner surface. Flotation experiments in a Hallimond tube and in a single bubble flotation tube show that model toner spheres are more readily floated than similar volume disks. High-speed motion pictures of particle/bubble interactions in a flowtube show differences in disk and sphere behavior. Spheres are deflected away from the bubble by flow but usually attach if they contact the bubble surface. Disks often collide with the bubble edge-on but immediately bounce off, seldom attaching to the bubble due to the very short contact time. Alternatively, disks (particularly small disk fragments) turn to the side as they approach the bubble but seldom attach due to a large thin-film drainage area.

To describe the motion of large disks around a bubble, a simple hydrodynamic model is constructed and used to conduct a parametric study of the effect of disk size and initial orientation on the efficiency of collision, E_c , attachment, E_a , and collection, $E=E_cE_a$, and to compare these results with those computed for spheres. Initial disk orientation is shown to significantly affect collision and attachment efficiencies, and a mean value of each is calculated by taking the average over a range of equally spaced initial disk orientations

assumed to be equally probable. Large disk-to-bubble radius ratios (> 0.1) are found always to yield greater collision efficiencies than those for equivalent spherical particles. An equivalent sphere is one with an equal disk volume, computed on the basis of a diameter-to-thickness aspect ratio of 40. Attachment efficiencies of large disks, on the other hand, are always lower than the values obtained for equivalent spheres. The decrease in E_a is always greater than the increase in E_c , so that the predicted collection efficiency E for disks is always less than that for spheres. These predictions for disks vs. spheres are in qualitative agreement with experimental observations.

Table of Contents

	<i>Page</i>
List of Figures	iii
List of Tables	vi
Chapter 1 Introduction	1
1.1 The Problem.....	1
1.2 Summary of this Work.....	2
Chapter 2 Literature Review and Background	4
2.1 Introduction	4
2.2 Differences Between Toners and Newsprint	4
2.3 The Flotation Process	6
2.3.1 Modeling the Flotation Process.....	6
2.3.2 Collision Efficiency	7
2.3.3 Attachment Efficiency.....	10
2.3.4 Stability of Attachment.....	17
2.3.5 Efficiency of Froth Retention	19
2.4 The Influence of Particle Size	21
2.5 Why Toners are Difficult to Float.....	22
Chapter 3 The Effect of Toner Electrostatic Properties on Flotation.....	24
3.1 Introduction	24
3.2 Materials and Methods	25
3.3 Results and Discussion	28
3.3.1 Toner Characterization	28
3.3.2 Zeta Potential Measurements.....	30
3.3.3 Hallimond Tube Flotation	35
3.3.4 Wemco Cell Flotation.....	37
3.4 Conclusion	39
Chapter 4 The Effect of Particle Shape on Flotation.....	40
4.1 Introduction	40
4.2 Theory	40
4.3 Experimental	43
4.4 Results and Discussion	51
4.5 Conclusions	61
Chapter 5 A Preliminary Hydrodynamic Modeling of the Flotation of Disk-Shaped Particles	62
5.1 Introduction	62
5.2 Review of Theory and Literature	62
5.3 Development of Model.....	64
5.3.1 Model Assumptions.....	64
5.3.2 Development of General Equations.....	65

5.3.3	Disk in Particle-Fixed Coordinates.....	67
5.3.4	Disk in Fixed-Space Coordinates.....	67
5.3.5	Equations for Angular Velocity.....	68
5.3.6	Equations for Translational Velocity.....	70
5.3.7	Solving the Ordinary Differential Equations	70
5.4	Results and Comparison to Experiment.....	71
5.4.1	The Effect of Initial Orientation on Collision Efficiency.....	75
5.4.2	The Effect of Initial Orientation on Attachment Efficiency	82
5.5	Conclusions	90
Chapter 6	Summary, Conclusions and Future Work.....	92
6.1	Summary and Conclusions.....	92
6.2	Recommendations for Future Work.....	94
	List Of References.....	95
APPENDIX A	Fortran Code of Model	102
A.1	Introduction	102
A.2	HMODP Program	103
A.2.1	Fortran Code.....	103
A.2.2	Sample Input File.....	118
A.2.3	Sample Output File.....	118
A.3	COLMOD Program.....	119
A.3.1	Fortran Code.....	119
A.3.2	Sample Input File.....	126
A.3.3	Sample Output File.....	126
A.4	VRCMOD Program	129
A.4.1	Fortran Code.....	129
A.4.2	Sample Input File.....	136
A.4.3	Sample Output File.....	136
A.5	Modification of Programs for Intermediate Flow	136

List of Figures

<i>Number</i>	<i>Page</i>
2.1 Relative shape and size of (a) a toner particle and (b) an agglomeration of newsprint ink particles.....	5
2.2 Particle collision and particle sliding at a bubble surface.	11
2.3 Spherical particle at flat gas-liquid interface.....	18
3.1 Schematic of the Hallimond tube used for flotation experiments.	27
3.2 Zeta potential of toners versus pH. Filled symbols are magnetic toners.	30
3.3 Advancing contact angle of toners versus pH. Filled symbols are magnetic toners.	31
3.4 Receding contact angle of toners versus pH. Filled symbols are magnetic toners.	32
3.5 Zeta potential in Ca and Na solutions at pH 5.5	32
3.6 Zeta potential in Ca and Na solutions at pH 9.....	33
3.7 Zeta potential in Ca and Na solutions at pH 11.1.....	33
3.8 Zeta potential in Na, Ca, and Al solutions.....	34
3.9 Zeta potential versus Hallimond tube flotation in a nonionic control surfactant (100 mg/l Triton™ X-100), the control plus an anionic surfactant (100 mg/l SDS), and the control plus a cationic surfactant (100 mg/l HTAB)	36
3.10 Zeta potential versus normalized Hallimond tube flotation (percent removal divided by percent removal of control).	37
3.11 Hallimond tube versus Wemco cell flotation for eight toners.	38
4.1 Predicted interactions of a disk and sphere as they approach a bubble.....	44
4.2 Schematic of the single bubble flotation tube.	47
4.3 Schematic of the flowtube apparatus used to observe particle/bubble interactions.	48
4.4 Mirror and camera set-up around the flowtube used to obtain two perpendicular views of the object on one frame of film.....	50

4.5	Disk and sphere flotation in the Hallimond tube and in the single bubble flotation tube.	52
4.6	Toner particles and bubbles photographed from two directions at right-angles to each other. Each picture is taken from one frame of a 16 mm film sequence. At the center is the bubble affixed atop a 1.02 mm diameter Teflon tube. The light spot in the middle of the bubble is due to the lighting. The bottom of the feedtube can be seen at the top of the picture. (a) Spheres attached to a 2.6 mm diameter bubble. The three spheres shown in the left view are in front of and behind the bubble in the right view and thus cannot be seen. (b) A 700 μm diameter toner disk approaching a 2.5 mm diameter bubble. (c) The same disk 5 frames or 7.0 ms later than (b) as it first collides with the bubble. (d) The same disk 6 frames or 8.5 ms later than (c) after it has bounced and turned to its side. The disk is not seen on the right because it is behind the bubble.	54
4.7	Trajectory of two spheres, drawn to scale, flowing around a bubble with one sphere attaching to the bubble. Each drawn sphere represents one frame of film or 1.4 ms.....	55
4.8	Disk, drawn to scale, colliding with a bubble, bouncing off, turning, and flowing around the bubble.	56
4.9	A disk, oriented parallel to the figure, colliding with and bouncing away from a bubble.	58
4.10	Small disk fragment, drawn to scale, flipping to side and missing bubble.....	59
5.1	Determination of r_c for a sphere flowing around a bubble.....	63
5.2	The orientation of the axis of revolution, z' , is described by two polar angles, α and β , where α is the angle formed between z' and the fixed-space z axis, and β is the angle formed between the projection of z' onto the fixed-space xy plane and the fixed-space x axis.	68
5.3	Movement of a large disk as observed from an experimental run and as predicted by the current model using the potential flow equations.	72
5.4	Disk movement as observed from an experimental run and as predicted by the current model using the potential flow equations.....	73
5.5	Predicted disk movement using the potential flow equations compared to using the intermediate flow equations.....	74
5.6	Disk orientation in xy plane for $\alpha = 0^\circ$	77
5.7	Disk orientation in xy plane for $\alpha = 90^\circ$, $\beta = 0^\circ$	77

5.8	Disk orientation in xy plane for $\alpha = 90^\circ$, $\beta = 90^\circ$	78
5.9	Dependence of rc on initial disk orientation for a disk/bubble radius ratio of 0.3 as predicted using equations for potential flow.	78
5.10	Dependence of rc on initial disk orientation for a disk/bubble radius ratio of 0.3 as predicted using equations for intermediate flow.	79
5.11	Comparison of disk and sphere collision efficiencies in potential flow.....	81
5.12	Comparison of disk and sphere collision efficiencies in intermediate flow.....	81
5.13	Contact radial velocity of a disk in potential flow with an initial orientation of $\alpha_o = 0^\circ$ and an undisturbed fluid velocity of 200 mm/s.	84
5.14	Contact radial velocity of a disk in intermediate flow with an initial orientation of $\alpha_o = 0^\circ$ and an undisturbed fluid velocity of 200 mm/s.	84
5.15	Contact radial velocity of a disk in potential flow with an initial orientation of $\alpha_o = 90^\circ$, $\beta_o = 0^\circ$, and an undisturbed fluid velocity of 200 mm/s.....	85
5.16	Contact radial velocity of a disk in intermediate flow with an initial orientation of $\alpha_o = 90^\circ$, $\beta_o = 0^\circ$, and an undisturbed fluid velocity of 200 mm/s.	85
5.17	Contact radial velocity of a disk in potential flow with an initial orientation of $\alpha_o = 90^\circ$, $\beta_o = 90^\circ$, and an undisturbed fluid velocity of 200 mm/s.	86
5.18	Contact radial velocity of a disk in intermediate flow with an initial orientation of $\alpha_o = 90^\circ$, $\beta_o = 90^\circ$, and an undisturbed fluid velocity of 200 mm/s.	87
5.19	Contact radial velocity of a disk in potential flow with an initial orientation of $\alpha_o = 40.368^\circ$, $\beta_o = 45^\circ$, and an undisturbed fluid velocity of 200 mm/s.....	87
5.20	Sphere collision efficiencies in potential flow for different ranges of contact radial velocities. Undisturbed fluid velocity = 200 mm/s.....	89
5.21	Disk collision efficiencies in potential flow for different ranges of contact radial velocities. Undisturbed fluid velocity = 200 mm/s.....	89

List of Tables

<i>Number</i>		<i>Page</i>
3.1	Toner descriptions.....	29
4.1	Advancing and receding contact angles measured on toner coated rods in deionized water.	51
4.2	Overall collection efficiencies for disks and spheres in the single bubble flotation apparatus and in the Hallimond Tube.....	53
4.3	Collision and attachment efficiencies for disks and spheres in the single bubble flotation tube.	60
5.1	Collision efficiencies at different contact radial velocity ranges in potential flow for a similar size disk and sphere.....	90

Acknowledgments

I wish to express my sincere appreciation to my advisor, Professor John C. Berg, for his expert guidance and generous support during my time as his graduate student. I also wish to express my thanks for the assistance and encouragement I received from the members of the Interfacial Phenomena Research Group from 1991 to 1996, especially from Bret Snyder, Dr. Jill Seebergh, Phil Harding, Jorge Sunkel, and Susie Stenkamp. I acknowledge the financial support from the Weyerhaeuser Foundation through the Fisker Fellowship, and express my appreciation to Dr. Tom Friberg of Weyerhaeuser for his gracious help throughout this project.

Special thanks go to my father, Don Schmidt, who first introduced me to the fascinating world of surface and colloid science, and who was a vital resource in helping me solve the problem of creating both model toner disks and spheres. Lastly, I wish to thank my wife, Julie, for her continual support, sustaining encouragement, and enduring patience during these graduate school years.

CHAPTER 1

Introduction

1.1 The Problem

The continuing reduction in landfill space and the political unpopularity of incinerators is leading to increased costs for the elimination of pulp and paper waste. This, along with the growth of the environmental movement, has led to an increase in demand, often through legislation, for more recycled content in pulp and paper products. But while the demand for more recycled fibers in paper products has increased, consumer expectations of paper quality have remained the same. This means that recovered post consumer waste cannot be used for paper making unless the recycled fibers can meet the high standards of brightness, cleanliness, and fiber strength that consumers expect. This generally requires the almost complete removal of ink and other contaminants from the recycled paper.

One method that has proven effective in removing ink and other contaminants is flotation deinking. Similar to mineral flotation, it involves adding collector chemicals (usually a surfactant) to the recycled pulp to make the ink surface hydrophobic. When air bubbles are passed through the paper slurry, the hydrophobic particles attach to the bubbles, float with the bubbles to the surface, and are removed with the resulting froth. This method has been used successfully with newsprint for many years.

One of the fastest growing sources of recycled fiber is office waste paper from laser writers and copy machines which print using a polymeric toner. Unfortunately, flotation has not been as successful at removing the toner from repulped paper slurries as it has been in removing conventional inks from newsprint.¹⁻³ It has been poorly understood why deinking flotation has not been completely effective because toners are already hydrophobic and should therefore easily attach themselves to the bubbles. A better understanding of

flotation as it applies to toners is required so that improved approaches towards ink removal can be developed.

1.2 Summary of this Work

The approach of this work has been to investigate fundamentally the reasons why toners are difficult to float. A literature review of the principles of flotation and how they relate to the flotation of toners is covered in Chapter 2. There are many variables that can affect flotation, but we have limited ourselves to the following areas:

- Toner electrostatic properties. Electrostatics will affect the repulsion between a toner particle and bubble and the attraction or repulsion between a functional group of a surfactant and the toner surface. A variety of toners were quantitatively characterized according to their electrostatic properties by measuring the zeta potential and the results were compared to flotation experiments. It was found that electrostatics actually plays a minor role in toner flotation, in part because toners are generally hydrophobic before the addition of collectors and should thus, in theory, already be floatable. This work is contained in Chapter 3.
- Experimental study on the effect of particle shape on flotation. Since toners were found to be already hydrophobic, it suggested that an additional mechanism was interfering with flotation. This led to an experimental investigation into the effect that the flat, plate-like shape of repulped toner particles has on flotation. It was found that disk-shaped toner particles have lower flotation rates than comparable size spheres. The reason for this, as observed using high-speed cinematography, was that disks either collide edge-on with a bubble, bouncing off due to the short contact time, or they rotate

to the side and fail to attach due to the large liquid drainage area separating the disk and bubble surfaces. Details of this research are covered in Chapter 4.

- Model study of the effect of particle shape and size on flotation. In the experimental studies, the disposition of the disk as it contacts the bubble was seen to be dependent upon disk size as well as the initial disk position and orientation. To investigate this further, a simple hydrodynamic model was developed to describe the motion of large disks in the vicinity of a bubble in flotation. The model was used to conduct a parametric study of the influence of disk size and initial orientation on the efficiency of collision, E_c , attachment, E_a , and collection, $E=E_cE_a$. Initial disk orientation was shown to significantly affect collision efficiency, and a mean value of E_c was calculated by taking the average over a range of equally spaced initial disk orientations assumed to be equally probable. Large disk-to-bubble radius ratios (> 0.1) were found always to yield greater collision efficiencies than those for equivalent spherical particles, where an equivalent sphere is one with an equal disk volume, computed on the basis of a diameter-to-thickness aspect ratio of 40. Computed attachment efficiencies for initial-orientation-averaged large disks, on the other hand, were always lower than the values obtained for equivalent spheres. The decrease in E_a was found to be always greater than the increase in E_c , so that the predicted collection efficiency E for disks was always less than that for spheres. All three of these predictions for disks vs. spheres were in qualitative agreement with experimental observations reported in Chapter 4. This work is explained in Chapter 5.

CHAPTER 2

Literature Review and Background

2.1 Introduction

Flotation was first applied to the separation of mineral ores in the late 19th century, and by the early 20th century it had become the primary method of recovery for a large variety of minerals.^{4, 5} It was first applied to the problem of removing ink particles from repulped slurries in the 1930's, but it was not until the 1950's that flotation deinking began to have widespread use.⁶ Flotation deinking has been especially effective in the treatment of newsprint, but the invention of new inks and new printing processes has led to waste papers that contain inks that are difficult to remove by conventional flotation methods.³ In particular, the widespread use of photocopy machines and laser printers, which print using a thermoplastic polymer called toner, has led to a large supply of toner-printed waste-papers that are difficult to deink by flotation.¹⁻³ Reasons for the poor flotation lie in the differences between toners and conventional printing inks, such as those in newsprint.

2.2 Differences Between Toners and Newsprint

Traditional newsprint inks consist of a pigment, i.e., carbon black, dispersed in a hydrocarbon carrier, such as vegetable oil.³ The ink carrier physically adsorbs onto the paper surface during the printing process. Before the ink can be removed by flotation, it must be separated from the paper fiber during the pulping phase. To accomplish this, caustic is added to help swell the fiber and hydrolyze the ink carrier, and a surfactant (classically oleic acid) is added to lift the ink from the fiber and emulsify it, similar to a laundering process. The oil-based ink, originally hydrophobic, is now hydrophilic from the addition of surfactant. Calcium, added as a collector, reacts with the oleic acid and makes the ink surface again hydrophobic. The small ink droplets agglomerate together and

these spherical, hydrophobic agglomerates stick to the bubbles and are removed with the froth.⁶⁻⁹

Toners differ from conventional inks in that, instead of having an oil- or water-based carrier, they are composed primarily of a thermoplastic resin, typically a styrene/acrylate or styrene/butadiene copolymer.^{2, 10} They generally contain 5-10 wt% dispersed carbon black as a pigment and small amounts of charge carrier and dry lubricants. Some toners also contain a large amount of iron oxide, added to give the toner magnetic properties.

In the printing process, toner powder is electrostatically transferred to the paper where, under heat and pressure, the powder is fused to itself and to the paper fibers to form large, flat particles on the page. The toner is removed from the fibers during pulping by adding caustic which swells the paper fibers, causing the toner to break up into flat flakes of sizes varying from 10 microns up to a millimeter.^{3, 11, 12} Unlike the small spherical ink droplets of newsprint, the large flakes are plate-shaped with abrupt edges, as shown schematically in Fig. 2.1.

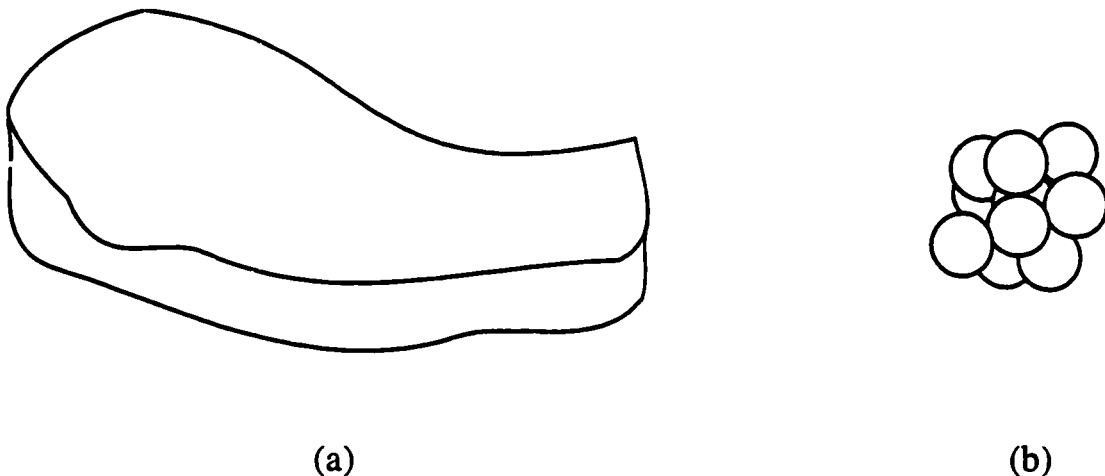


Figure 2.1 Relative shape and size of (a) a toner particle and (b) an agglomeration of newsprint ink particles.

Once the toner is separated from the fiber, it should still be hydrophobic. The flotation of toners should thus be quite similar to the flotation of naturally hydrophobic minerals such as talc, graphite, paraffin, molybdenite, sulfur, and high-rank unoxidized coal. These minerals do not require a collector for separation by flotation unless there is contamination by polar species on the particle surface such that the surface becomes hydrophilic.¹³ What is primarily needed in these systems is an adequate frother that does not destroy the hydrophobicity of the particle surface. Thus, unlike the flotation of newsprint, the flotation of toners should depend less on collector chemistry and more on the choice of an effective frother.^{2, 14} To understand why toners do not float satisfactorily, one first needs to understand some basic principles of the flotation process.

2.3 The Flotation Process

2.3.1 *Modeling the Flotation Process*

Flotation is often considered as a series of separate but consecutive events or steps of particle-bubble interactions. They are generally identified as:¹⁵⁻¹⁸

- 1) the approach of a particle to a bubble in the flow field surrounding the bubble;
- 2) the formation of a thin liquid film between the particle and the bubble, the rupture of this film and the formation of a dynamic three-phase contact;
- 3) the stabilization of the particle/bubble aggregate against all detachment forces existing in the environment; and
- 4) the transfer of the particle/bubble aggregate into the froth and being retained by the froth until removed from the system.

It is common practice to assume that each step has a probability of taking place and that the total probability of a particle being collected will be the product of these separate probabilities. The probability of a collision between a single particle and a bubble during the first step is the collision efficiency, E_c . After collision, the probability of a particle

attaching to a bubble in the second step is the attachment efficiency, E_a . The probability that subsequent detachment will not occur in step three is the stability efficiency of the particle/bubble aggregate, E_s . Lastly, the efficiency of particle transfer to the froth is E_f . The overall collection efficiency, E , is the product of these efficiencies:

$$E = E_c E_a E_s E_f \quad (2.1)$$

The overall collection efficiency can be included in a kinetic equation to describe the total removal of particles from a given cell volume:

$$\frac{dn_p}{dt} = -z_c n_p n_b E_c E_a E_s E_f \quad (2.2)$$

where t is time, z_c is the number of collisions per unit time if effects of the flow field are ignored, n_p is the number of particles, and n_b is the number of bubbles. The four steps in flotation will be discussed in more detail in the following sections.

2.3.2 Collision Efficiency

The collision efficiency is commonly defined as the probability that a random particle, whose center lies within the volume swept out by a rising bubble, will collide with that bubble. If we call the center of the rising bubble's path the bubble centerline, only particles that are initially within a critical radial distance, r_c , from the centerline will make contact with the bubble surface. The collision efficiency is defined as the area within the critical radius divided by the cross sectional area of the bubble:

$$E_c = \frac{\pi r_c^2}{\pi R_b^2} = \left(\frac{r_c}{R_b} \right)^2 \quad (2.3)$$

For large particles, it is possible that r_c will be greater than the bubble radius, R_b . Thus, E_c , as defined in this manner, is not a true efficiency because it is possible to obtain

values greater than one. However, it is the most commonly used definition because of the relative ease of incorporating it into kinetic equations that describe the flotation rate (as will be seen in Chapter 4).

Collision efficiency is strongly dependent upon the flow field around the bubble. A number of studies have been conducted which examine the collision process of spherical particles in flotation from hydrodynamic principles.^{4, 15, 17-24} The flow field is highly dependent upon the bubble Reynolds number:

$$Re_b = \frac{2R_b u_b \rho_f}{\eta} \quad (2.4)$$

where u_b is bubble velocity, ρ_f is fluid density, and η is fluid viscosity. The flow field also depends upon the degree of retardation on the bubble surface due the adsorption of surfactants.

Assuming Stokes flow ($Re_b \ll 1$) with completely rigid bubbles and spherical particles, Gaudin⁴ has shown that:

$$E_c = \frac{3}{2} \frac{R_p^2}{R_b^2} \quad (2.5)$$

where R_p is the particle radius. For potential flow ($Re_b \gg 500$) and completely unretarded, free movable bubble surfaces, Sutherland¹⁵ has shown that:

$$E_c = 3 \frac{R_p}{R_b} \quad (2.6)$$

The details of the flow field around a bubble are not modeled well by either the Stokes or the potential flow assumption because rising air bubbles in water typically have a Reynolds number of the order of 100-400. Flint and Howarth²⁵ and later Reay and Ratcliff¹⁹ numerically solved the Navier-Stokes equations to determine the probability of

collision for intermediate Reynolds numbers. Weber and Paddock²⁰ obtained a quantitative expression for collision efficiency by using a curve-fit solution to the numerical solution of the Navier-Stokes equation for spherical particles and rigid spherical bubbles:

$$E_c = \frac{3}{2} \left[1 + \frac{(3/16) \text{Re}_b}{1 + 0.249 \text{Re}_b^{0.56}} \right] \left(\frac{R_p}{R_b} \right)^2 \quad (2.7)$$

Nguyen-Van and Kmet^{26, 27} recently modified this equation to more accurately apply to higher density particles.

Yoon and Luttrell²² determined particle trajectories for Reynolds numbers up to 100 by deriving an empirical stream function by curve-fitting streamline patterns available in the literature.²⁸ The resulting equation for collision efficiency is:

$$E_c = \left[\frac{3}{2} + \frac{4 \text{Re}_b^{0.72}}{15} \right] \left(\frac{R_p}{R_b} \right)^2 \quad (2.8)$$

Their expression was found to closely agree with E_c values determined experimentally from the flotation of very hydrophobic coal samples (where E_a was assumed to be unity). This equation has been suggested for ink and sticky particle sizes up to 100 μm in size.²⁹

At the University of Maine, Pan, Paulsen, Johnson, Bousfield, and Thompson^{24, 30-32} developed a hydrodynamic model of the motion of one or more spherical particles around bubbles using Stokesian dynamics.³³ Stokesian dynamics assumes that the only interaction between the bubble and the particle is through lubrication or viscous forces. The equations are applicable when the particle is close to the bubble and when the particle Reynolds number is in the Stokes regime. The computer model calculates the net force and torque on every particle at every point in time and then updates a given particle's velocity, angular velocity, and position. When the particle and bubble approach to within a critical gap distance, attachment is assumed to take place, and the particle is considered captured by

the bubble. This model was used to study the effects of flotation time, particle size, and bubble capture radius on flotation efficiency.

The models above assume that the particles to be removed by flotation are spherical in shape. Models to describe the flotation of disk-shaped particles have not been treated in the literature, perhaps because particles often encountered in flotation are quasi-spherical and because of the additional complications in accounting for orientation effects. A preliminary hydrodynamic model to calculate collision efficiency for disk-shaped particles is presented in Chapter 5.

2.3.3 Attachment Efficiency

Once a particle contacts the bubble surface, the thin liquid film separating them must thin, rupture, and recede to form a strong, three-phase contact, or else attachment will not take place. The interactions at contact can be classified as two types¹⁸ (Fig. 2.2):

- 1) collision or impact interactions, in which the bubble surface is strongly deformed and, unless the three-phase contact is formed quickly, the particle will rebound from the bubble surface;
- 2) sliding interactions, where the particle slides along the bubble surface, with only a very weak deformation of the bubble surface.

Impact interactions should predominate when the particles are large, the particle velocities are high relative to the bubble, and the particles are directed radially towards the bubble surface.¹⁸ If the particle does not immediately attach at impact, it will rebound, possibly several times, until kinetic energy is sufficiently dissipated so that a sliding interaction can predominate. A common assumption in the literature is that the more forcefully a particle impacts a bubble, the more likely is the attachment, as the particles will literally pierce through the bubble surface.¹³ However, it has also been suggested that with

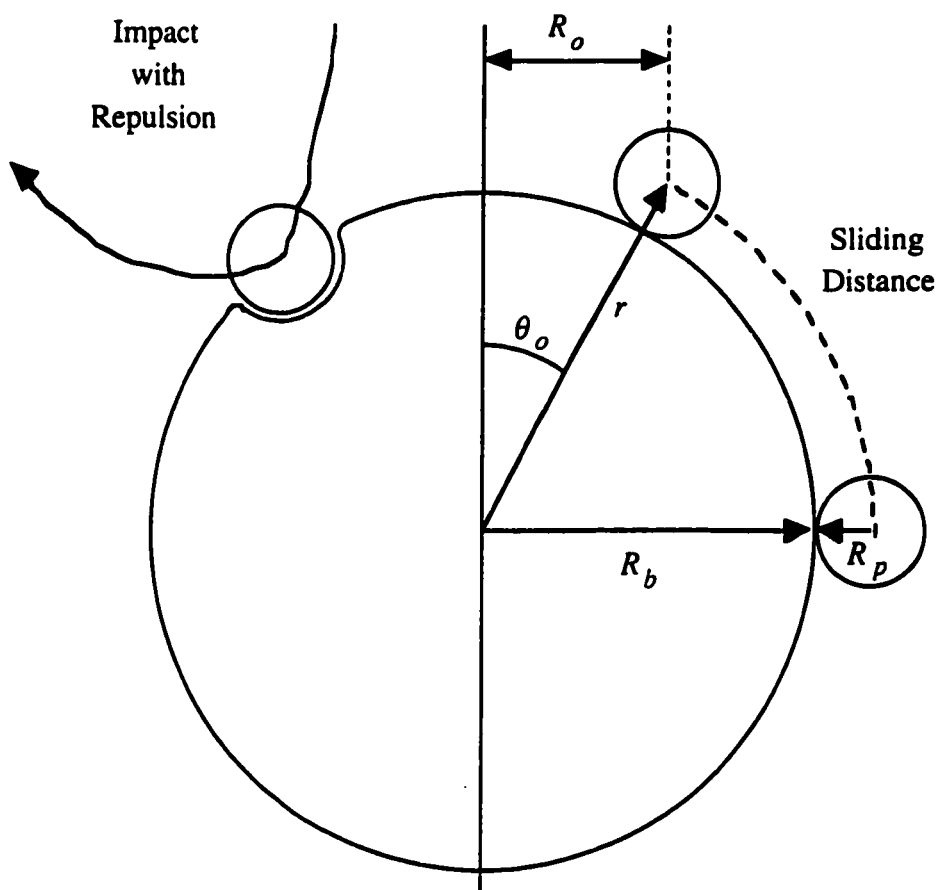


Figure 2.2 Particle collision and particle sliding at a bubble surface.

increasing particle and bubble size and with increasing particle density, the probability of attachment will decrease due to particles rebounding from the surface.³⁴ The second assumption is supported by experimental results of Stechemesser and Weber, as reported by Schulze,¹⁸ that show that even extremely hydrophobic, spherical particles do not attach during the first collision. Observations by this author (see Chapter 4) give further support to the conclusion that strong collisions do not immediately result in attachment.

For the most part, attachment is assumed to occur during the sliding interaction. For attachment to take place, the thin liquid-film that separates the particle and the bubble must thin and rupture, and a three-phase contact line must be formed. The time for this to happen is known as the induction time,³⁵ t_i . Attachment will occur only if the time that the sliding particle is in contact with the bubble, t_{sl} , is greater than the induction time. This means that the particle must travel a finite distance along the bubble surface before attachment takes place. The distance traveled will depend upon the angle of incidence, θ_i , at which the particle strikes the bubble.²² It is often assumed that if θ_i is less than a limiting angle θ_o , then t_{sl} will be greater than t_i and attachment will occur. From Fig. 2.2, E_a can be defined as the area inscribed by the limiting radius, R_o , to the area inscribed by the sum of all bubble and particle radii ($R_b + R_p$) or

$$E_a = \frac{R_o^2}{(R_b + R_p)^2} = \sin^2 \theta_o \quad (2.9)$$

The sliding time can be determined from the incident angle and the sliding velocity of the particle as determined by the tangential velocity of the streamline, v_t , by the following integration:

$$t_{sl} = \int_{\theta_o}^{\theta_m} \frac{R_b + R_p}{v_t} d\theta \quad (2.10)$$

where θ_m is the position at which the streamline will move a particle away from the bubble surface. For potential flow it is equal to $\pi/2$. For intermediate Reynolds numbers it is significantly less, as shown by Dobby and Finch^{36, 37} and Nguyen Van.³⁸

The first derivation of sliding time by Sutherland in 1948¹⁵ assumed potential flow and a completely unretarded bubble surface. Sutherland's model, as corrected by Dobby and Finch,³⁶ is:

$$t_{sl} = \frac{2(R_b + R_p)}{u_b \left(2 + \left(\frac{R_b}{R_b + R_p} \right)^3 \right) + 2v_s} \ln \left(\cot \frac{\theta_i}{2} \right) \quad (2.11)$$

where u_b is the bubble velocity and v_s is the particle settling velocity.

Flint and Howarth,²⁵ from photographic results, observed that potential flow theory was valid for particles only up until they approached within one or two particle diameters from the bubble surface, at which point large discrepancies from theory were observed. To better describe particle behavior close to bubbles under flotation conditions, Dobby and Finch^{36, 37} derived an equation for completely retarded bubbles (bubbles whose rate of rise is slowed due to adsorption of surfactant at the air/water interface) and for medium values of Reynolds number:

$$t_{sl} = \left(\frac{\theta_m - \theta_i}{180} \right) \frac{\pi(R_b + R_p)}{\overline{v_\theta}} \quad (2.12)$$

where $\overline{v_\theta}$ is the average tangential velocity of the particle at the surface found by using an average dimensionless surface vorticity and an average value of the sine function.

Yoon and Luttrell²² used an empirical stream function to calculate sliding time for intermediate Reynolds numbers up to 100:

$$t_{sl} = \frac{R_b + R_p}{u_b \frac{R_p(45 + 8 \text{Re}^{0.72})}{30R_b}} \ln \left(\cot \frac{\theta_i}{2} \right) \quad (2.13)$$

Their model does not account for particle sedimentation, but is still applicable for particles with low density, such as in coal flotation.³⁸

Nguyen Van³⁸ proposed a model that includes the effect of centrifugal force for Reynolds numbers up to 400 and for particle size to bubble size ratios (R_p/R_b) up to 0.1.

For inertialess particles, an analytical expression results:

$$t_{sl} = \frac{R_b + R_p}{u_s(a^2 + B^2)} \left\{ a \ln \left| \frac{\tan \frac{\theta_m}{2}}{\frac{\theta_i}{2}} \right| + B \ln \left| \frac{(a + B \cos \theta_m) \sin \theta_i}{(a + B \cos \theta_i) \sin \theta_m} \right| \right\} \text{ for } a \neq B$$

$$t_{sl} = \frac{R_b + R_p}{2u_s a} \left\{ \ln \left| \frac{\tan \frac{\theta_m}{2}}{\frac{\theta_i}{2}} \right| + \frac{1}{1 + \cos \theta_m} - \frac{1}{1 + \cos \theta_i} \right\} \text{ for } a = B \quad (2.14)$$

where u_s is the slip bubble (bubble-liquid relative) velocity and the parameters a and B are calculated by a numerical solution to the Navier-Stokes equations.

Hewitt, Fornasiero, and Ralston³⁹ reported that their experimental results followed trends of E_a with bubble and particle size similar to that predicted by Dobby and Finch,³⁶ ³⁷ Yoon and Luttrell,²² and Li *et al.*⁴⁰ Results were closest to those predicted by the approach by Schulze,⁴¹ which allows for bubble surfaces of different degrees of retardation

Since sliding time is primarily controlled by the hydrodynamics of flow around the bubble, improvements in attachment efficiency by the addition of surfactants generally come about because of a decrease in the induction time. Measuring the induction time in flotation is difficult. If other steps, including the collision efficiency, are known or can be accurately predicted, then the induction time can be backed out from the flotation results.³⁹ Another approach is to measure the drainage rate of a thin liquid film between a bubble and a flat surface⁴² or between a bubble and a bed of particles⁴³ and qualitatively relating that to induction time. Measurements with these methods always result in calculated induction

times much higher than true flotation values due to the differences between the static measurement and the dynamic encounter event in actual flotation.⁴⁴

The induction time depends upon the stability of the thin film. Thin-film stability is an area with a well developed literature, and many good reviews on this subject and its application to flotation can be found elsewhere.^{13, 44-47} Only a few salient features will be dealt with here.

Most of the time of induction is taken up by film drainage. Two limiting cases for film drainage can be considered as first approximations:¹⁸ Reynolds' equation for the case of a plane-parallel thin film of radius R_f given by

$$t_{FR} = \frac{3\eta R_f^2}{4h_{crit}^2 F k} \quad (2.15)$$

and Taylor's equation for a solid sphere approaching a rigid wall with "point contact":

$$t_{FT} = \frac{6\pi\eta R_p^2}{F} \ln \frac{R_p}{h_{crit}} \quad (2.16)$$

where h_{crit} is the critical film thickness of film rupture, F is the driving force of approach, and the factor k is 4 for completely unretarded bubbles and 1 if they are completely retarded.

The critical film thickness is the thickness of the film when the "disjoining pressure" drops to zero. The disjoining pressure,⁴⁸ $P(h)$, is a function of film thickness and represents the difference between the pressure within the bubble and the pressure in the bulk liquid adjacent to the solid particle surface. It is thought to have three sources:

$$P(h) = P_{elec} + P_{vdW} + P_{steric} \quad (2.17)$$

where P_{elec} is the electrostatic or Coulombic forces which arise when the ionic atmospheres on the two surfaces of the wetting film overlap, P_{vdW} is the van der Waals forces that result from the molecular interactions of the molecules of the film with the particle and with each other, and P_{steric} is the steric forces resulting from the formation of polymolecular layers with specific properties on the surface of the particle.^{16, 44, 49} In general, P_{elec} and P_{steric} are repulsive and P_{vdW} is attractive. It has recently been recognized that there exists another attractive force, sometimes termed a hydrophobic interaction, which has been shown to increase with increasing surface hydrophobicity.^{50, 51}

It is generally very difficult to calculate h_{crit} from interparticle interaction energies. Often an experimental critical rupture thickness of a thin film separating a bubble and a flat sample plate is measured and assumed to be related to h_{crit} in the real flotation attachment process.⁵²⁻⁵⁵ Schulze and Bizer⁵⁶ have also developed an empirical correlation of h_{crit} to surface tension, σ , and advancing contact angle θ_a :

$$h_{crit} = 23.3 \left[\sigma (1 - \cos \theta_a) \right]^{0.16} \quad (2.18)$$

Paulsen, Pan, Bousfield, and Thompson⁵⁷ have recently developed a model for disjoining film rupture in which they consider viscous, surface tension, London-van der Waals dispersion, and hydrophobic attraction forces. Film drainage times were calculated in terms of the magnitude of the hydrophobic attraction and the characteristic wavelength which was assumed to be associated with particle dimension. The model predicted that intermediate size particles would be preferentially floated, which is consistent with flotation experiments.

It has been experimentally shown by Anfruns and Kitchener⁵⁸ that particles with angular or rough surfaces will more easily rupture the thin film, thus increasing their likelihood of being removed by flotation. Some models have been proposed to account for the existence of tips of edges, but there are not enough experimental results to confirm the

model assumptions.¹⁸ Because of this and the difficulties in understanding the interparticle interactions, no successful model for induction time has yet been developed.^{38, 39}

2.3.4 Stability of Attachment

Once the particle is fully attached to the bubble, the capillary attachment force must be great enough to withstand all of the detachment forces or the particle will be stripped from the bubble before it can be caught up in the foam. Nutt⁵⁹ was the first to investigate the adhesion of a spherical particle to a liquid-air interface. In reference to Fig. 2.3, he found that the capillary force for a spherical particle on a flat liquid-air surface was:

$$F_{ca} = 2\pi R_p \sigma \sin \phi \sin(\theta - \phi) \quad (2.19)$$

where θ is the liquid-solid advancing contact angle.

The other forces that will be acting on the spherical particle include the force of gravity, the static buoyancy force of the immersed part of the particle, the hydrostatic pressure, the capillary pressure in the gas bubble which acts on the contact area of the attached particle, and detaching forces resulting from acceleration in an external field of flow.^{17, 41}

If $\theta \ll 90^\circ$ and the particle diameter is smaller than 300 μm , the hydrostatic force can be neglected and the contacting angle at the maximum attachment force, ϕ_m , can be approximated as:

$$\phi_m = \frac{\theta}{2} \quad (2.20)$$

and the maximum capillary attachment force will be:⁵⁹

$$F_{ca, \max} = \pi R_p \sigma (1 - \cos \theta) \quad (2.21)$$

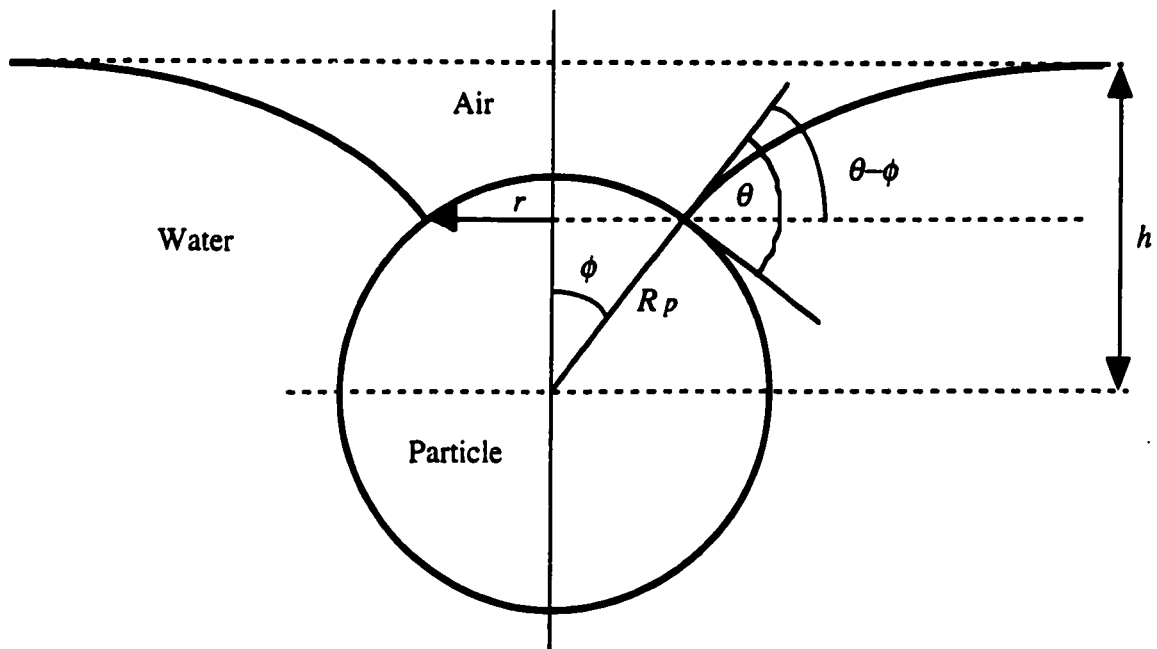


Figure 2.3 Spherical particle at flat gas-liquid interface.

When the hydrostatic force cannot be neglected, Baichenko and Listovnichii⁶⁰ have shown the following to be applicable if $R_p/R_b \ll 1$ and $R_p^2/a^2 \ll 1$:

$$\phi_m \cong \frac{\theta}{2} - \frac{1}{6} \frac{R_p^2}{a^2} \sin \frac{\theta}{2} - \frac{R_p}{2R_b} \sin \theta \quad (2.22)$$

where

$$a = \left(\frac{\sigma}{\rho_{Fl} g} \right)^{\frac{1}{2}} \quad (2.23)$$

For non-spherical particles, the situation is more complex. Ellipsoidal geometries^{59, 61} as well as cylindrical and prismatic shapes on liquid interfaces⁶² have been modeled. The adhesive force of irregularly shaped particles has been estimated by assuming an approximate average value of R_p of the particles.⁶³

Janczuk^{64, 65} has looked at the attachment of a bubble to a flat solid surface with small area and has derived the following:

$$F_{ca} = \frac{R_b \sigma \sin^2 \theta}{2} \left(\frac{4}{2 + \frac{3}{2} \sqrt{4 - \sin^2 \theta} - \frac{1}{8} (4 - \sin^2 \theta)^{\frac{3}{2}}} \right)^{\frac{1}{3}} \quad (2.24)$$

Janczuk found equation (2.24) to be in good agreement with experimentally measured detachment forces of bubbles in water on sulfur and graphite surfaces.⁶⁴ The relationship was also found to hold with Teflon surfaces although there were greater differences between measured and calculated values.⁶⁵

Stratton⁶⁶ assumed a simple geometry of a bubble adhering to a flat solid surface, and making some geometric assumptions, derived the force of capillary adhesion to be:

$$F_{ca} = 2\pi R_b \sigma (1 - \cos^2 \theta) \quad (2.25)$$

Stratton experimentally found a correlation between equation (2.25) and the flotation of hot melts and laser printed toners.

To find the stability of attachment from the above equations, it is usually assumed that E_s is exponentially distributed⁴¹ such that:

$$E_s = 1 - \exp\left(\frac{F_d - F_a}{F_d}\right) \quad (2.26)$$

where F_d is the sum of all detachment forces.

2.3.5 Efficiency of Froth Retention

Most flotation modeling assumes that the probability of the particle being retained in the froth is unity so very little information about modeling E_f is available in the literature.

However, changing frother type or even flotation conditions may increase selectivity by allowing material to drain from the froth back into the slurry.⁶⁷ In the 50's, Wrobel^{68, 69} reported that froth selectivity decreases with an increase in the molecular weight of the nonpolar group of the frother and decreases with an increase of the molecular weight of the polar group. The carrying power of the frother was shown to have an opposite trend, increasing with the molecular weight of the nonpolar hydrocarbon chain and increasing markedly with an increase in the molecular weight of the polar group, in particular with the number of carbon atoms.

Frothers come in two general categories: those that also act as collectors such as long-chain fatty acids, and those that don't. Frothers whose purpose is solely to create a froth are most commonly nonionic surfactants, and they can be divided into three main groups: alcohols, alkoxys, and polyglycols.⁷⁰

Alcohol frothers generally have 4 to 10 carbon atoms arranged in a linear, branched, cyclical, or aromatic form. They show less tenacity, lower water retention, and more brittle froths than most other frother groups.⁷¹ They are most effective for fine to medium size particles such as the floatation of smaller sized coal particles in the range of 75 to 250 μm .⁷²

The alkoxy group, such as 1,1,3-triethoxybutane, is rather new and has not seen much industrial use.⁷¹ It has frother properties similar to alcohols.⁷⁰

The polyglycol group is most typically represented by the polypropylene glycol methyl ethers: $\text{CH}_3-(\text{O}-\text{C}_3\text{H}_6)_n-\text{OH}$ and the polypropylene glycols: $\text{H}-(\text{O}-\text{C}_3\text{H}_6)_n-\text{OH}$ where n for both is commonly 3 to 7. These compounds generally form froths consisting of fine, tightly knit bubbles that are more persistent than froths from associated alcohols. The larger molecular polyglycols are more effective at floating larger size particles but have less selectivity than corresponding alcohols.⁷¹ For example, they are effective in removing coal particles in the size range of 150 to 500 μm .⁷²

In the last decade, research towards improving recovery of larger particles has led to a new group of polyglycol frothers given by the formula $\text{ROH} \cdot n$ alkylene oxide units, where R varies from four to six aliphatic carbon atoms.⁷⁰ The most successful of these have come from the reaction of propylene oxide (PO) and/or butylene oxide (BO) with aliphatic alcohols. For two known examples, Hexanol•2 PO and Hexanol•BO, larger copper sulfide particles (up to 300 μm) were recovered than with hexanol (up to 110 μm) or the corresponding polyglycol (up to 150 μm).⁷¹ However, this increase in coarse particle recovery comes at the expense of lower fine particle recovery.

The choice of frother type and concentration may affect E_f to some degree, but it should only be responsible for small differences in removal or selectivity. It is reasonable to assume that, in general, E_f has a value that is fairly high and that major differences in flotation are due to processes which happen in earlier steps.

2.4 The Influence of Particle Size

Next to particle hydrophobicity, particle size is the most significant parameter in flotation. Particles generally have difficulty floating if they are either too large (coarse) or too small (fine). Trahar⁷³ suggests explaining the behavior of different sizes in terms of a trade off between E_c and $E_a \cdot E_s$. E_c is known to be directly related to particle size and not related to surface hydrophobicity. E_a is inversely related to induction time, so it will be directly related to hydrophobicity and inversely related to particle size. E_s is dependent on the adhesion force between particle and bubble, which is also directly related to the hydrophobicity and inversely related to the particle size. Thus fine particles, which are assumed to have short induction times and strong forces of attachment ($E_a \cdot E_s$ close to one) primarily do not float because they do not collide with the bubbles ($E_c \ll 1$). Coarse particles, which are assumed almost always to collide with the bubble (E_c about 1), have shorter induction times and must endure stronger detachment forces ($E_a \cdot E_s \ll 1$), but are

also sensitive to increases in hydrophobicity ($E_a \cdot E_s$ increases) such that the larger the particle size, the greater the hydrophobicity required for successful flotation.

If we can assume that the advancing contact angle is a sufficient measurement of the hydrophobicity of the particle surface, then for each particle size there is a critical advancing contact angle below which flotation does not occur.⁷⁴ Several attempts have been made to model maximum flotation size as a function of contact angle and other parameters,^{17, 75} but application of these models to experiments has been difficult.^{73, 74}

2.5 Why Toners are Difficult to Float

In toner flotation, it is most important to remove the larger particles since they cause large ink specks in the recycled product. As discussed above, large particles do not float because either 1) they do not attach to the bubble after collision because they either are deflected from the bubble surface or the contact time is too short for the thin film to rupture; or 2) the particle initially attaches to the bubble but is not retained because the detachment forces from gravity and the surrounding flow are greater than the attachment forces. When poor flotation is due to the failure of a particle to either attach initially or remain attached to the bubble, the primary method of increasing flotation is to increase the hydrophobicity of the particle. It has also been shown that the poor flotation of repulped toners may be due largely to the continued presence of paper fiber still attached to toner particle surfaces.⁷⁶ The study suggested that as many as 65% of toner particles greater than 100 μm which exist the repulper may retain some amount of fiber.

A third possibility exists with toners. Since they are plate-shaped, they may change orientation as they flow around the bubble. This could cause changes in the probability of collision as well as the likelihood of attachment as will be discussed in Chapters 4 and 5.

An understanding of which mechanism is most important in hindering toner flotation, as well as the relationship between the important variables in this mechanism, will

aid in predicting the flotation response under given conditions. This may also lead to strategies towards improving flotation effectiveness either through the addition of more effective flotation reagents, improving the design of the mechanical flotation cell, or better controlling the size and shape of the toner particles in the pulping process.

CHAPTER 3

The Effect of Toner Electrostatic Properties on Flotation

3.1 Introduction

The objective of this study was to characterize quantitatively a variety of representative toners according to their electrostatic properties and to investigate how these relate to flotation. Toners contain known ionic surfactant constituents, such as charge carrying compounds and small amounts of metallic stearates, and changes in electrostatic properties, as characterized by the zeta potential,⁷⁷ can significantly affect the flotation efficiency, as has been shown in many mineral flotation processes.^{4, 13, 78} Zeta potential is generally a strong function of pH and commonly varies from a strongly negative to a strongly positive value over a large pH range. The pH at which the zeta potential is zero is known as the isoelectric point (IEP) and it is at this point that flotation is most effective.¹³

The zeta potential also aids in predicting how surfactants acting as collectors will adsorb onto a surface. For example, the head group of a cationic surfactant will more strongly adsorb to a negatively charged surface. The exposed hydrophobic tail of the adsorbed surfactant lowers the particle's surface energy, which in turn increases the adhesive strength between the particle and the bubble. Sometimes, the introduction of an anionic or cationic surfactant can lead to a high like charge on both the toner and the air bubble resulting in an electrostatic repulsion between them.

A better understanding of the electrostatics of toner systems might lead to a more effective choice of a collector. In this study, we sought to investigate the zeta-potential of toners and examine its effect of the hydrophobicity of the toner surface, as measured by contact angles, and on toner flotation in model flotation environments.

3.2 Materials and Methods

Eight toners representing six manufacturers, two laser printers, and both low- and high-capacity copy machines were selected. The compositions were obtained from Material Safety Data Sheets. Toners were used in the powder form as received from the manufacturers before printing. Densities were measured by a Micromeritics AccuPyc 1330 V2.01 pycnometer. Particle size was measured using the Horiba Model CAPA-500 Centrifugal Particle Size Analyzer.

Zeta potentials were measured by a Rank Brothers Mark II Particle Micro-electrophoresis apparatus. Attempts were made to duplicate the zeta-potential results using a Matec ESA-8000 and a Malvern Zetasizer 2c, but these failed because the particle size of the toner powder, about 10 μm in diameter, exceeded the upper size limits of both machines. Due to the strong hydrophobicity of the powder, toners were first dispersed in a 2.5 g/l solution of Triton™ X-100 in deionized water. The zeta-potentials of freshly prepared dispersions were found typically to have a time-dependence on a scale of hours, so dispersions were allowed to sit overnight before the experiment and come to equilibrium.

The pH was adjusted just before measurement by addition of HCl or NaOH. Conductivity was adjusted by adding NaCl. Conductivity was kept constant at about 120 $\mu\text{S/cm}$ for midrange pH values. Hydrochloric acid was added to lower the pH to about 2.8 and this raised the conductivity to about 850 $\mu\text{S/cm}$. Likewise, additions of sodium hydroxide increased conductivity to about 550 $\mu\text{S/cm}$ for toner solutions tested at pH 11.2. The pH and conductivity were measured with a Radiometer PHM 84 and CDM 83 immediately before measurement of zeta potential. To investigate the effect of multivalent cations, experiments at three pH values were repeated using $\text{Ca}(\text{OH})_2$ and CaCl_2 to adjust pH and conductivity. Experiments at a pH 4.2 were also performed with $\text{Al}(\text{OH})_3$ and AlCl_3 .

To measure contact angles on toners, the powdered toners were melted in a sand bath and thin fibers of perimeter 0.65-0.9 mm were drawn out with a glass stirring rod. Advancing and receding contact angles of the fibers were measured with a dynamic contact angle balance as described by Berg.⁷⁹ The pH and conductivity of probe solutions were adjusted so that the solutions were identical to those used in zeta potential measurements.

Flotation experiments were carried out with a modified Hallimond tube as described by Fuerstenau *et al.*⁸⁰ and Larsson *et al.*⁷ and with a 2.5 liter Wemco flotation cell. The modified Hallimond tube, shown in Fig. 3.1, worked best with model ink system, that is, ink solutions with no paper fiber present. It allowed for accurate control of gas flow, flotation time, and cell agitation so that changes in flotation efficiency were only attributable to toner type, pH, or chemical reagents.

Hallimond-tube flotation experiments were carried out for the eight toners in three different solutions: 1) a control solution containing 100 mg/l of Triton™ X-100 (octylphenoxy polyethoxyethanol with 9-10 ethoxy units, technical grade from Sigma Corp.) in deionized water; 2) 100 mg/l sodium n-dodecyl sulphate (SDS, technical grade from Fisher Scientific Co.) and 100 mg/l Triton™ X-100 in deionized water; and 3) 100 mg/l *n*-hexadecyltrimethyl-ammonium bromide (HTAB, reagent grade from Fluka) and 100 mg/l Triton™ X-100 in deionized water. No salts or pH conditioners were added but pH was measured and found always to be between 5 and 6.

The procedure for Hallimond tube tests was as follows. Between 30 and 40 mg of non-magnetic toner or between 40 and 60 mg of magnetic toner was measured into a 10 ml beaker. Approximately 5 ml of surfactant solution was added. Toner was dispersed by vigorous stirring with a stirbar for at least 20 minutes after which the dispersion was added to the bottom flask of the Hallimond tube along with a magnetic stirbar. The magnetic stirrer was turned on and kept at a constant setting for all experiments. The top section of the Hallimond tube was attached and approximately 65 ml of surfactant solution was added

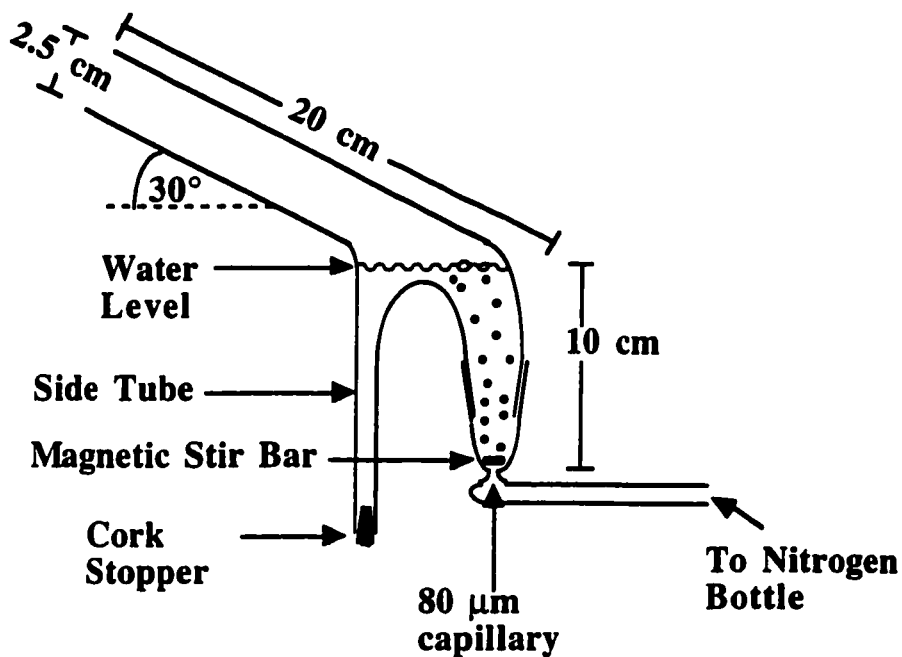


Figure 3.1 Schematic of the Hallimond tube used for flotation experiments.

until the liquid level was just barely above the top of the recovery tube. Nitrogen flow was introduced at a controlled rate of 40 ml/min. Any foam coming out of the top of the Hallimond tube was caught in a 250 ml beaker.

After ten minutes, nitrogen flow was shut off and floated toner was collected from the recovery tube into the 250 ml beaker. The dispersion remaining in the bottom flask of the Hallimond tube was collected into a second 250 ml beaker. Both dispersions were diluted to 50 ml by addition of deionized water. The toner content of the three fractions was determined by U/V/VIS spectrometry at 580 nm with a Bausch & Lomb Spectronic 20 instrument. Absorption was found to increase linearly with toner concentration. Recovery was defined as:

$$\frac{(\text{absorption of floated dispersion})}{(\text{abs. of floated disp.})(\text{abs. of remaining disp.})} \times 100\% \quad (3.1)$$

Flotation in the Wemco cell was performed on paper printed with one of the eight toners. About 13 g of printed paper was added to 2 liters of one of three solutions: 1) 5 mg/l of Triton™ X-100 in deionized water; 2) 5 mg/l SDS, 5 mg/l Triton™ X-100 in deionized water; or 3) 5 mg/l HTAB, 5 mg/l Triton™ X-100 in deionized water. All surfactant solutions included 0.00325 M NaOH yielding a pH of between 11 and 12. The mixture was repulped in a Messmer Instruments Disintegrator MarkIIIC for 75,000 cycles (25 min.). The slurry was transferred to the Wemco cell and flotation was begun. One-half to one liter of additional deionized water was added during flotation to maintain the liquid level. Flotation runs lasted two minutes and the temperature was about 24° C.

After flotation, a single, 16 cm-diameter handsheet was made from the slurry. After drying, the handsheet was analyzed on both sides with image analysis. Total dirt was measured on eight randomly chosen areas on the handsheet. This was compared to the total dirt measured on a control handsheet, prepared by the same procedure but omitting the flotation step, to give the percentage toner removal.

3.3 Results and Discussion

3.3.1 Toner Characterization

A description of the eight toners tested is given in Table 3.1. Toners are classified as either one or two-component toners. Both types of toner are made up of primarily carbon black dispersed in a thermoset copolymer such as styrene/butadiene or styrene/acrylate, but the two-component or magnetic toners also contain varying amounts of iron oxide in the form of magnetite, making them significantly denser and subject to a magnetic field, as shown in the table. Both toners also contain charge carrying compounds, such as quaternary ammonium salt or chromium chelate, and small amounts of metallic stearates which act as dry lubricants in the printing process.⁸¹

Table 3.1 Toner descriptions.

Toner	Source	Resin	Additives	Magnetic?	Density (g/cm ³)
A	Canon NP-115 Copier	Unknown	Unknown	yes	1.55
B	Pitney Bowes 750A	Unknown	Dye	no	1.17
C	Heattek Laser Writer	Unknown	Unknown	yes	1.49
D	Xerox 5042	Styrene/acryl copolymer	Amorphous silica, zinc stearate	no	1.17
E	Xerox 5065	Styrene/buta- diene copolymer	Rosin acid, quatarnary ammonium salt	slightly	1.27
F	Xerox 1090	Styrene/acryl copolymer	Quaternary ammonium salt	no	1.14
G	Sharp 8570	Styrene/acryl copolymer	Quaternary ammonium salt	no	1.14
M	Apple Laser Writer	Styrene/acryl copolymer	Salicylic acid chromium chelate	yes	1.52

All toners were found to be nearly monodispersed, with an average particle diameter of 8 to 12 microns. This falls well within the reported values of 8 to 15 microns.¹⁰ These results were confirmed by observations under a light field microscope as well as by scanning electron micrographs of all tested toners.⁸¹

The size of toner particles after printing is more complex. The spherical toner particles fuse during printing to form large, flat layers against the paper. Upon repulping, these layers break up to form smaller, plate-shaped particles of toner. Observed under a light field microscope, these toner particles typically range in size from 10 up to 350 microns in diameter but are only about 10 to 30 microns in thickness. Results with image analysis also show that a few particles can be as big as 1000 microns in diameter.

3.3.2 Zeta Potential Measurements

Zeta potentials of the toners were measured over a pH range of 3 to 11. The data are displayed in Fig. 3.2. Magnetic toners are represented by filled symbols.

As seen in Fig. 3.2, all of the toners tested were found to be anionic above a pH of 4, becoming more negative with increasing pH. Early experiments had indicated that toners dispersed in water could be either cationic or anionic, but contrary to our expectations, no cationic toners were found. Also, there was no difference between the zeta potential curves of magnetic and non-magnetic toners. Although it appears from the figure that a maximum negative zeta potential is being observed at a pH of around 8, it must be noted that the higher conductivity at the highest and lowest pH measurements will compress the double layer, resulting in a lower zeta potential than would otherwise have been observed. It is expected that if constant conductivity could have been achieved, the most negative zeta potential would have been seen at the highest pH.

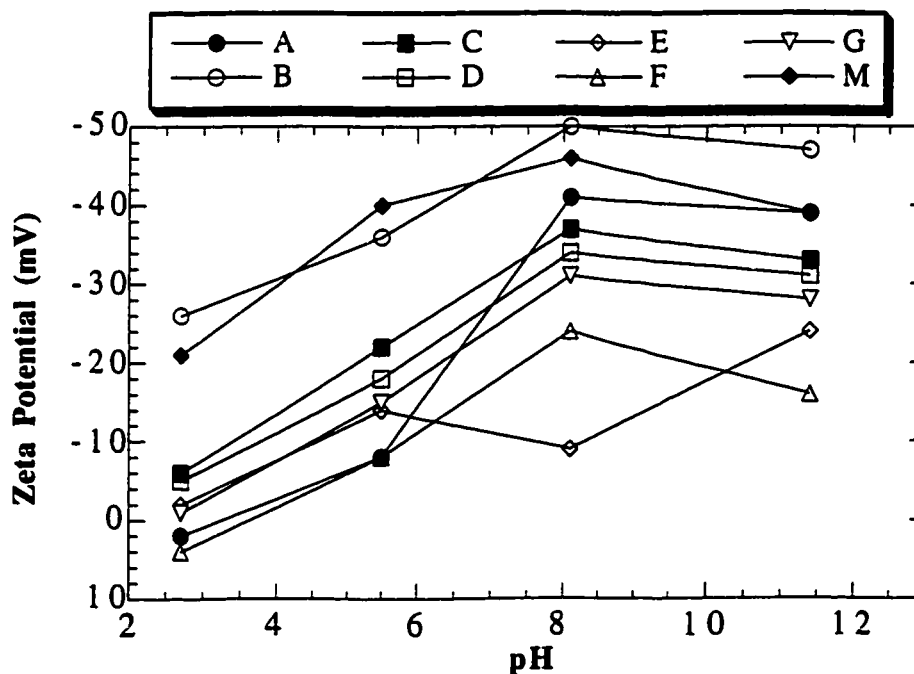


Figure 3.2 Zeta potential of toners versus pH. Filled symbols are magnetic toners.

Contact angle measurements are shown in Fig. 3.3 and 3.4. Both the advancing and receding contact angles are large, indicating a high degree of hydrophobicity across the pH range. There is little dependence upon pH, except perhaps for toners A and B which both have low receding contact angles at high pH. The receding contact angle is most sensitive to hydrophilic regions on the surface,⁸² so this may be indicative of polar functional groups in the toner polymer coming to the surface. Since the functional groups are probably ionized and increase the negative zeta potential, this also explains why toner A and B have the most negative zeta potentials at high pH.

Calcium is commonly present in industrial deinking plants, and it was speculated that the divalent calcium ion might specifically adsorb onto the toner surface, changing the zeta potential from negative to positive. To investigate this possibility, the experiments were repeated for all eight toners at pH values of 5.5, 9, and 11 using calcium hydroxide

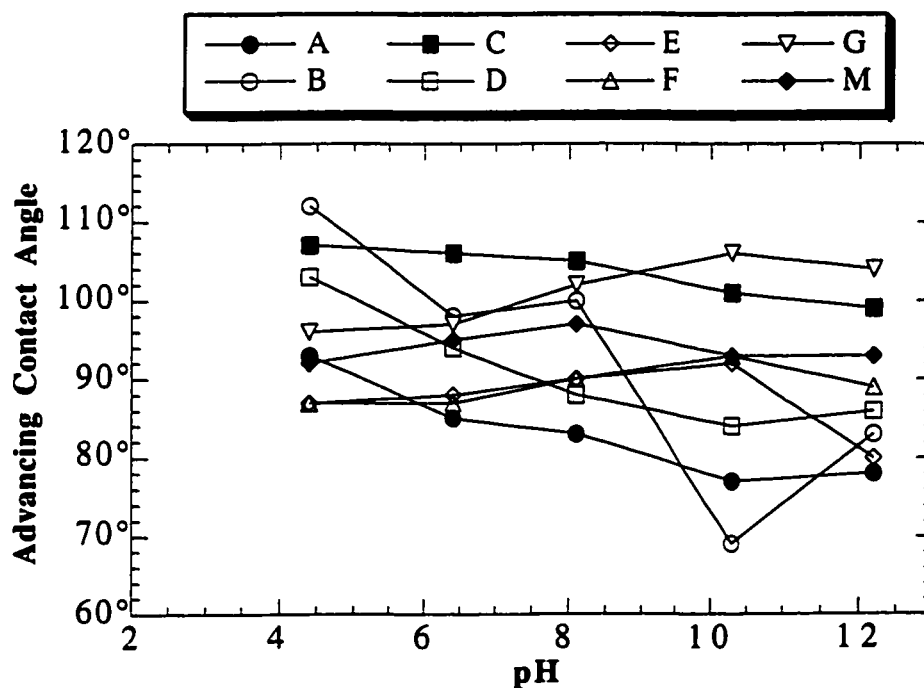


Figure 3.3 Advancing contact angle of toners versus pH. Filled symbols are magnetic toners.

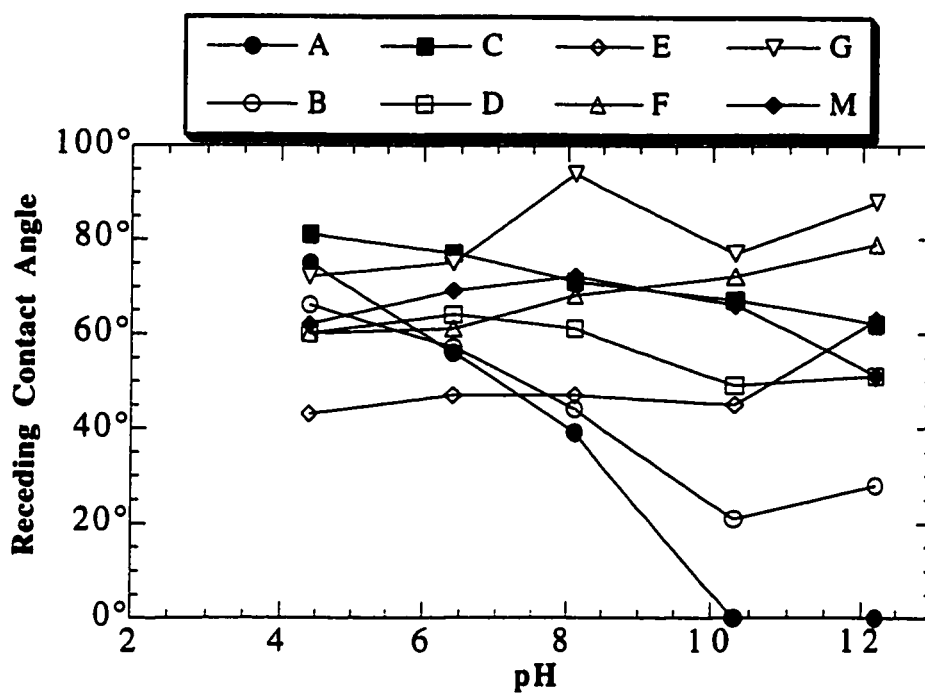


Figure 3.4 Receding contact angle of toners versus pH. Filled symbols are magnetic toners.

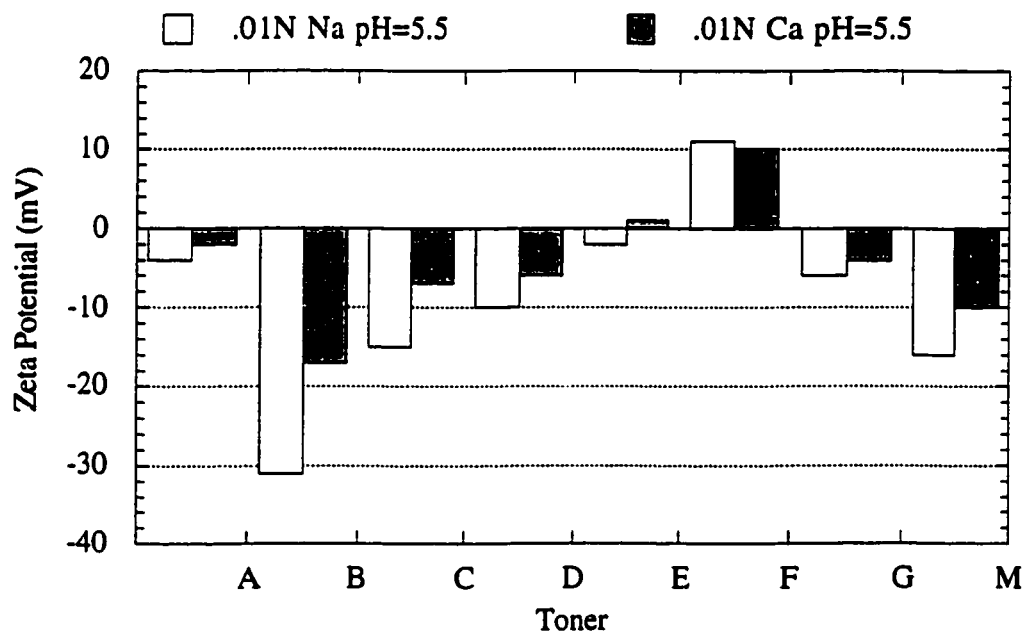


Figure 3.5 Zeta potential in Ca and Na solutions at pH 5.5

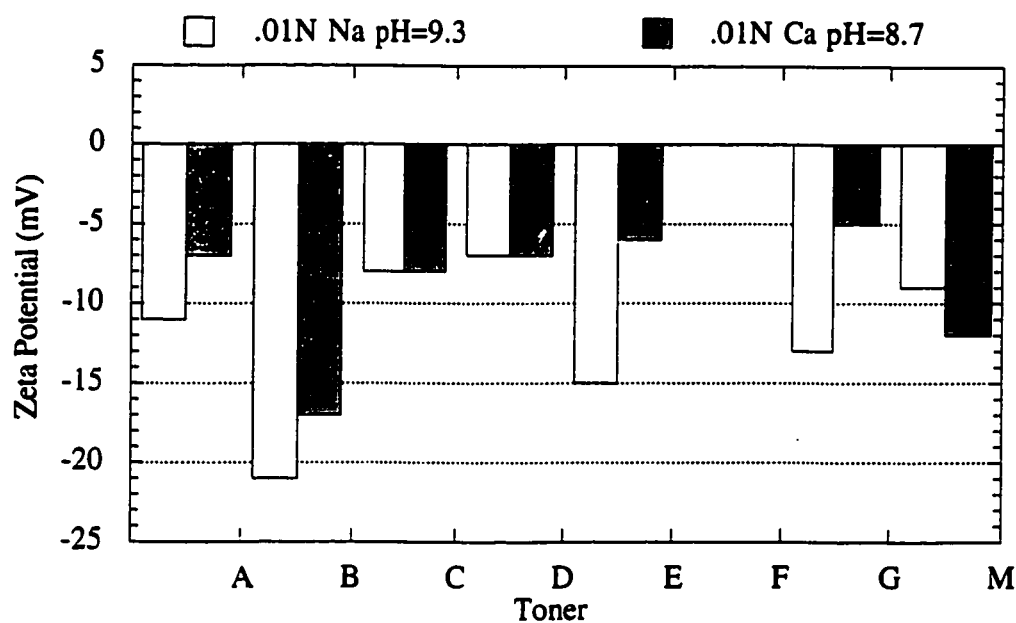


Figure 3.6 Zeta potential in Ca and Na solutions at pH 9.

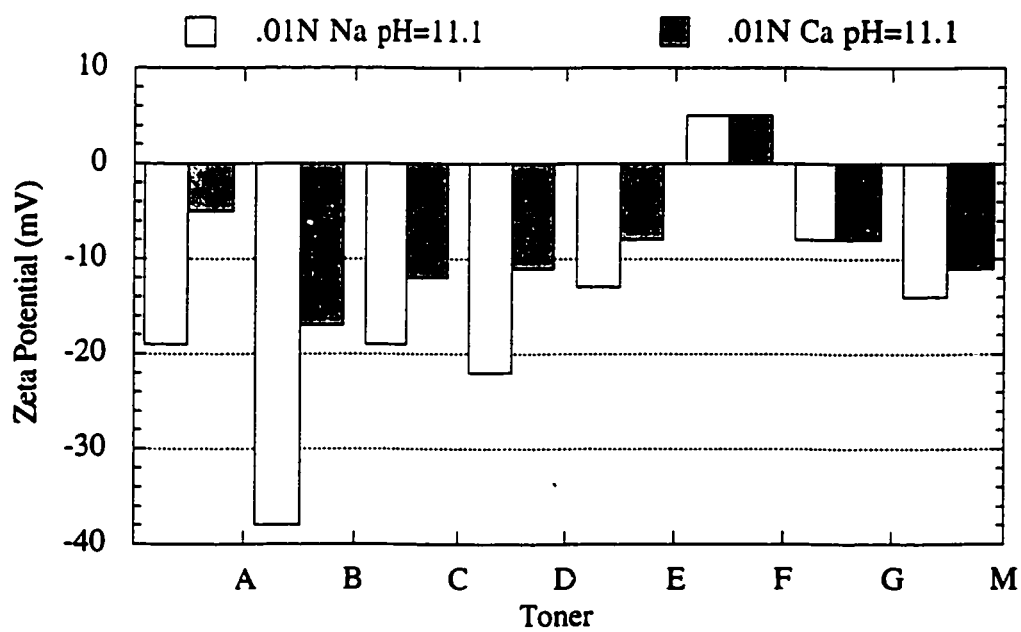


Figure 3.7 Zeta potential in Ca and Na solutions at pH 11.1.

and calcium chloride to adjust the pH and conductivity. The results of these experiments are shown in Figs. 3.5-3.7.

The calcium solutions followed the same trend as the sodium solutions with respect to pH, i.e., the zeta potential became more negative at higher pH. Calcium reduced the magnitude of the zeta potential compared to sodium, probably because of a greater collapse of the electrostatic double-layer due to the divalency of the calcium cation (as would be predicted from the DLVO theory⁷⁷).

The zeta potentials of the toners in an AlCl_3 solution were also measured. Because Al^{+3} ions are only present below a pH of about 5, measurements were taken only at a pH of 4.2. The results are compared with the sodium and calcium solutions in Fig. 3.8. Similar to the calcium solution, the magnitude of the zeta potential was even lower, probably due to the trivalent aluminum cation continuing to shrink the double-layer. Toner A did show a positive zeta potential, but this may be due to the low pH since earlier measurements with sodium showed the zeta potential becoming positive below a pH of 4.

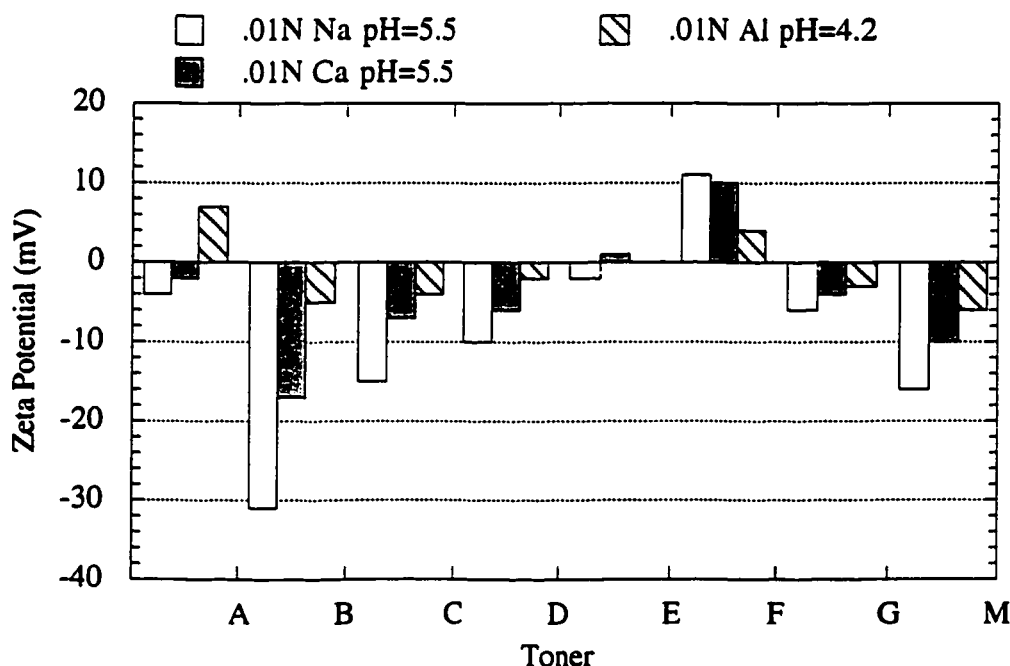


Figure 3.8 Zeta potential in Na, Ca, and Al solutions.

It was concluded that multivalent cations do not adsorb to the toner surface in significant amounts. One surprising result was that toner F sometimes exhibited cationic properties. We found that the zeta potential of toner F exhibited a time dependent behavior of the order of hours. The zeta potential of F would often start slightly positive and then quickly drop until, after several hours, it eventually reached a stable negative value. For consistent results, a standardized procedure was thereafter followed in which the toner dispersions are stored for a set time before measuring the zeta-potentials.

3.3.3 Hallimond Tube Flotation

Hallimond tube experiments were originally attempted at 5 mg/l for all surfactants so as to better compare with the Wemco flotation experiments. However, it was almost impossible to disperse the toner at such a low surfactant concentration. To insure good dispersion, 100 mg/l was chosen as the surfactant concentration.

To determine repeatability, six Hallimond tube flotation experiments were conducted consecutively with toner B. The average flotation of toner was 46% and the 95 percent confidence limit was calculated to be 4.6%. This leads to the conclusion that differences in recovery of less than 5% should not be seen as statistically significant.

Figure 3.9 shows a graph of zeta potential versus Hallimond tube flotation of toner in the nonionic control surfactant (Triton™ X-100), the control plus an anionic surfactant (SDS), and the control plus a cationic surfactant (HTAB). As can be seen from the scatter of control data, there is no relationship between zeta potential and removal of toner. However, the two toners with the highest zeta potential, B and M, have as high or higher toner removal with the addition of HTAB versus just the control alone. In order to see how significant this might be, the flotation data of Fig. 3.9 were normalized with respect to the control solution by dividing the percent removal of a given solution by the percent removal of the control. The results are shown in Fig. 3.10.

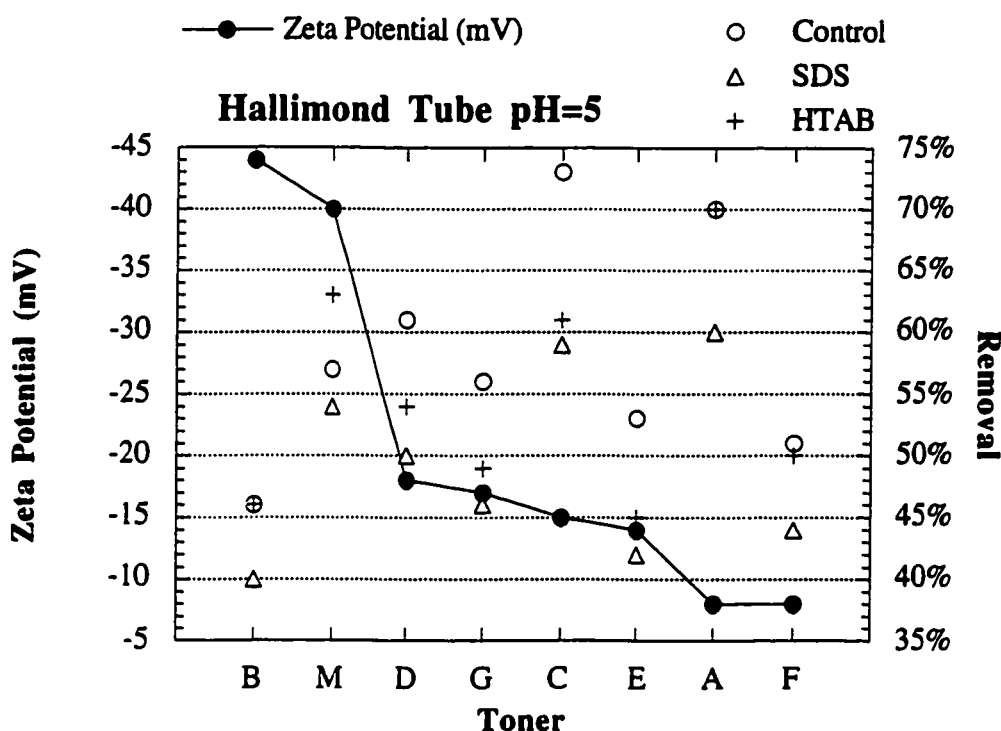


Figure 3.9 Zeta potential versus Hallimond tube flotation in a nonionic control surfactant (100 mg/l Triton™ X-100), the control plus an anionic surfactant (100 mg/l SDS), and the control plus a cationic surfactant (100 mg/l HTAB).

Figure 3.10 shows a possible relationship between zeta potential and toner removal with a cationic surfactant. The first six toners on the graph suggest a trend in which the more negative zeta potentials have a higher recovery rate when a cationic surfactant is added to the dispersion. This could be explained by the cationic surfactant adsorbing to the toner with the charged polar head-group facing down, leaving the hydrophobic tail sticking out and thus making the toner surface more hydrophobic and more likely to adhere to a bubble. However, the trend fails with toners A and F, the toners with the lowest zeta potential, and thus we cannot conclude that this trend is valid for all toners.

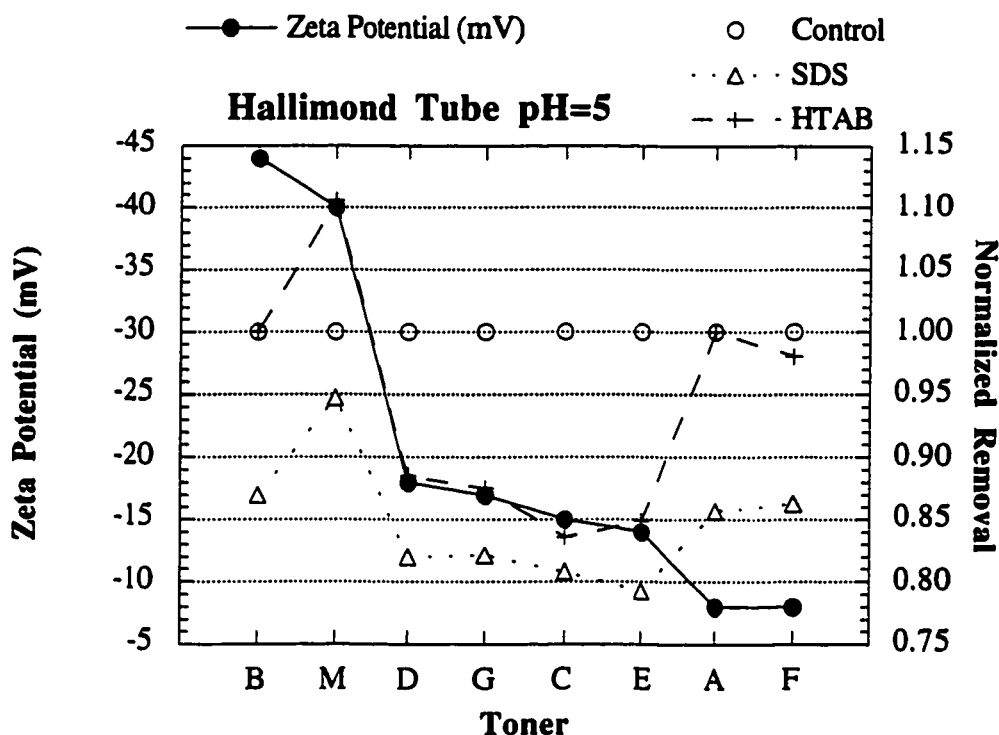


Figure 3.10 Zeta potential versus normalized Hallimond tube flotation (percent removal divided by percent removal of control).

3.3.4 Wemco Cell Flotation

The modified Hallimond tube gives reproducible results that are sensitive to changes in toner surface chemistry and solution chemistry. However, the results do not always correlate well with those obtained from an industrial flotation cell due to differences in attachment mechanism, suspension, and bubble size.⁸³ Because of this, it is important to compare Hallimond tube experiments with flotation experiments conducted in larger lab top flotation cells or even pilot plant flotation cells if possible before making definite conclusions regarding flotation.

Hallimond-tube flotation results are compared to results in a benchscale Wemco flotation cell in Fig. 3.11. Instead of a direct correlation, an almost inverse correlation is observed. In particular, toners A, C, and M are generally easiest to remove with the

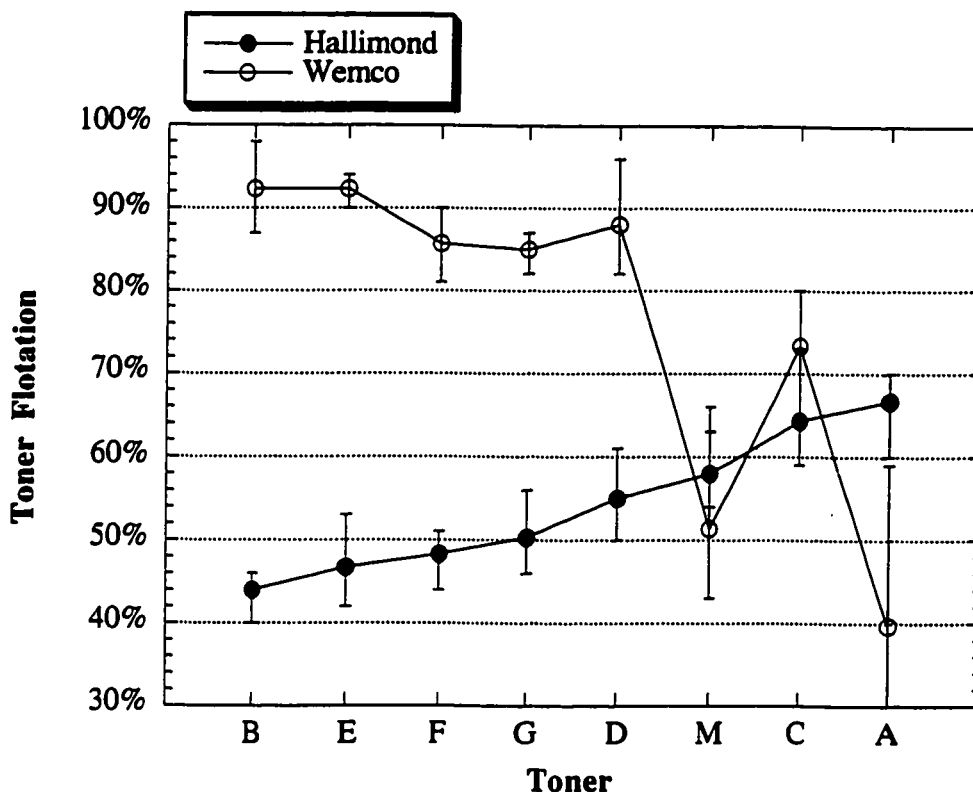


Figure 3.11 Hallimond tube versus Wemco cell flotation for eight toners.

Hallimond tube, but the hardest to remove using the Wemco cell. This may be because these toners are magnetic. The unprinted toners are all the same size, about 10 microns in diameter, but the three magnetic toners have a higher density than the non-magnetic toners, 1.5 g/ml vs. 1.15 g/ml. In the Hallimond tube, being dense is an advantage to removal. The dense toners have greater momentum and are more likely to collide with a bubble rather than follow the stream lines around it. The dense toners also settle to the bottom of the tube faster, where they have greater chance of contacting the bubbles.

In the Wemco cell, particle size is determined by the pulping process, and not all toners will break up the same way. The magnetic toners may break up as larger flakes than the non-magnetic making them more difficult to remove. Also, the heavier flakes of

magnetic toners may not remain attached to a bubble as readily as the lighter, non-magnetic toners and thus may not float as effectively.

3.4 Conclusion

All eight toners tested were found to be anionic in solutions of neutral pH and above, and all were hydrophobic over a pH range of 4-12. It was found that zeta potential does not play a major role in flotation. This was not surprising considering the hydrophobicity of the toner surfaces. Work by Arbiter *et al.*⁸⁴ showed that no relation existed between zeta potential and contact angle or floatability for many hydrophobic solids, including molybdenite, graphite, and paraffin wax. For most hydrophobic solids, the composition and potential of the interface is determined only by the aqueous phase. Contributions by the solid phase are generally due to charged hydrophilic sites on anisotropic surfaces. Because toner surfaces have few charged hydrophilic sites, zeta potential has little correlation with floatability.

It was also observed that flotation of unprinted toner powder in a Hallimond tube did not predict the flotation of printed toners in a flotation cell. However, the Hallimond tube is still useful to compare qualitatively the flotation of a single type of unprinted toner in different surfactant solutions because the toner size is always controlled, and thus differences in removal will be due only to changes in toner surface properties.

Work in this area led to a further investigation into the effect of surfactant concentration on zeta potential and contact angles of toners, in which it was demonstrated that the surface chemical concept of hemi-micellization, familiar in mineral flotation, was also applicable to polymeric toners in surfactant solutions.¹⁴ Further experiments with toner flotation in the Hallimond tube also led to an investigation into the effect of froth stability and wettability on toner flotation, as detailed elsewhere.⁸⁵

CHAPTER 4

The Effect of Particle Shape on Flotation⁸⁶

4.1 Introduction

In Chapter 3 and in an earlier investigation,⁸¹ it was found that eight random toners were all hydrophobic over a pH range of 4-12. In general, toners are naturally hydrophobic particles and should theoretically be easily removed with only the addition of a frother.^{2, 13, 14} It has been shown that the poor flotation of repulped toners may be due largely to the continued presence of paper fiber still attached to as many as 65% of the toner particles exiting the repulper.⁷⁶ However, the shape of the toner after repulping may also play a role in the effectiveness of flotation.

In the paper repulping process, the toner breaks up into large, flat, plate-shaped particles that differ significantly from the smaller, spherical particles of conventional inks.^{3, 11, 12} These plate-shaped particles could interfere with the particle/bubble attachment process and hinder flotation. The objective of the present research was to investigate the role of toner particle shape in the flotation process. The first task was the creation of model toner disks and spheres of the same toner, particle volume, and density. Differences in the flotation performance between these particles were examined using flotation experiments and by observing single particle/bubble interactions.

4.2 Theory

In a batch flotation cell, the fractional removal of particles, R , is commonly modeled as a first order rate process:

$$\frac{dR}{dt} = k(1 - R) \quad (4.1)$$

where t is time and k is a rate constant. R is defined as:

$$R = \frac{C_o - C}{C_o} \quad (4.2)$$

where C is the number of particles per unit volume or particle concentration and C_o is particle concentration at $t = 0$. Thus, at any given time, $C = N/V_r$ where N is the total number of particles present in the cell and V_r is the reference cell volume.

The total number of particles collected by one bubble (N_b) rising through a well-mixed suspension of particles is:

$$N_b = E \left(\frac{\pi D_b^2 L}{4} \right) C \quad (4.3)$$

where D_b is bubble diameter, L is the path length through which the bubble rises through the suspension, and E , the overall collection efficiency introduced in Chapter 2, represents the probability that a particle whose center is within the path of a rising bubble will be removed by that bubble. This relationship holds true when the bubble is large (≈ 1 mm diameter) and the particles are not excessively large.⁸⁷ Theoretically, particles up to 2 mm in diameter can be floated,¹⁷ but in industrial practice, flotation effectiveness begins to fall off for particle sizes greater than around 300 μm .⁸⁸

For a given gas volumetric flow rate, G_{fr} , at a fixed pressure, the number of bubbles formed per unit time, B_{rate} , is:

$$B_{rate} = \frac{G_{fr}}{\pi D_b^3 / 6} \quad (4.4)$$

In this equation, D_b is the average bubble diameter and should take into account the size distribution of bubbles formed as well as any changes in size due to the decrease in

local pressure as the bubble rises in the flotation cell. The total rate of removal of particles, N , from a flotation cell can be given by:

$$-\frac{dN}{dt} = \left(\frac{G_f}{\pi D_b^3 / 6} \right) \left(E \frac{\pi D_b^2 L}{4} C \right) = \frac{3}{2} \frac{G_f EL}{D_b} C \quad (4.5)$$

Since $C = N/V_r$,

$$-\frac{dC}{dt} = \frac{3}{2} \frac{G_f EL}{D_b V_r} C \quad (4.6)$$

or in terms of removal:

$$\frac{dR}{dt} = \frac{3}{2} \frac{G_f EL}{D_b V_r} (1 - R) \quad (4.7)$$

By comparison of equations (4.1) and (4.7), the rate constant can now be shown to be:

$$k = \frac{3G_f EL}{2D_b V_r} \quad (4.8)$$

The rate constant is thus dependent upon gas flow rate, average bubble size, length of bubble rise (which is approximately the cell height), cell volume, and most critically, upon the overall collection efficiency.

As explained in Chapter 2, it is common practice to break down the flotation process into four steps that must occur in sequence for a particle to be removed. First, the particle must collide with the bubble. Second, the thin liquid film separating the particle and bubble must drain and rupture for true contact or attachment to be established. Third, the particle must remain attached to the bubble as it rises to the surface, and finally the particle must be successfully transferred to the froth. The overall collection efficiency can be expressed as the product of the efficiency of these steps:

$$E = E_c E_a E_s E_f \quad (4.9)$$

where E_c is the collision efficiency, E_a is the attachment efficiency, E_s is the stability efficiency of the particle/bubble aggregate, and E_f is the efficiency of particle transfer to the froth.

For medium-sized particles ($\approx 100 \mu\text{m}$) and larger, the smallest of these four factors is generally the attachment efficiency of the particle to the bubble. For attachment to take place, the time required for the thin film to drain and rupture, the induction time, must be less than the time of contact. Induction time will depend upon several factors including the hydrophobicity of the particle and the size of the drainage area. Optimum attachment of a hydrophobic particle to a bubble will take place when there is a small drainage area linked with a prolonged contact time.

The path that an element of fluid takes as it flows around a bubble is the streamline of flow. Our initial hypothesis was that as a flat-shaped particle, shown on the left side of Fig. 4.1 as a disk, approaches a bubble, it turns due to the streamlines of flow around the bubble such that its large side becomes parallel to the bubble surface. This produces a greater drainage area compared to the case of a similar volume sphere. The larger contact area requires greater time for film drainage and rupture, and thus lowers the probability of disk attachment.

4.3 Experimental

Model toner disks were created by printing solid black circles with either a Pitney Bowes 750A photocopier (toner B from Chapter 3) or an Apple Laser Writer (toner M from Chapter 3) onto a transparency coated with a 2 wt% solution(water) of poly(vinyl alcohol) (PVA). The PVA was 99+% hydrolyzed, of molecular weight 85,000 to 146,000, obtained from Aldrich Chemical Company, Inc. The PVA solution was applied using a

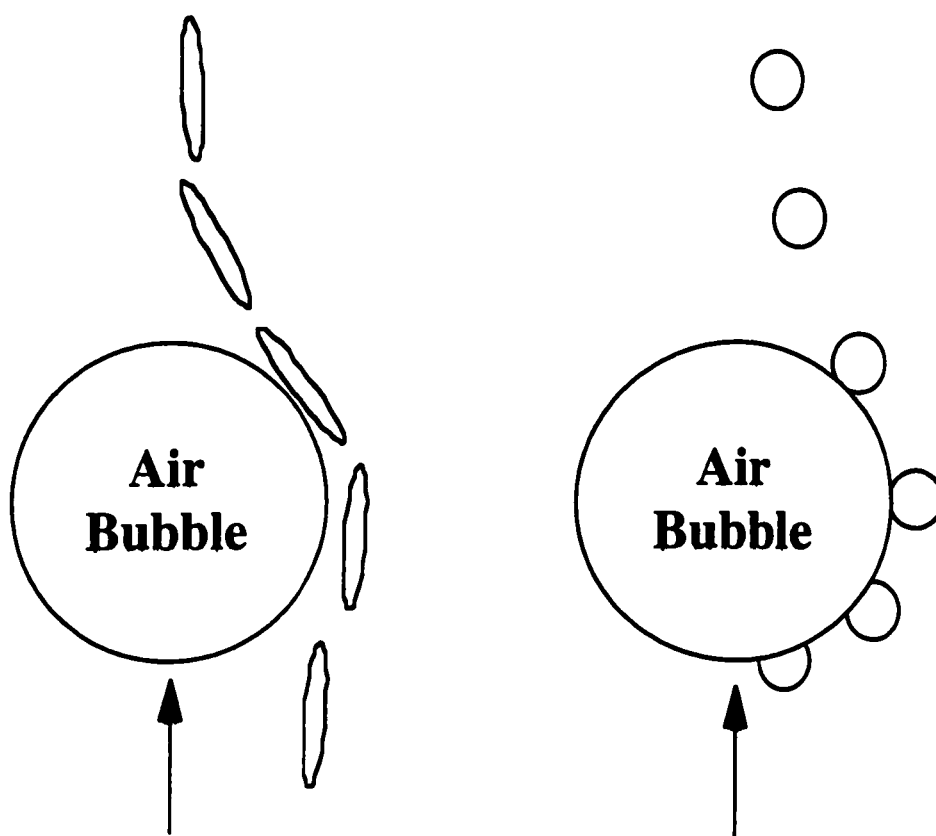


Figure 4.1 Predicted interactions of a disk and sphere as they approach a bubble.

#30 wire wound rod which rested on both ends on Scotch® 3M tape attached at each long edge of the transparency.

After printing, the transparency was cut into strips and soaked for about 10 minutes in 60°C deionized water. The PVA dissolved and the toner disks floated off the transparency and were recovered. Disks were washed twice in 60°C deionized water to insure removal of any residual PVA. Toner disks from both the laser printer and the photocopier were 650 to 850 μm in diameter and 10 to 20 μm in thickness. Average disk diameter was 730 μm which was well within the floatable range of the laboratory flotation

cells. The Apple Laser Writer toner contained iron oxide and thus those disks had a higher density than the photocopier disks (1.52 g/cm^3 versus 1.17 g/cm^3).

So far, we have only been able to create toner spheres with the photocopier toner, so only photocopier disks were used in comparisons with spheres. Toner spheres were created by dissolving 1.5 grams of the Pitney Bowes photocopier toner into 6 grams of ethyl acetate and, with a syringe, injecting small droplets of the mixture into a tall bath of deionized water. The droplets had a density slightly less than water. As the droplets rose, ethyl acetate diffused out of the toner and into the water, eventually leaving solid spheres behind. Toner spheres, being more dense than water, settled to the bottom. Spheres were collected and stored in deionized water at 60°C overnight to drive off remaining solvent. Sphere sizes ranged from $50 \text{ }\mu\text{m}$ to $300 \text{ }\mu\text{m}$ in diameter so a 65 mesh sieve was used to collect spheres of size $200 \text{ }\mu\text{m}$ to $300 \text{ }\mu\text{m}$, corresponding to the same volume as that of the disks. Disks and spheres were stored in deionized water and refrigerated to inhibit bacterial growth.

Because the methods of creating toner spheres and disks are very different, it is necessary to measure the surface properties of each to ensure that differences in flotation are not simply due to differences in hydrophobicity between the two particles. The contact angle, a convenient measurement of surface hydrophobicity, cannot be easily measured on small particles, so methods were sought to create similar surfaces on more convenient shapes. At the same time that the spheres were created, several 0.10 cm-diameter, copper-wire rods were immersed in deionized water and coated with toner by passing one end of the rod through a drop of the toner-ethyl acetate mixture formed at the end of the syringe. The rods were stored in deionized water at 60°C overnight to drive off any remaining ethyl acetate and were subsequently stored in the same container as the spheres.

To mimic the surface of a disk, photocopier-toner powder was melted onto copper-wire rods in an oven at 90°C . The melted-toner rods were then placed into a small beaker

of deionized water, heated to 60°C, and allowed to cool. The rods were stored in the same manner as the disks. Advancing and receding contact angle for all rods were determined with a dynamic contact angle balance as described by Berg.⁷⁹

Flotation experiments were conducted using both a Hallimond tube and a single bubble flotation tube. The Hallimond tube was constructed as described by Fuerstenau *et al.*⁸⁰ and Larsson *et al.*⁷ and is shown schematically in Fig. 3.1. A known number of toner disks or spheres were placed for 5 minutes in 10 ml of a 0.4 mM solution of 1-hexanol (added as a frother) so that any adsorption of the surfactant onto the toner surface could have time to reach equilibrium. The particles were then added to the right-hand tube and the entire assembly was filled with the 0.4 mM 1-hexanol solution. Nitrogen was flowed at 20 ml/min for two minutes. Floated particles were removed via the left side tube, counted, and compared to the number of particles not floated to determine the fraction removed by flotation.

The single bubble flotation tube was adapted from a design by Anfruns and Kitchener⁵⁸ and is shown schematically in Fig. 4.2. A known concentration of disks or spheres was conditioned in a 0.4 mM 1-hexanol solution. By manipulating two 3-way stopcocks, the suspended particles were brought into a known length of tubing by vacuum. A single bubble was formed and allowed to rise through the particles and into a collecting cell at the top, where the bubble was captured, bubble size measured, and the number of particles attached to the bubble counted.

Finally, to observe particle movement around a bubble, a flowtube apparatus was built as shown schematically in Fig. 4.3. A bubble was affixed to the end of a 24-gauge Teflon tube. Water flows down the flowtube at a constant, adjustable velocity to mimic the hydrodynamics of a free bubble rising in water. Particles enter through a feed tube that is centered just above the bubble. A Plexiglas box full of water surrounds the viewing area to

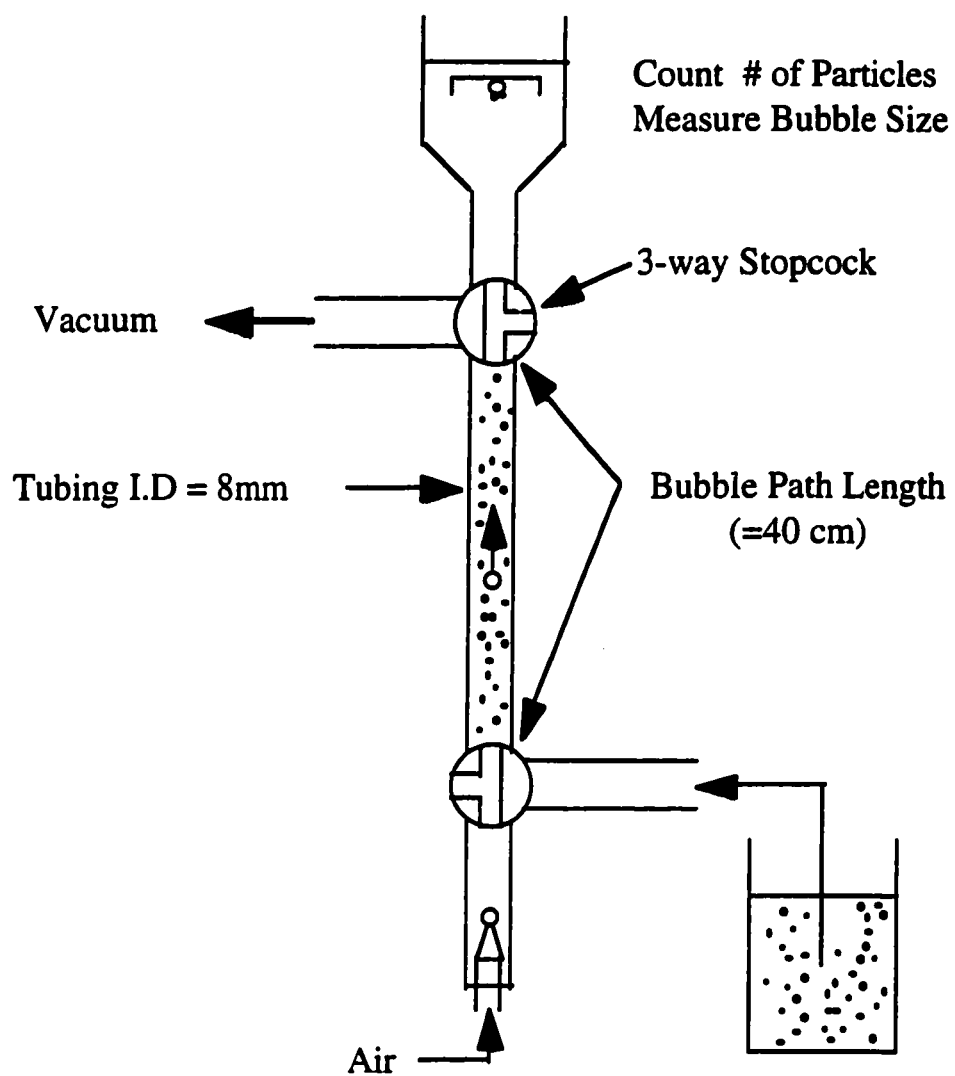


Figure 4.2 Schematic of the single bubble flotation tube.

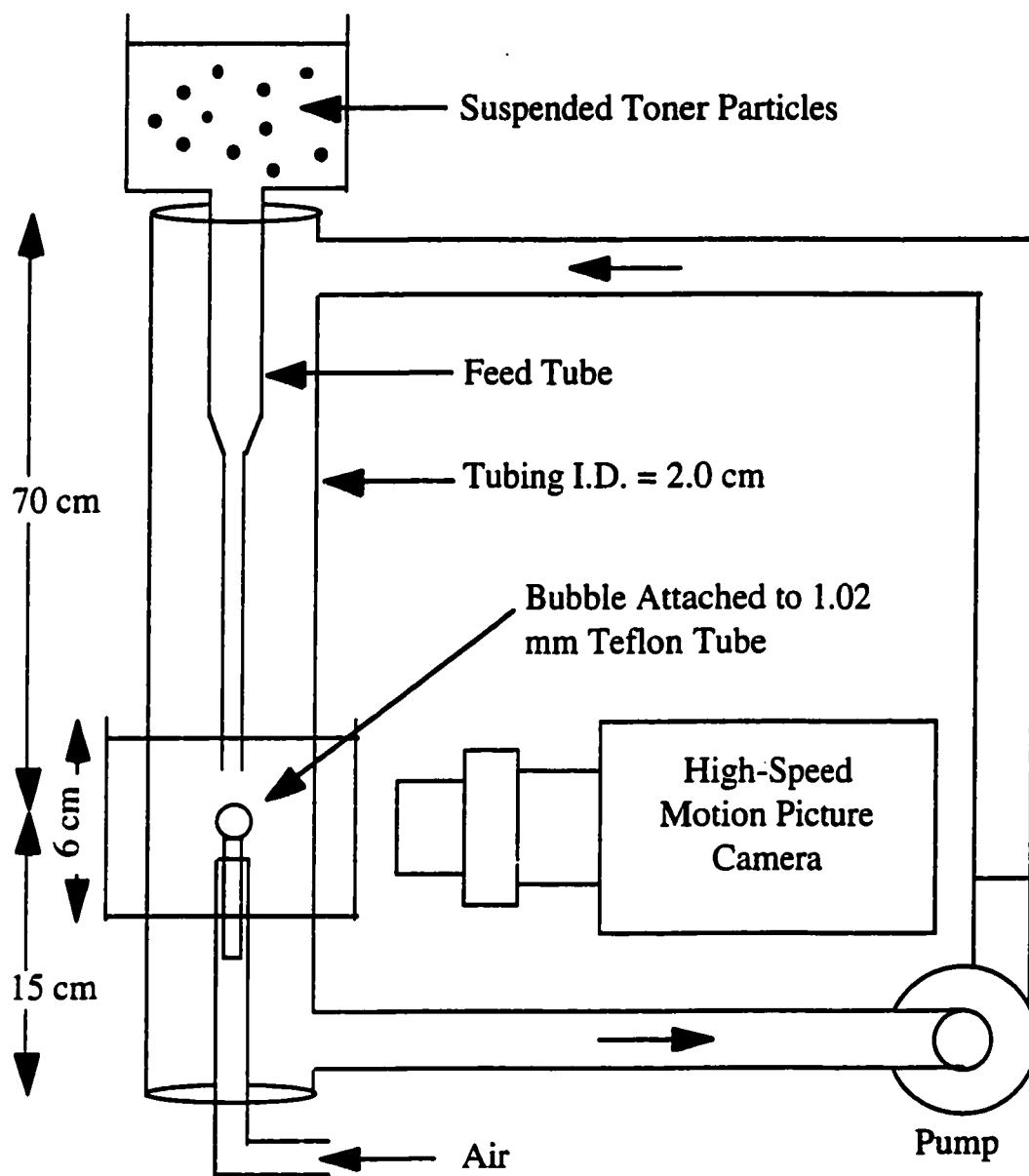


Figure 4.3 Schematic of the flowtube apparatus used to observe particle/bubble interactions.

minimize distortion. A 0.4 mM 1-hexanol solution was used in the flowtube so that the solution chemistry would be the same as that in the flotation experiments.

Particles colliding and interacting with bubbles have been observed before with high-speed motion photography by Spedden and Hannan⁸⁹ and Whelan and Brown,⁹⁰ with a stroboscopic method by Schulze and Gottschalk,⁹¹ and with high-speed video by Batchelder and Li,⁹² but all of these observations were with spherical or roughly spherical particles. This is the first study we are aware of that looks at the interaction of plate-shaped particles with a bubble.

Particle/bubble interactions were recorded with a Photosonics 1-B 16 mm high-speed motion picture camera running at 700-800 frames per second. High-speed pictures were necessary because the events of collision and attachment are very rapid, of the order of milliseconds. To obtain a three-dimensional representation of particle movement, a mirror set-up, as shown in Fig. 4.4, was used to record two orthogonal images of the bubble and particle at the same time, on the same frame of 16 mm film. Size and position of particles and bubbles were determined by image analysis of the film with a Vanguard Motion Analyzer.

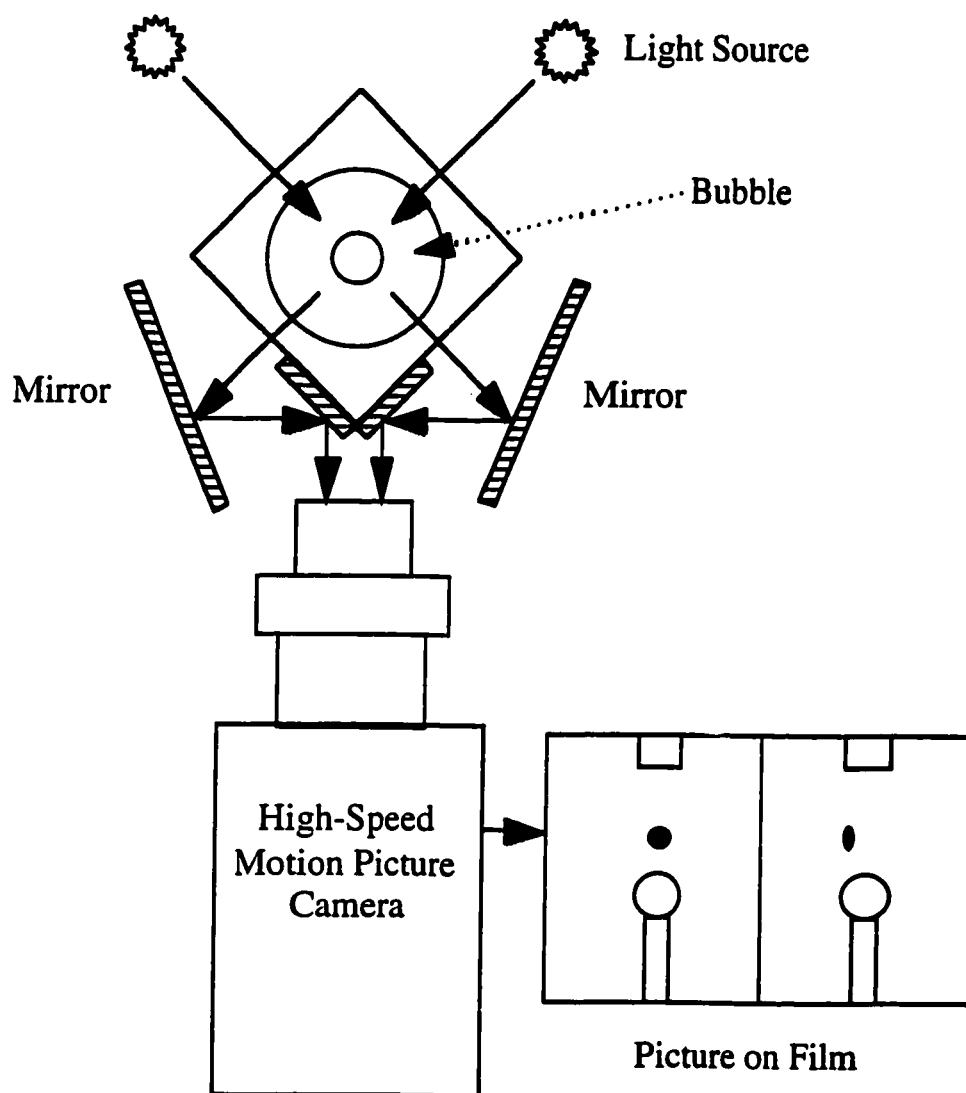


Figure 4.4 Mirror and camera set-up around the flowtube used to obtain two perpendicular views of the object on one frame of film.

4.4 Results and Discussion

Contact angle measurements on the toner coated rods are shown in Table 4.1. There was no significant difference between either the advancing or receding contact angles, indicating that the hydrophobicity of the disk and sphere surfaces are similar.

Flotation results are summarized in Fig. 4.5. Hallimond tube removal is the percent of particles floated in two minutes. Single bubble collection is the total sum of particles attached to 15 separate bubbles that were allowed to rise through the tube. For both apparatuses, there was a dramatic difference in the flotation of disks and spheres. Only 32% to 36% of the disks were floated in the Hallimond tube, compared to 75% to 80% flotation for spheres. After letting 15 bubbles rise through the single bubble apparatus, only 6 disks were captured versus 36 spheres for the same conditions.

From equation (4.3), E for the single bubble collection apparatus can be shown to be:

$$E = \frac{4N_b}{\pi D_b^2 LC} \quad (4.10)$$

Using this relationship, E for the flotation of disks and spheres was calculated. The results are shown in the first column of Table 4.2. E for the flotation of disks and spheres in the Hallimond tube was also determined by measuring flotation at five different

Table 4.1 Advancing and receding contact angles measured on toner coated rods in deionized water.

Toner coating process:	Surface similar to:	Advancing contact angle	Receding contact angle
Melting	Disk	78 ± 7	38 ± 8
Ethyl Acetate	Sphere	75 ± 4	40 ± 6

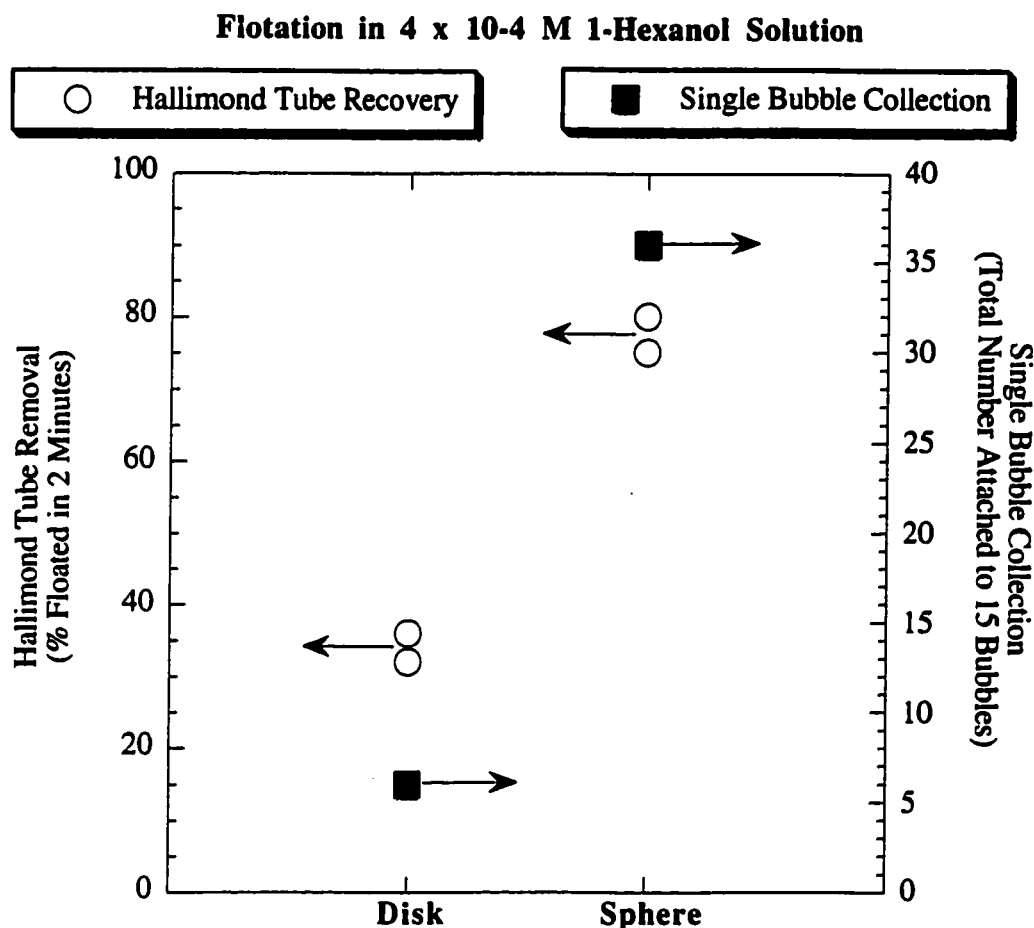


Figure 4.5 Disk and sphere flotation in the Hallimond tube and in the single bubble flotation tube.

times, calculating from this data a rate constant, k , and then using k in equation (8) to calculate E . The resulting Hallimond tube collection efficiencies showed similar trends to the single bubble flotation results, as shown in Table 4.2.

Although they are of the same volume, disks have a much larger longest particle dimension than spheres. It is not always clear how this will affect flotation, since it will both increase collision efficiency and decrease the stability efficiency of the particle/bubble aggregate. We assumed the decrease in the stability efficiency in our apparatuses was negligible and tried to account for changes in collision efficiency as explained later.

Table 4.2 Overall collection efficiencies for disks and spheres in the single bubble flotation apparatus and in the Hallimond Tube.

Particles	<i>E</i> Single Bubble	<i>E</i> Hallimond Tube
Disks	0.07 ± 0.03	0.06 ± 0.01
Spheres	0.4 ± 0.1	0.14 ± 0.02

Figure 4.6(a) shows two spheres which attached to a bubble after collision. The trajectory of a captured sphere is shown in Fig. 4.7 on the left where the path of the particle is oriented such that it is within the plane of the figure. The sphere that misses contacting the bubble, shown on the right, is included here for comparison. Both spheres and bubble are drawn to scale and each drawn sphere represents the movement in one frame of film.

It was observed that as the spheres approach the bubble they were deflected. If a sphere was already several hundred microns away from the bubble centerline as it approached the bubble, as with the outside sphere in Fig. 4.7, it would usually fail to contact the bubble and attach. However, if a sphere did contact the bubble, it had a good probability of attaching and remaining stuck to the bubble. This behavior of the spheres is qualitatively similar to that predicted by a flotation model developed by Pan, Paulsen, Johnson, Bousfield, and Thompson.^{24, 30, 32}

The results for the disks colliding with the bubble were unexpected. Figure 4.6(b)-(d) shows a typical picture of a disk approaching, colliding, and flowing around a bubble as taken from three separate frames of a 16 mm film sequence. The two perpendicular views on one frame allows the three-dimensional position and orientation of the disk to be determined by image analysis. As the disk approached a bubble, it was not strongly deflected before collision, neither did it turn, but collided edge-on. The entire trajectory of a typical disk/bubble interaction is shown in Fig. 4.8. Here it can be seen that the disk

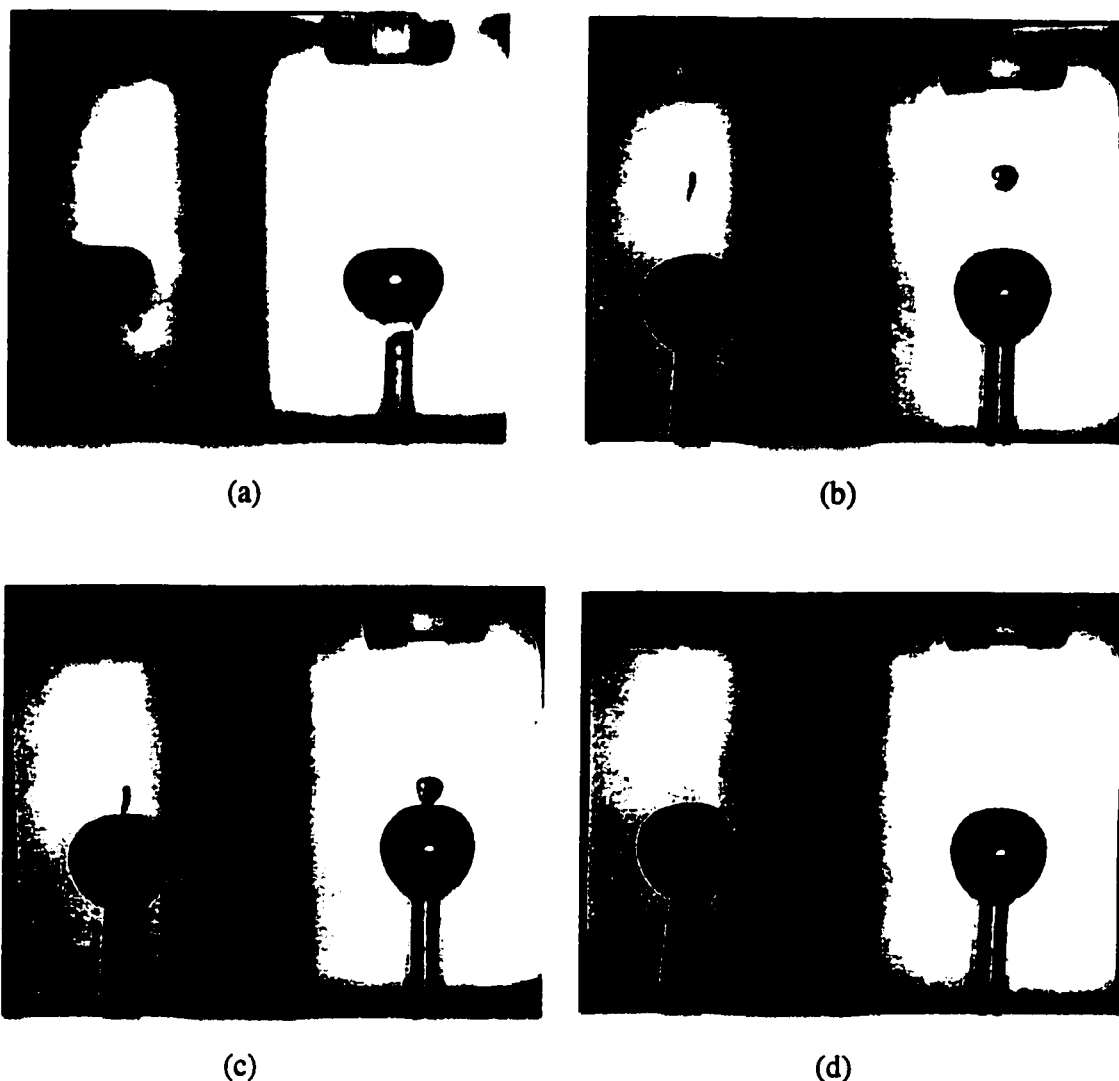


Figure 4.6 Toner particles and bubbles photographed from two directions at right-angles to each other. Each picture is taken from one frame of a 16 mm film sequence. At the center is the bubble affixed atop a 1.02 mm diameter Teflon tube. The light spot in the middle of the bubble is due to the lighting. The bottom of the feedtube can be seen at the top of the picture. (a) Spheres attached to a 2.6 mm diameter bubble. The three spheres shown in the left view are in front of and behind the bubble in the right view and thus cannot be seen. (b) A 700 μm diameter toner disk approaching a 2.5 mm diameter bubble. (c) The same disk 5 frames or 7.0 ms later than (b) as it first collides with the bubble. (d) The same disk 6 frames or 8.5 ms later than (c) after it has bounced and turned to its side. The disk is not seen on the right because it is behind the bubble. (The full video tape of the 16 mm film is on file at the Department of Chemical Engineering at the University of Washington.)

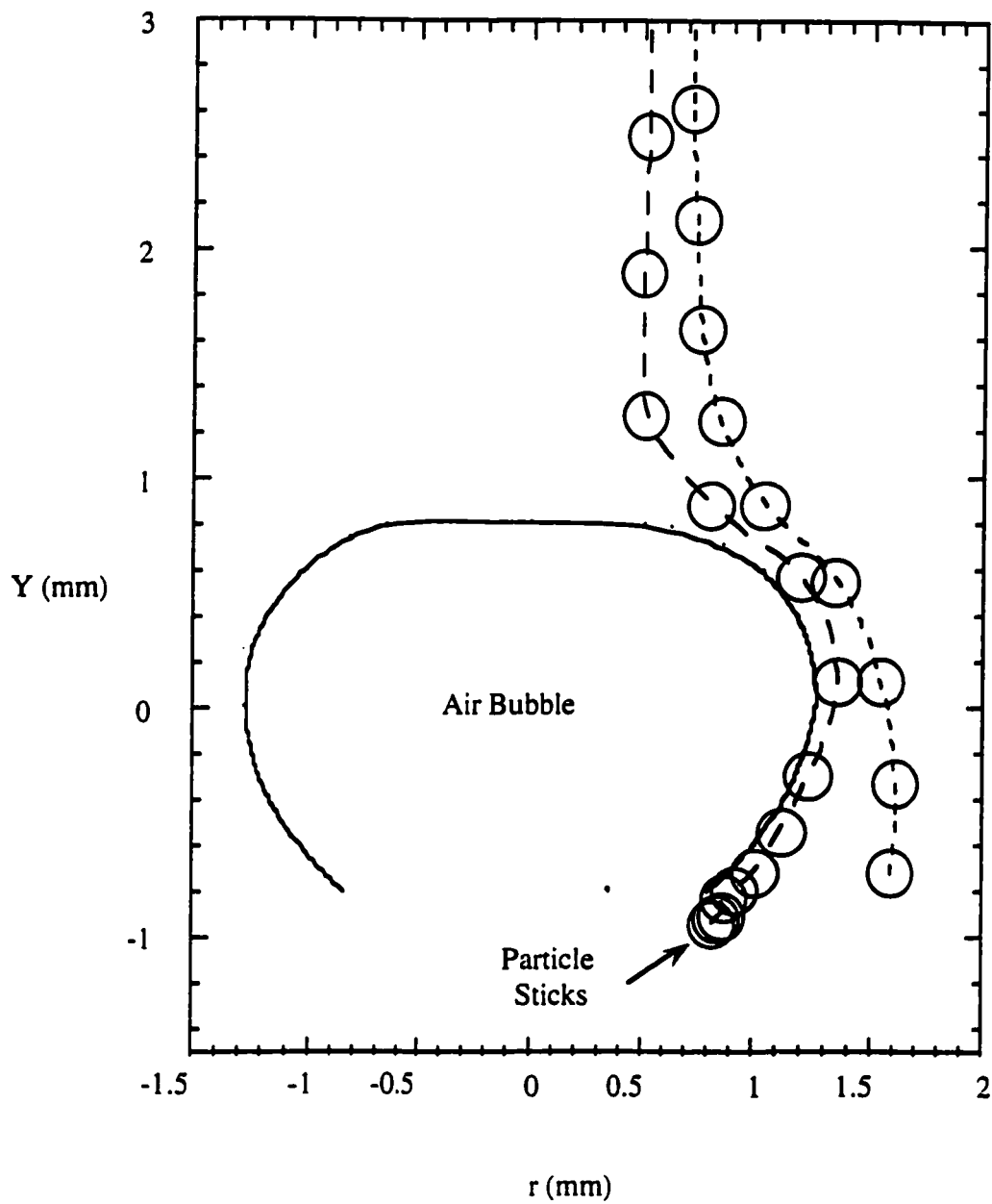


Figure 4.7 Trajectory of two spheres, drawn to scale, flowing around a bubble with one sphere attaching to the bubble. Each drawn sphere represents one frame of film or 1.4 ms.

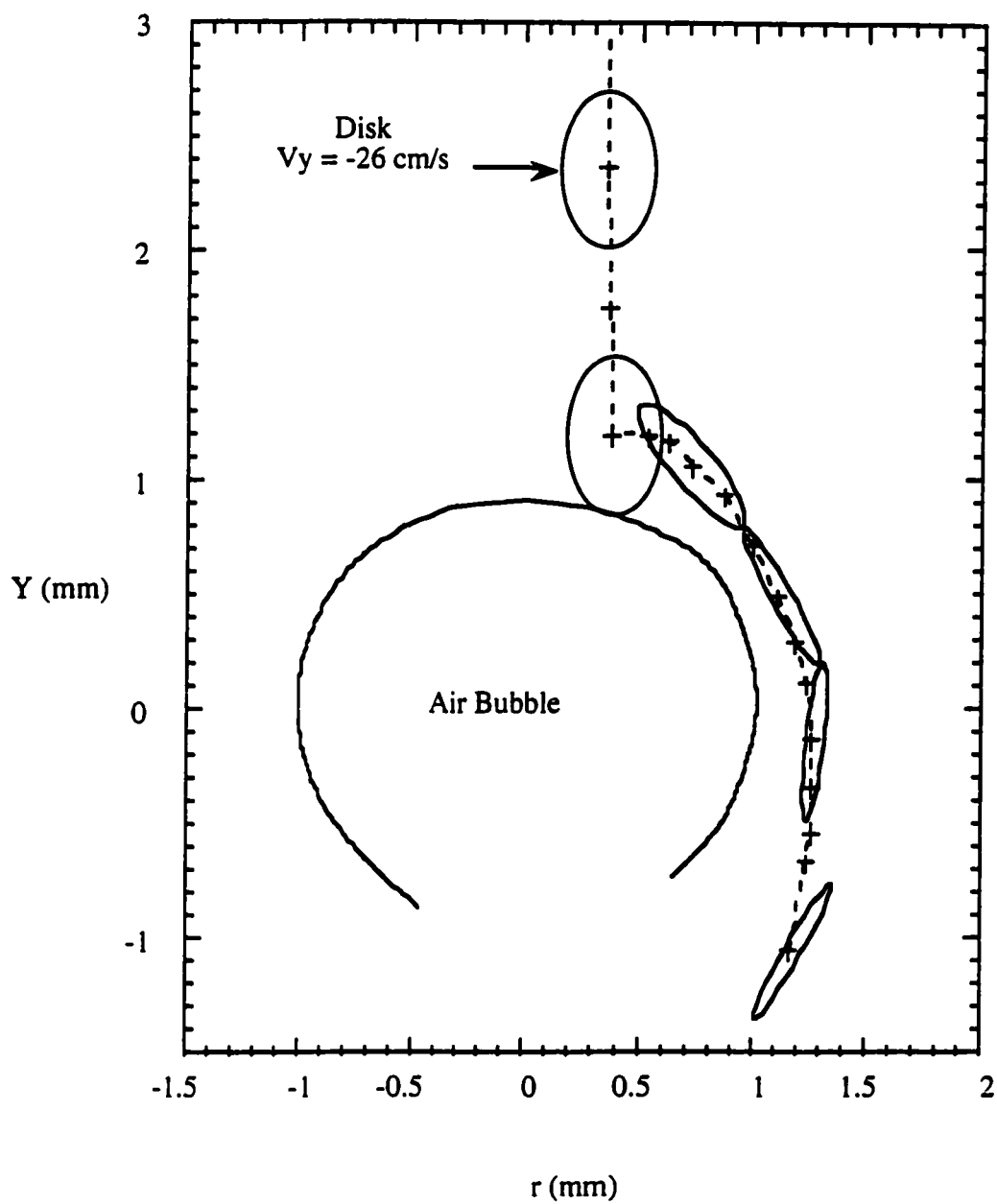


Figure 4.8 Disk, drawn to scale, colliding with a bubble, bouncing off, turning, and flowing around the bubble.

bounced, and then flipped over to its side and flowed around the bubble without attachment. The bounce occurred in less than a millisecond, and after turning to its side, the disk usually never came into contact with the bubble again. Occasionally a disk would bounce away from the bubble without flipping over. An example of such a trajectory is shown in Fig. 4.9, where the disk is oriented parallel to the page.

The initial collision in both of these cases is so rapid that the thin film separating the particle and bubble does not have time to drain and rupture, despite the very small contact area. This seems to contradict the commonly-held belief that particles colliding with a sufficiently high momentum should be able to pierce the surface of the bubble.¹³

Experiments with the toner disks created by the Apple Laser Writer which have a higher density than the photocopier disks (1.52 g/cm^3 versus 1.17 g/cm^3) did not lead to any disks piercing the bubble surface. In fact, the two different disks appeared to behave identically with respect to their interactions with the bubble.

After the initial collision, it was very rare for a disk to contact the bubble surface again. Once bouncing and flipping to the side, they flow around the bubble as shown in Fig. 4.6(d). This lack of contact during flow around the bubble may be due to the large drainage area that is set up between the bubble surface and the flat side of the disk, preventing the disk from getting too close to the bubble during the time it circles the bubble. Thus attachment of disks to a bubble in the flowtube apparatus happened much less frequently than the attachment of spheres.

From Figs. 4.9 and 4.10, it appears that the disks are not being deflected by the streamlines of flow around the bubble as were the spheres. However, this is not the case. The disks are being deflected, but because they are such wide particles, they collide with the bubble while the degree of deflection is still small. This suggests that there might be more disk deflection and reorientation before collision for disks of smaller size. We did see evidence that our hypothesis of disks turning before collision may dominate for the smaller

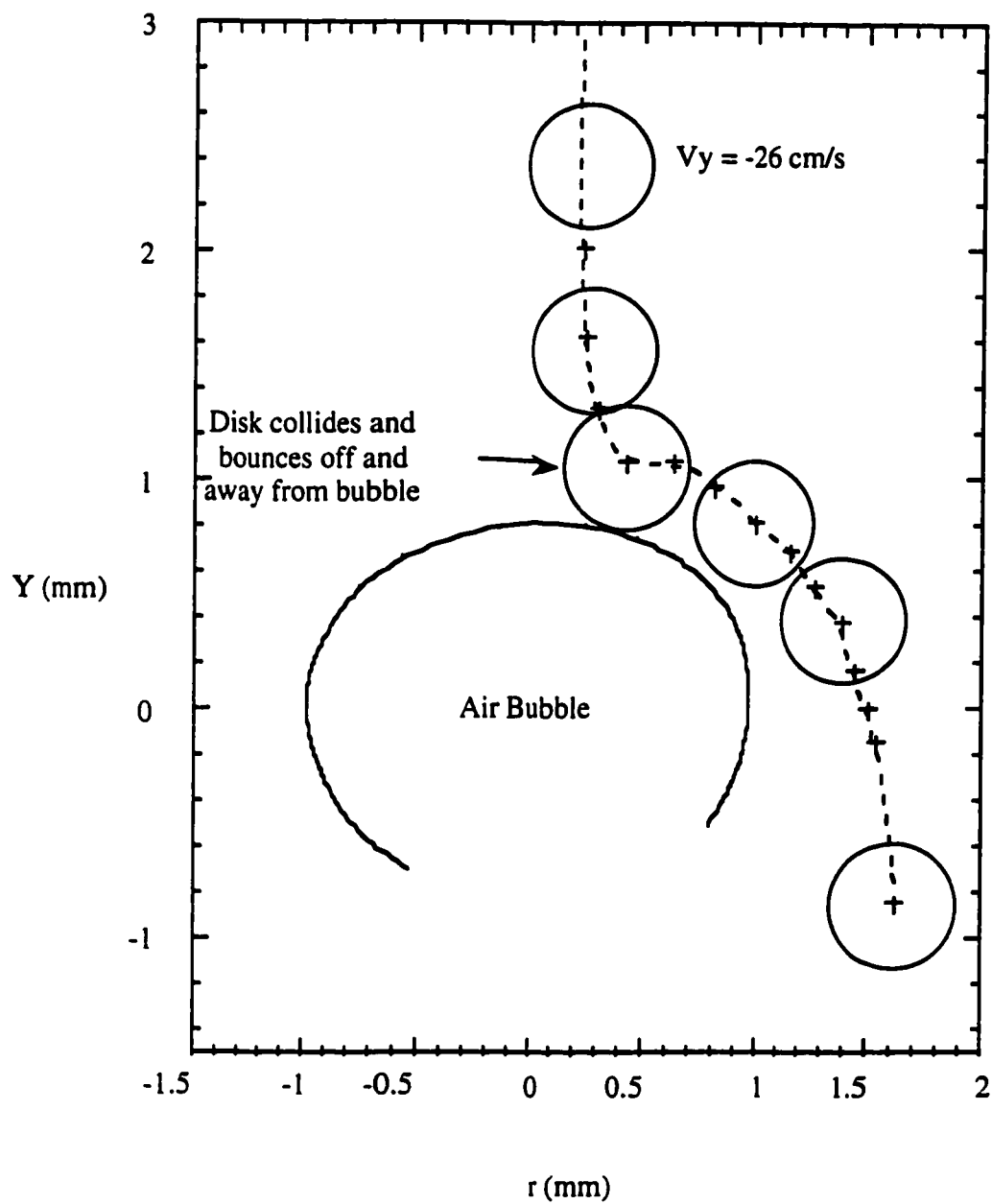


Figure 4.9 A disk, oriented parallel to the figure, colliding with and bouncing away from a bubble.

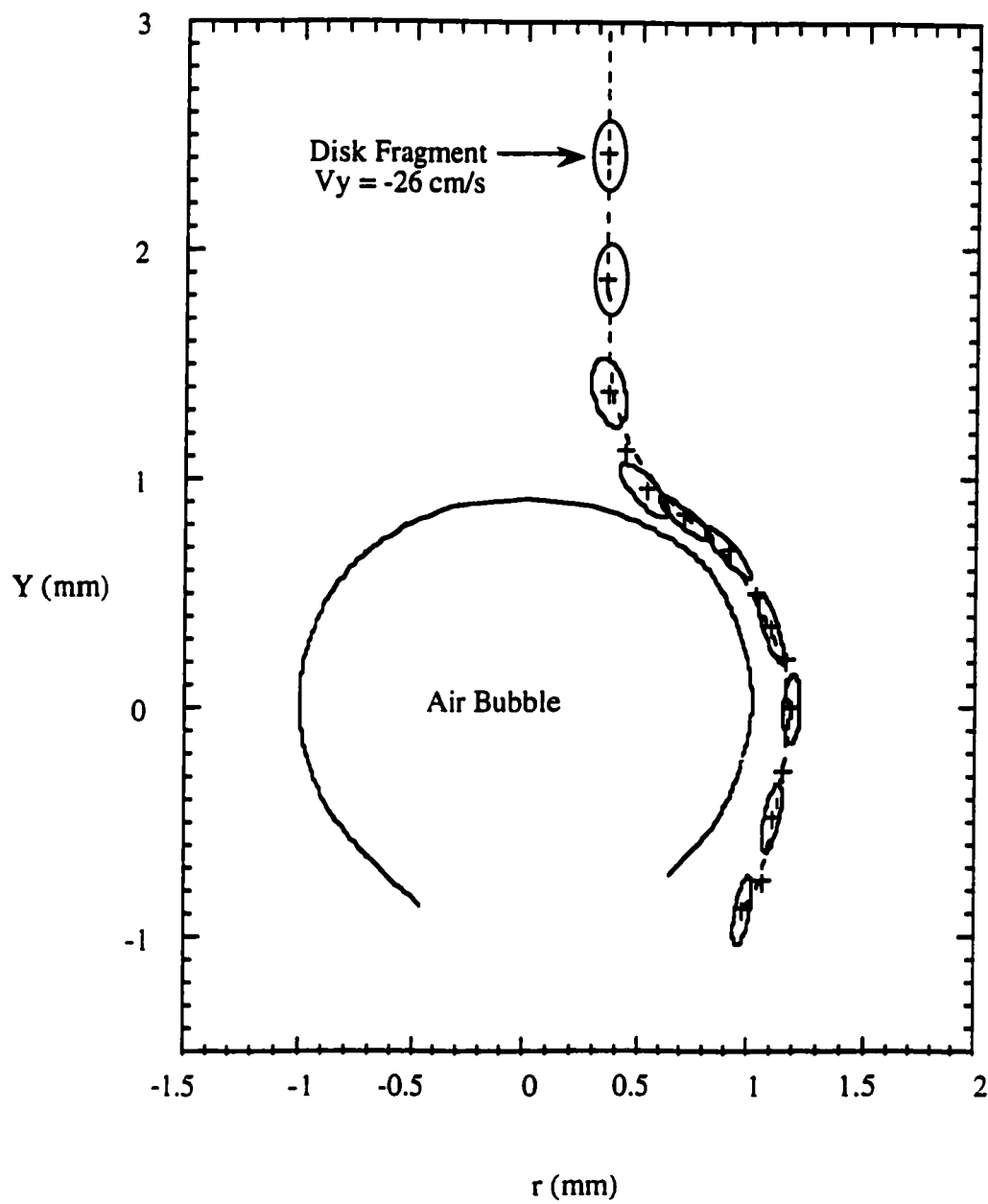


Figure 4.10 Small disk fragment, drawn to scale, flipping to side and missing bubble.

sizes. Figure 4.10 shows a small disk fragment interacting with a bubble. The fragment turned as it approached the bubble, as originally assumed, and the resulting large drainage area between it and the bubble surface hindered attachment.

A drawback of the flowtube apparatus was that disks exiting from the feed tube were always oriented vertically due to the hydrodynamics of flow within the circular feed tube. Thus, no observations of disks approaching the bubble with a horizontal orientation were made. Initial orientation is obviously an important factor in how a disk will interact with a bubble, and we would anticipate that horizontally-oriented disks might be deflected as are spheres. Disks in a typical flotation cell will have random orientations although it is possible that certain cell geometries could favor one orientation due to the hydrodynamics of the flow.

From image analysis of the flowtube observations, we were able to calculate approximate values for the collision efficiency as shown in the third column of Table 4.3. For disks, the collision efficiency was computed to be approximately 0.8, significantly greater than the range of 0.15 to 0.35 estimated for the spheres. This is because spheres are more likely to be deflected by the streamlines of flow around the bubble before they can make contact with the bubble surface.

In the single-bubble flotation apparatus, a froth is unnecessary, and turbulence is negligible. Therefore, flotation can be assumed to depend only upon the efficiency of collision and the efficiency of attachment. By dividing the overall collection efficiency, E

Table 4.3 Collision and attachment efficiencies for disks and spheres in the single bubble flotation tube.

Particles	E Single Bubble	E_c	E_a
Disks	0.07 ± 0.03	0.8	0.09
Spheres	0.4 ± 0.1	0.15 - 0.35	≈ 1.0

by E_c , the attachment efficiency, E_a , can be calculated. The result, shown in Table 4.3, was almost the reverse of that of the collision efficiencies. Almost all sphere collisions resulted in attachment, whereas only 5% of the disks attached after collision. The attachment efficiency can never be greater than one, so the collision efficiency range estimated for the spheres may be low.

Because collision and attachment efficiencies are strongly affected by even very small changes in flotation chemistry or flotation cell geometry, it is not expected that the above values will be directly applicable to other types of flotation cells. However, the qualitative behavior observed in these experiments is expected to be applicable to flotation in general.

4.5 Conclusions

Disks or plate-shaped particles do not float as well as spheres because they cannot meet the required conditions for optimum particle/bubble attachment, viz. a small drainage area linked with a prolonged contact time. Either they collide with bubbles edge-on, giving a small contact area, but also a short contact time, resulting in the particle bouncing off before attachment can occur, or they flip to the side before contact, giving a long contact time but a large drainage area which takes too long to drain and rupture for attachment to take place. This may help to explain why the flotation of toner particles from repulped slurries is often difficult to accomplish.

CHAPTER 5

A Preliminary Hydrodynamic Modeling of the Flotation of Disk-Shaped Particles⁹³

5.1 Introduction

In Chapter 4, we experimentally investigated the difference in flotation of toner disks and spheres. It was found that although disks had a higher collision efficiency with the bubble than similar-size spheres, they had a lower probability of attaching to the bubble after contact had taken place. Low attachment efficiency was due to two types of behavior: 1) disks either collided with the bubble edge-on and bounced off, failing to attach due to the very short contact time, or 2) disks rotated to the side before collision and had difficulty attaching due the large drainage area separating the disk and bubble surfaces. Disk behavior was observed to relate closely to size, with the larger disks usually exhibiting the first behavior and smaller disks and fragments the second.

The objective of the research of this chapter was to investigate computationally the role of particle shape (i.e., disk vs. sphere) and size in flotation by developing a simple hydrodynamic model of disk movement around a bubble. Disks were modeled as circular and infinitely thin. The model, in the form of a computer program, was used to conduct a parametric study of the effect of disk size and initial orientation on the efficiency of collision, attachment, and collection, and to compare these results with those computed for spheres.

5.2 Review of Theory and Literature

Of particular interest in the investigation of particle/bubble interactions is the critical initial displacement distance from the vertical bubble centerline, r_c , at which the particle and bubble will just make contact as the particle flows around the bubble. This is shown

schematically for the case of a sphere in Fig. 5.1. The initial distance between the particle and bubble in the y direction must be large enough such that any particle movement away from the centerline before reaching this starting point is negligible.

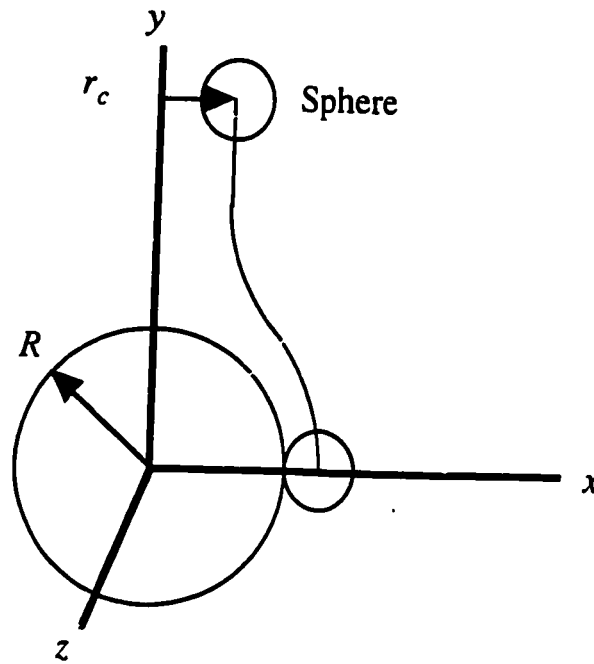


Figure 5.1 Determination of r_c for a sphere flowing around a bubble.

It is common practice to define the collision efficiency, or probability of collision, as the area within this critical displacement radius divided by the cross sectional area of the bubble:

$$E_c = \frac{\pi r_c^2}{\pi R_b^2} = \left(\frac{r_c}{R_b} \right)^2 \quad (5.1)$$

Because r_c always increases with increasing particle size, it is possible for r_c to become greater than the bubble radius, R_b , for large particles. Thus, E_c is not a true efficiency because it is possible to obtain a value greater than one.

A number of studies have been conducted which examine the collision of spherical particles with bubbles in flotation from hydrodynamic principles.^{15, 17, 19-24} In the case where inertial effects and gravity are ignored, r_c for a sphere in a known flow field generally depends only upon the ratio of the sphere radius, a , to the bubble radius, R_b . The resulting expression for r_c can be substituted into equation (1) to yield an equation for collision efficiency. For example, assuming there exists a potential flow field around a bubble and that the center of a sphere will exactly follow the streamlines of flow, the collision efficiency equation for a sphere is:¹⁵

$$E_c = 3 \frac{a}{R_b} \quad (5.2)$$

For a disk, r_c is affected by an additional variable, viz. initial disk orientation. Models to describe the flotation of disk-shaped particles have not been treated in the literature, perhaps because particles often encountered in flotation are quasi-spherical and because of the additional complications in accounting for orientation effects.

5.3 Development of Model

5.3.1 Model Assumptions

For this initial treatment, a number of simplifying assumptions are made. Bubbles are assumed to be spherical, which should hold true for rising air bubbles up to about 1 mm diameter, after which their shape begins to become flattened, i.e. oblate.⁹⁴ Initially, flow around the bubble was approximated as potential flow, which is a reasonable approximation for Reynolds numbers above 1000.⁹⁵ Rising bubbles typically have a Reynolds number value of the order of several hundred, but Flint and Howarth,²⁵ from photographic results, observed that particles still followed potential flow theory until they approached close to the bubble surface, after which large discrepancies from theory were

observed. To observe how a different flow field would affect the results, the flow around the bubble in later runs was approximated by using an empirical stream function developed by Yoon and Luttrell²² for a Reynolds number of 100, hereafter referred to as "intermediate flow".

Although flow around the bubble is easy to approximate, the flow in the immediate vicinity of a disk requires solving the Navier-Stokes equations for a particle in a non-linear flow field. Solutions to the equations of motion exist only for the simplified case of an ellipsoidal particle in linear one-dimensional irrotational flow, as given by Jeffery,⁹⁶ or two-dimensional irrotational flow, as given by van de Ven.⁹⁷ To model disk motion for our system, further simplifications were required. It was assumed that the particle density was effectively the same as that of the water, a reasonable approximation for non-magnetic toner particles, which have a density of approximately 1.15 g/cm³. Particle density neutrality implies that 1) disks do not settle due to gravity, and 2) there are no inertial effects. Thus, the model used assumed an inviscid flow, with the flow in the fluid perfectly transferred to the disk.

5.3.2 *Development of General Equations*

From the above suppositions, the force exerted on any point of a rigid, 2-dimensional disk is directly proportional to the difference between the velocity of that point, \mathbf{u} , and the velocity that the fluid would have at that point if that disk were not present, \mathbf{v} . The total force experienced by the disk is the summation of all forces across the disk surface:

$$\mathbf{F} = \int k(\mathbf{v} - \mathbf{u}) dA \quad (5.3)$$

where k is an arbitrary constant with units of mass per unit time. The torque about the origin is similarly approximated as:

$$\mathbf{T} = \int \mathbf{r} \times k(\mathbf{v} - \mathbf{u}) dA \quad (5.4)$$

where \mathbf{r} is a position vector that describes the distance and direction of a point from the disk origin. The velocity of a point on the disk is defined by the disk velocity at the origin, \mathbf{U} , and the angular velocity about the origin, $\boldsymbol{\omega}$:

$$\mathbf{u} = \mathbf{U} + \boldsymbol{\omega} \times \mathbf{r} \quad (5.5)$$

Because inertial effects are ignored, the disk instantaneously assumes a translational and angular velocity such that the force and torque go to zero. From equations (5.3) - (5.5):

$$\mathbf{F} = \int k(\mathbf{v} - \mathbf{U} - \boldsymbol{\omega} \times \mathbf{r}) dA = \mathbf{0} \quad (5.6)$$

$$\mathbf{T} = \int \mathbf{r} \times k(\mathbf{v} - \mathbf{U} - \boldsymbol{\omega} \times \mathbf{r}) dA = \mathbf{0} \quad (5.7)$$

Expanding equation (5.7):

$$\begin{aligned} & k \int (\mathbf{r} \times \mathbf{v} - \mathbf{r} \times \mathbf{U} - \mathbf{r} \times (\boldsymbol{\omega} \times \mathbf{r})) dA \\ &= k \int (\mathbf{r} \times \mathbf{v} - \mathbf{r} \times \mathbf{U} - \boldsymbol{\omega}(\mathbf{r} \cdot \mathbf{r}) + \mathbf{r}(\mathbf{r} \cdot \boldsymbol{\omega})) dA = \mathbf{0} \end{aligned} \quad (5.8)$$

By symmetry arguments, $\mathbf{r} \times \mathbf{U}$ and $\mathbf{r}(\mathbf{r} \cdot \boldsymbol{\omega})$ cancel out in the integral. Because $\boldsymbol{\omega}$ is a constant, it is moved in front of the integral. Dividing by k , separating and rearranging results in:

$$\boldsymbol{\omega} = \frac{\int \mathbf{r} \times \mathbf{v} dA}{\int \mathbf{r} \cdot \mathbf{r} dA} \quad (5.9)$$

Expanding equation (5.6), dividing out k , and moving \mathbf{U} out of the integral yields:

$$\mathbf{U} = \frac{\int (\mathbf{v} - \boldsymbol{\omega} \times \mathbf{r}) dA}{\int dA} \quad (5.10)$$

Solving the integrals contained in equations (5.9) and (5.10) is simplified if the variables are expressed in a convenient coordinate system, such as polar coordinates.

5.3.3 Disk in Particle-Fixed Coordinates

A disk in particle-fixed coordinates (x', y', z') , is defined as

$$x'^2 + y'^2 = a^2, \quad z' = 0 \quad (5.11)$$

where a is the disk radius and the disk center is at the axis origin. Any point on the disk can also be easily described in polar coordinates, r and θ , and the transformation from polar to Cartesian particle-fixed coordinates is

$$x' = r \cos \theta, \quad y' = r \sin \theta, \quad z' = 0 \quad (5.12)$$

where $0 \leq r \leq a$ and $0 \leq \theta < 2\pi$.

5.3.4 Disk in Fixed-Space Coordinates

The position of a disk in space is described by the location of its origin, O , which has three components, O_x , O_y , and O_z . The orientation of a disk is described by the rotation of the particle-fixed coordinate system from the fixed-space system. This is represented by the orientation of the axis of revolution, z' , which is described by two polar angles, α and β , where α is the angle formed between z' and the fixed-space z axis, and β is the angle formed between the projection of z' onto the fixed-space xy plane and the fixed-space x axis, as shown in Fig. 5.2. For a given disk position and orientation, any point on the disk can be described by the polar coordinate variables, r and θ , the position of

the disk origin, O_x , O_y , and O_z , and the two rotation angles, α and β . The transformation into fixed-space coordinates, (x, y, z) , results in:⁹⁷

$$x = r \cos \theta \cos \alpha \cos \beta - r \sin \theta \sin \beta + O_x \quad (5.13)$$

$$y = r \cos \theta \cos \alpha \sin \beta + r \sin \theta \cos \beta + O_y \quad (5.14)$$

$$z = -r \cos \theta \sin \alpha + O_z \quad (5.15)$$

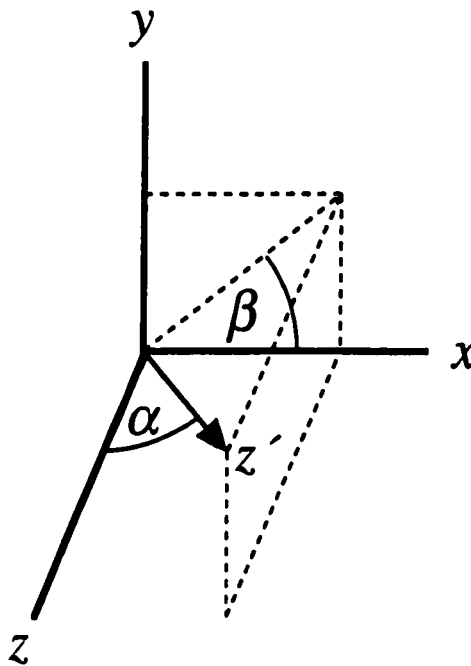


Figure 5.2 The orientation of the axis of revolution, z' , is described by two polar angles, α and β , where α is the angle formed between z' and the fixed-space z axis, and β is the angle formed between the projection of z' onto the fixed-space xy plane and the fixed-space x axis.

5.3.5 Equations for Angular Velocity

Solving equation (5.9) in terms of polar coordinates and breaking it up into ω_x , ω_y , and ω_z , results in the following:

$$\omega_x = \frac{2}{\pi a^4} \int_0^{2\pi} \int_0^a (r_y v_z - r_z v_y) r dr d\theta \quad (5.16)$$

$$\omega_y = \frac{2}{\pi a^4} \int_0^{2\pi} \int_0^a (r_z v_x - r_x v_z) r dr d\theta \quad (5.17)$$

$$\omega_z = \frac{2}{\pi a^4} \int_0^{2\pi} \int_0^a (r_x v_y - r_y v_x) r dr d\theta \quad (5.18)$$

The fluid velocity, v , is defined by the potential flow equations for flow around a sphere, where the sphere, (i.e. bubble) is centered at the axis origin.

$$v_x = v_\infty R_b^3 \frac{3xy}{2(x^2 + y^2 + z^2)^{5/2}} \quad (5.19)$$

$$v_y = -v_\infty \left(1 - R_b^3 \frac{2y^2 - x^2 - z^2}{2(x^2 + y^2 + z^2)^{5/2}} \right) \quad (5.20)$$

$$v_z = v_\infty R_b^3 \frac{3zy}{2(x^2 + y^2 + z^2)^{5/2}} \quad (5.21)$$

In these equations, v_∞ is the undisturbed fluid velocity far away from the bubble surface.

Substituting equations (5.13) - (5.15) into equations (5.19) - (5.21) gives the fluid velocity in terms of polar coordinates. The position vector, \mathbf{r} , of any point on the disk can also be expressed in polar coordinates.

$$r_x = x - O_x = r \cos \theta \cos \alpha \cos \beta - r \sin \theta \sin \beta \quad (5.22)$$

$$r_y = y - O_y = r \cos \theta \cos \alpha \sin \beta + r \sin \theta \cos \beta \quad (5.23)$$

$$r_z = z - O_z = -r \cos \theta \sin \alpha \quad (5.24)$$

Substitution of equations (5.19) - (5.24) into equations (5.16) - (5.18) results in integrals which can be numerically solved given constant values for α , β , O_x , O_y , O_z , R_b , V_∞ , and a .

5.3.6 Equations for Translational Velocity

From equation (5.10), U can also be expressed in terms of polar coordinates and broken up into U_x , U_y , and U_z :

$$U_x = \frac{1}{\pi a^2} \int_0^{2\pi} \int_0^a (v_x - \omega_y r_z + \omega_z r_y) r dr d\theta \quad (5.25)$$

$$U_y = \frac{1}{\pi a^2} \int_0^{2\pi} \int_0^a (v_y - \omega_z r_x + \omega_x r_z) r dr d\theta \quad (5.26)$$

$$U_z = \frac{1}{\pi a^2} \int_0^{2\pi} \int_0^a (v_z - \omega_x r_y + \omega_y r_x) r dr d\theta \quad (5.27)$$

The variables within the integral are defined in equations (5.16) - (5.24) and these integrals can also be solved numerically if α , β , O_x , O_y , O_z , R_b , V_∞ , and a are known. The integrals above and the integrals for angular velocity were solved using a Romberg integration algorithm and Simpson's rule,⁹⁸ as explained in Appendix A.

5.3.7 Solving the Ordinary Differential Equations

The purpose of the model was to follow the change in disk position (O_x , O_y , and O_z) and orientation (α and β) with respect to time (t) given an initial position (O_{x0} , O_{y0} , and O_{z0}) and orientation (α_0 and β_0) and known values for a , R_b , and V_∞ . The five dependent variables can be expressed as linked ordinary differential equations:

$$\frac{dO_x}{dt} = U_x \quad (5.28)$$

$$\frac{dO_y}{dt} = U_y \quad (5.29)$$

$$\frac{dO_z}{dt} = U_z \quad (5.30)$$

$$\frac{d\alpha}{dt} = \omega_y \cos \beta - \omega_x \sin \beta \quad (5.31)$$

$$\frac{d\beta}{dt} = \omega_z - \frac{\omega_x \cos \beta + \omega_y \sin \beta}{\tan \alpha} \quad (5.32)$$

These equations were solved with a Fortran computer program using the classical fourth-order Runge-Kutta method.⁹⁸ The Fortran code and a description of the program are found in Appendix A.

5.4 Results and Comparison to Experiment

Using the potential flow equations, the model predicted the same general disk behavior as observed experimentally. Figure 5.3 compares the movement of an actual disk to movement as predicted from the model for disks with the same starting position, starting orientation, and size. Similar to the experimental run, the model predicted only a small deflection before the disk collided edge-on with the bubble.

More difficult to model was the case in which the disk turned to its side as it approached the bubble. A comparison of the predicted movement using the potential flow equations compared to actual observed motion is shown in Fig. 5.4. The model underestimates the degree of disk turning and deflection. This is probably due to two reasons: 1) the failure of the potential flow equations to accurately predict the flow streams close to the bubble surface, and 2) the model's neglect of lubrication forces that come into play as the disk closely approaches the bubble surface.⁹⁹ However, the general motion

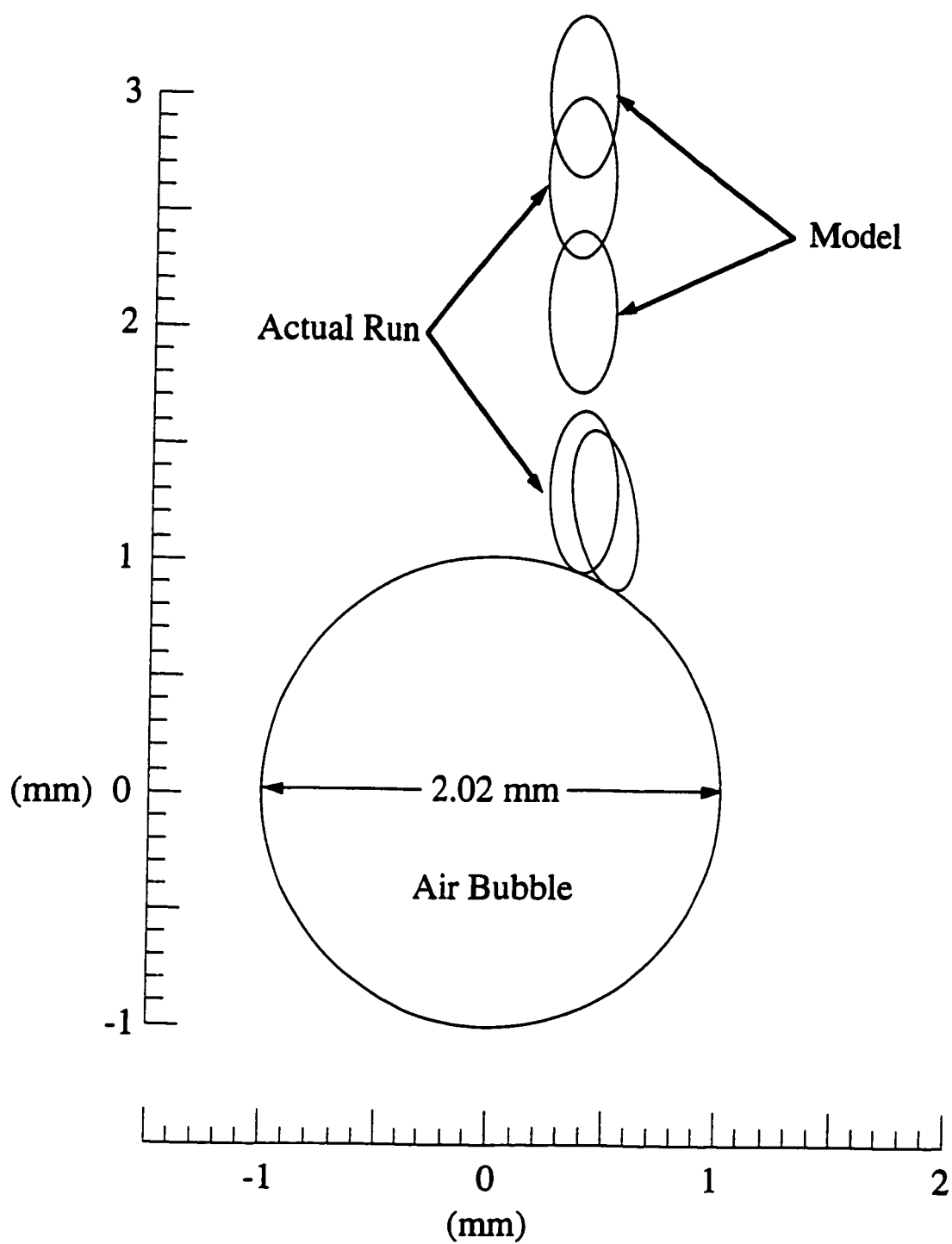


Figure 5.3 Movement of a large disk as observed from an experimental run and as predicted by the current model using the potential flow equations.

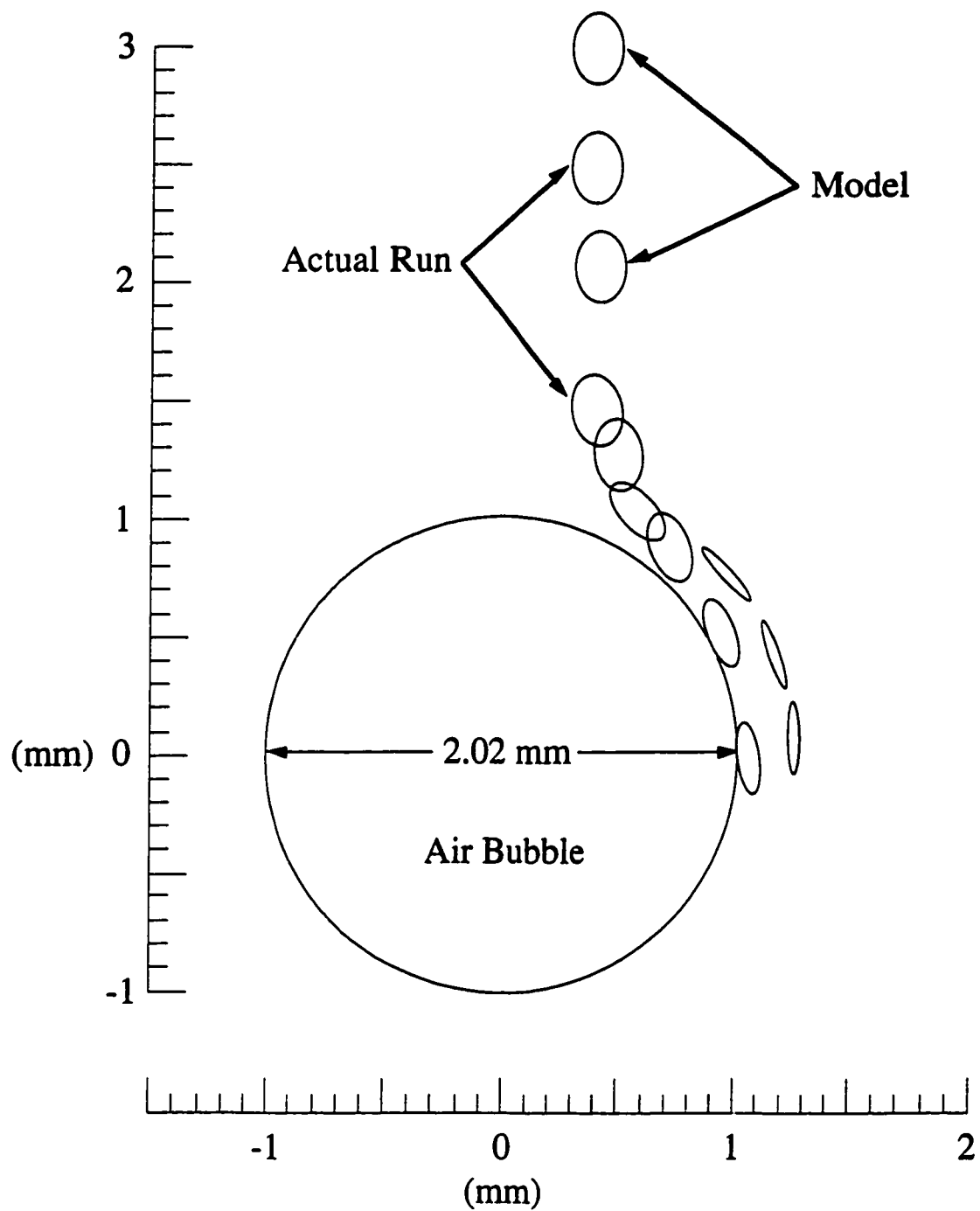


Figure 5.4 Disk movement as observed from an experimental run and as predicted by the current model using the potential flow equations.

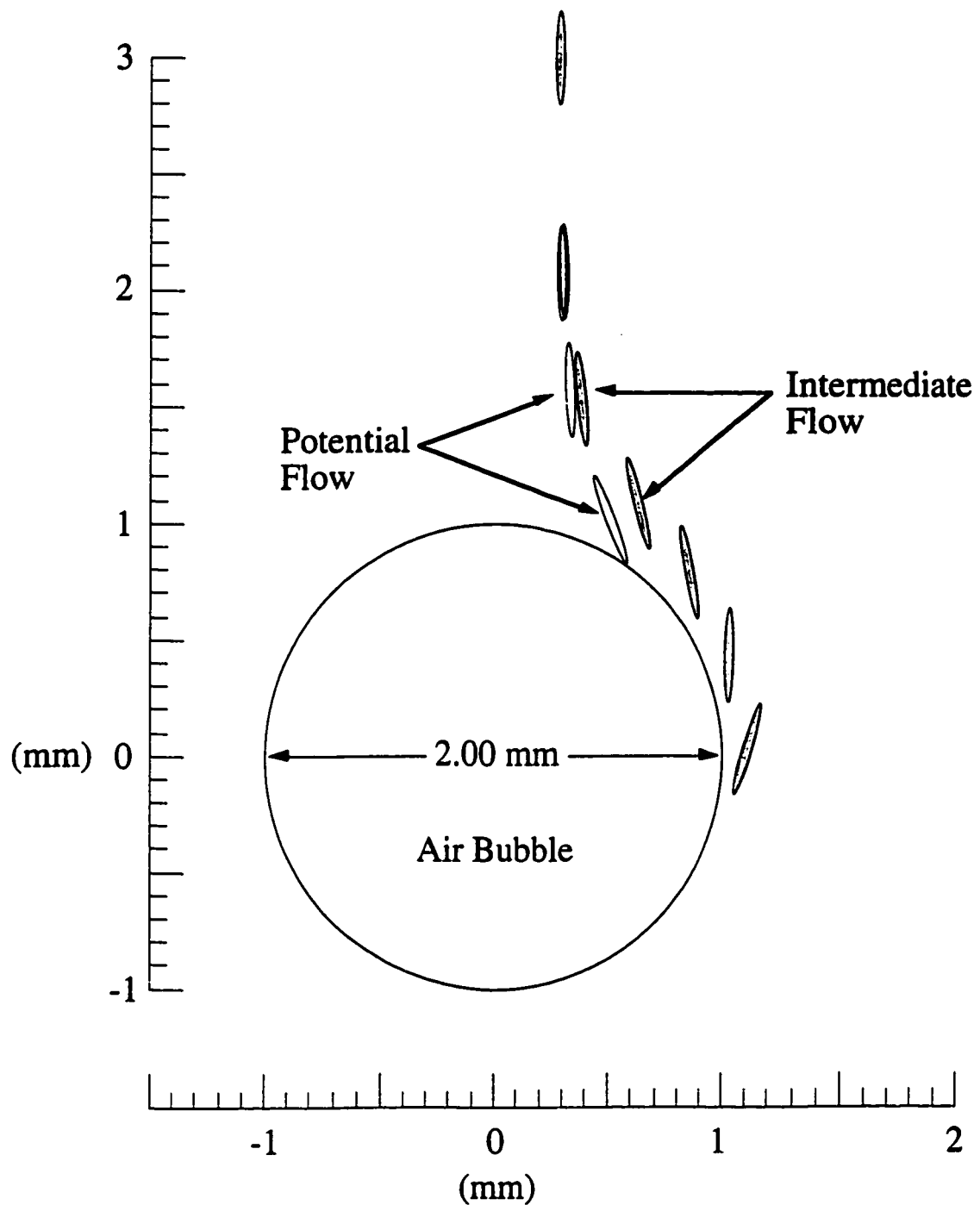


Figure 5.5 Predicted disk movement using the potential flow equations compared to using the intermediate flow equations.

predicted by the model is qualitatively similar to experiment, and thus the use of the model to conduct a parametric study of disk behavior should be valid.

Whereas the fluid velocity at the bubble surface in potential flow is at a maximum, the empirical stream function for intermediate flow guarantees that the surface velocity will be zero. How this affected disk motion is illustrated in Fig. 5.5. The disk in intermediate flow has a greater deflection from the bubble centerline and undergoes more clockwise rotation than the disk in potential flow. The greater deflection decreases collision efficiency, while the increased rotation leads to more collisions along the disk side than was seen in potential flow.

Surprisingly, the potential flow equations predicted movement closer to what was seen experimentally for large disks than the intermediate stream function. This may be because the disk inertia, unaccounted for in the model, balances out with the no-slip boundary condition that exists near the bubble surface and which is partially taken into account with the intermediate flow equations. It is expected that the intermediate stream function will be more accurate for smaller disk sizes.

5.4.1 *The Effect of Initial Orientation on Collision Efficiency*

Because the flow is cylindrically symmetric around the bubble, it was necessary only to examine disk motion in one plane that intersects the vertical bubble centerline. The xy plane was chosen for convenience, so for all disks, the initial values of O_z , i.e., O_{z0} , were taken to be zero.

There are three principal disk orientations. The first is when the plane of the disk passes through the vertical bubble centerline (or y axis) as shown in Fig. 5.6. In the xy plane, this is the case when $\alpha = 0^\circ$. The second orientation is when the disk is parallel to the flow, and its normal is perpendicular to the vertical bubble centerline as shown in Fig. 5.7. In the xy plane, this corresponds to $\alpha = 90^\circ$, $\beta = 0^\circ$. In the third orientation, the plane

of the disk is perpendicular to the direction of flow, as shown in Fig. 5.8. In this case, $\alpha = 90^\circ$, $\beta = 90^\circ$.

As mentioned previously, the initial orientation of a disk-shaped particle greatly affects the critical initial displacement distance, r_c . Figure 5.9 shows how r_c varies with changes in initial orientation for a fixed disk and bubble size ratio using the equations for potential flow. The largest r_c/R_b value, 0.95, is observed when $\alpha_0 = 0^\circ$ while the smallest r_c/R_b value, 0.38, is observed when $\alpha_0 = 90^\circ$, $\beta_0 = 0^\circ$.

Similar trends were predicted for the same disk/bubble radius ratio using the equations for intermediate flow as shown in Fig. 5.10. The largest r_c/R_b value, 0.69, is again observed when $\alpha_0 = 0^\circ$. However, the maximum and minimum peaks for $\alpha_0 > 0^\circ$ have shifted to the right, and now the minimum r_c/R_b value is closer to the orientation of $\alpha_0 = 90^\circ$, $\beta_0 = 45^\circ$.

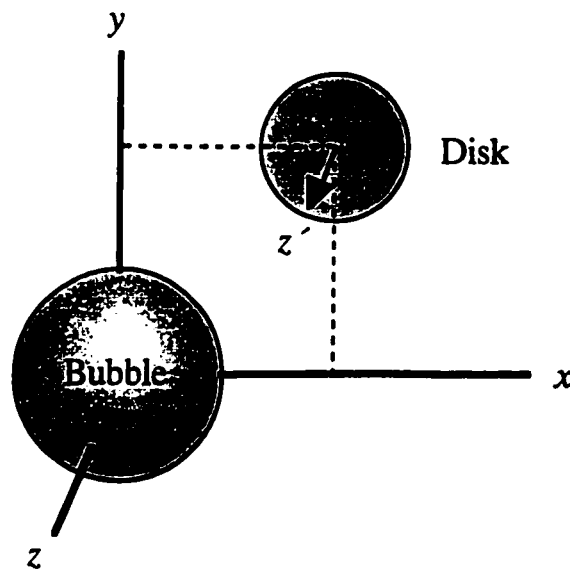


Figure 5.6 Disk orientation in xy plane for $\alpha = 0^\circ$.

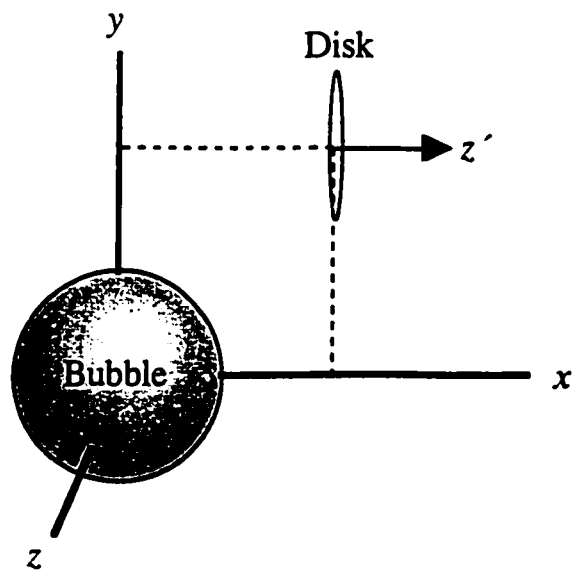


Figure 5.7 Disk orientation in xy plane for $\alpha = 90^\circ$, $\beta = 0^\circ$.

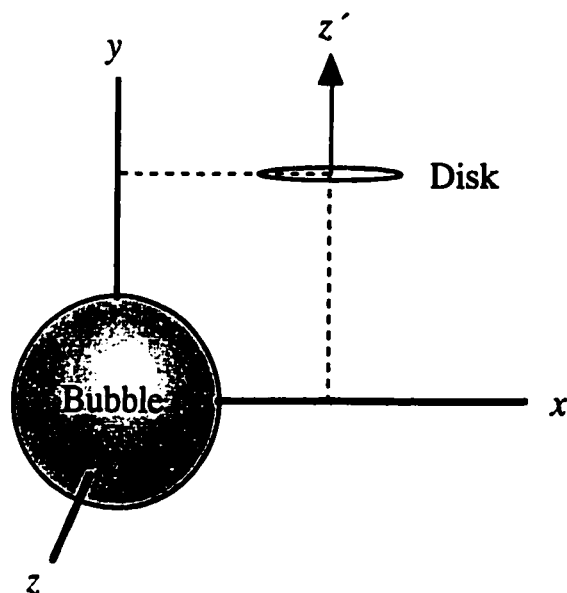


Figure 5.8 Disk orientation in xy plane for $\alpha = 90^\circ$, $\beta = 90^\circ$.

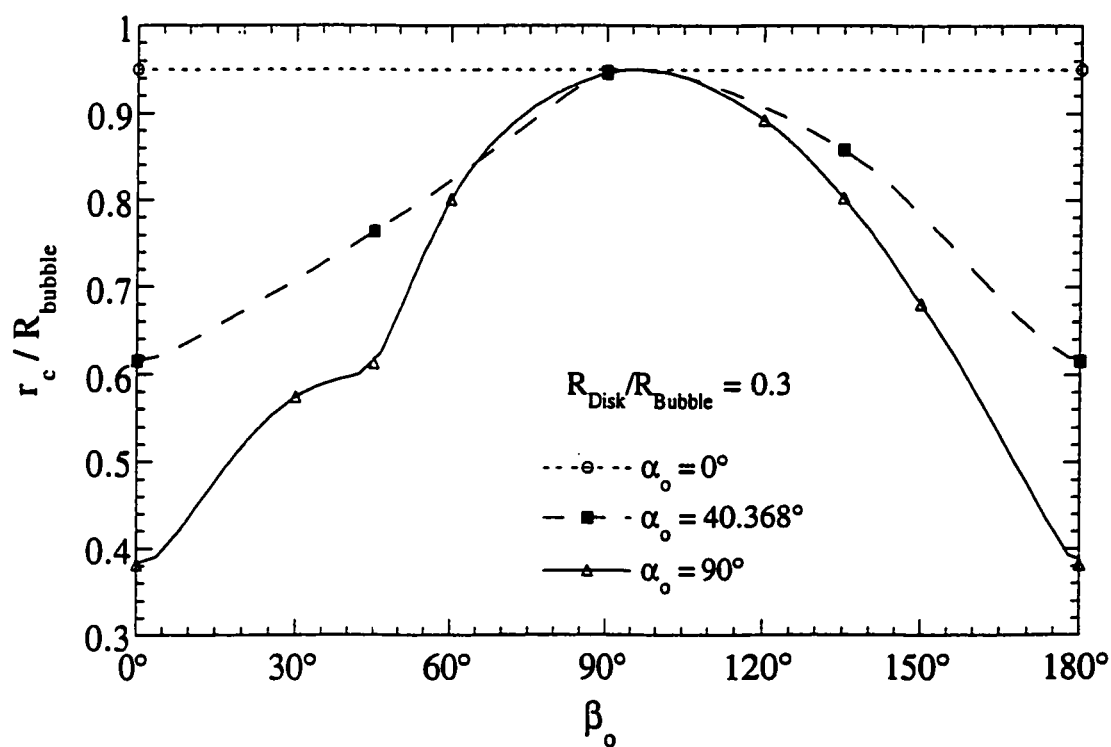


Figure 5.9 Dependence of r_c on initial disk orientation for a disk/bubble radius ratio of 0.3 as predicted using equations for potential flow.

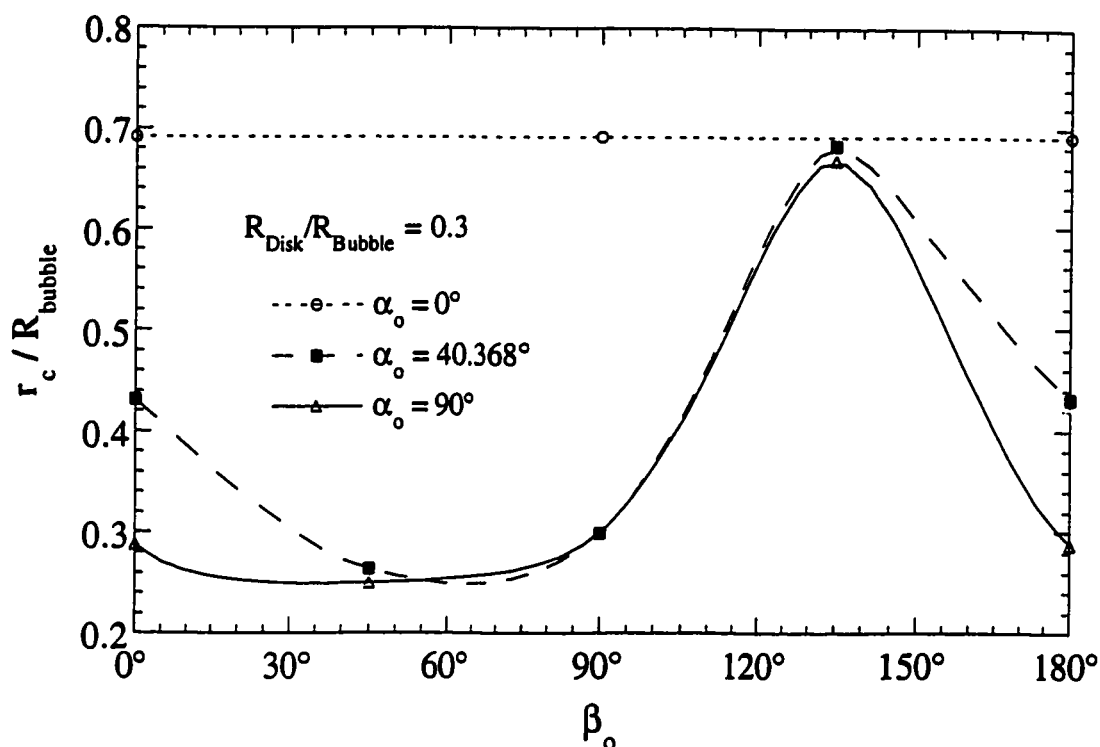


Figure 5.10 Dependence of r_c on initial disk orientation for a disk/bubble radius ratio of 0.3 as predicted using equations for intermediate flow.

The efficiency of collision at a given initial disk orientation for a given disk-to-bubble radius ratio is obtained by squaring r_c/R_b . It was assumed that disks have an equal probability of beginning at any given initial orientation, a good assumption for flotation where particles are constantly being mixed. The net efficiency of collision, E_c , of the disk was calculated by averaging the collision efficiencies over a range of equally spaced orientations for the same disk-to-bubble radius ratio. Similar to the sphere E_c , the disk E_c was dependent only upon the size of the disk, the size of the bubble, and the flow profile assumed to exist around the bubble.

Figures 5.11 and 5.12 compare the collision efficiencies of a sphere and a disk using the potential flow and intermediate flow equations. In comparing spheres and disks of the same *radius*, the sphere always has a higher collision efficiency than the disk.

However, the reverse is usually true when comparing disks and spheres of similar *volume*. Volume comparisons are highly dependent upon the disk aspect ratio, defined as the diameter divided by the thickness. An equivalent sphere was defined as one with the same volume as a disk computed on the basis of an aspect ratio of 40, which was a typical value for the experimental runs.

Both graphs are consistent with experimental results: large disks always have a higher probability of collision than equivalent spheres. For example, assuming potential flow, a disk of radius 300 μm and width 15 μm approaching a 1 mm-radius bubble will have a collision efficiency of 0.6, about twice the collision efficiency of a similar volume, 100 μm -radius sphere. Assuming intermediate flow, the same size disk will have a collision efficiency of 0.19, 2.7 times as large as the collision efficiency of 0.070 for the sphere.

Calculations using the curve fits of collision efficiency for potential flow, as plotted in Fig. 5.11, show that even very small disks have a higher collision efficiency than equivalent spheres. However, similar calculations for intermediate flow show that disks only have a higher collision efficiency when the disk-to-bubble radius ratio is greater than 0.14. It is expected that the intermediate flow prediction is more realistic.

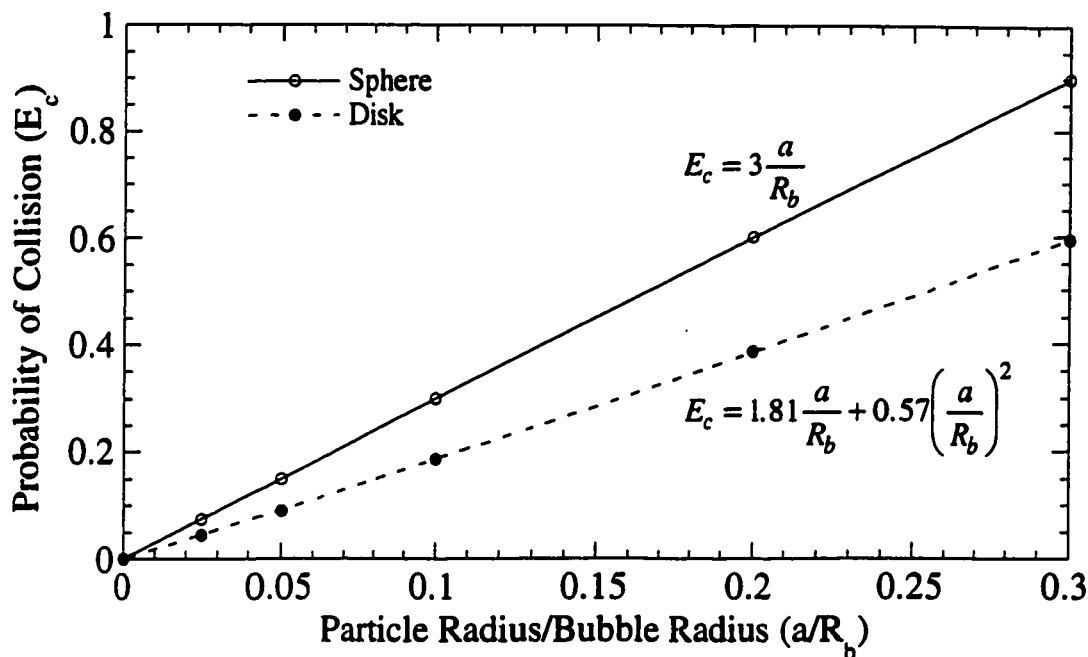


Figure 5.11 Comparison of disk and sphere collision efficiencies in potential flow.

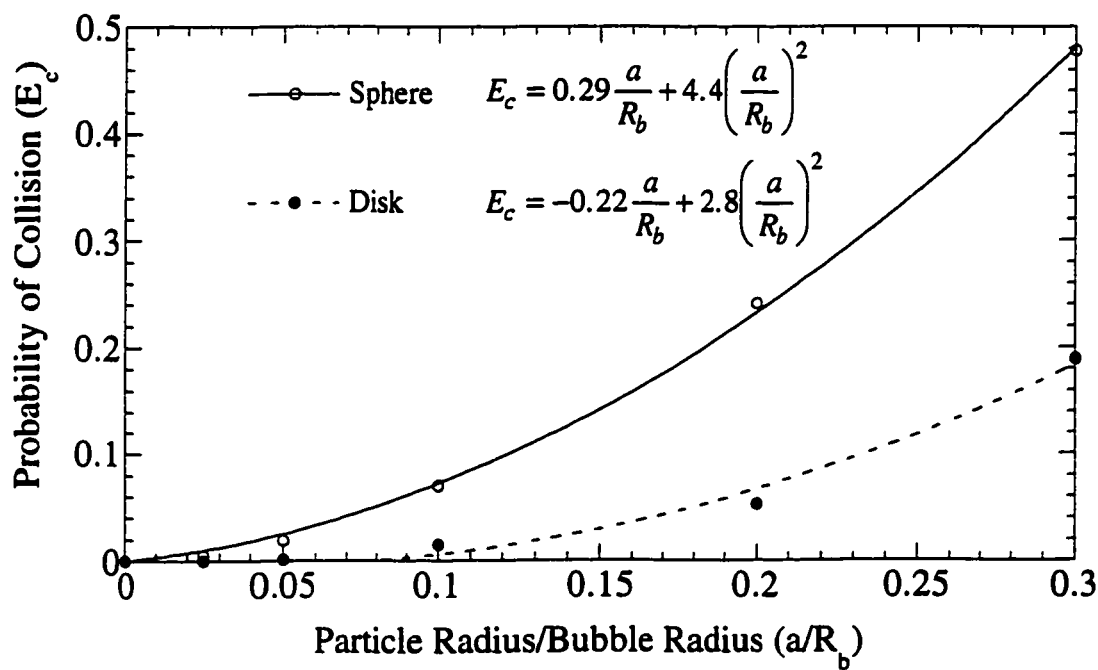


Figure 5.12 Comparison of disk and sphere collision efficiencies in intermediate flow.

5.4.2 *The Effect of Initial Orientation on Attachment Efficiency*

Attachment of a particle to a bubble after collision depends upon the time of contact between the particle and bubble surface and the time for film drainage and rupture, also called induction time. In Chapter 4, it was observed that disk-shaped toner particles that collide at high velocity bounce off the bubble surface and have little chance of attaching. Such an effect has been observed with more spherically-shaped particles in other experimental observations,⁸⁹⁻⁹¹ but while spherical particles tend to contact the bubble several times after the initial collision, disks almost never contact the bubble a second time due to rotation of the disk during the bounce. Such an inverse relationship between velocity and attachment efficiency is not uncommon, having also been seen for the collection of solid particles with liquid drops.¹⁰⁰

Although the model cannot predict disk motion after contact, disk velocities at the time of contact can be calculated and comparisons made. The velocity of the particle at the point of contact can be broken up into radial and tangential components. Of particular interest is the contact radial velocity. The higher the contact radial velocity, the more likely the particle will bounce off the bubble, and the lower the probability of attachment.

For a sphere, the contact radial velocity depends upon the magnitude of the ratio of the sphere radius to the bubble radius, the initial position of the sphere, and the velocity of the undisturbed fluid flow. For a disk, the contact radial velocity also depends upon the initial orientation. For all of the following results, the velocity of the undisturbed flow was taken as 200 mm/s, which is the bubble rise velocity of a bubble 1 to 2 mm in diameter.¹⁰¹

Figure 5.13 shows how the contact radial velocity ($-U_{rc}$) varies with initial position and disk size for a disk in potential flow and with an initial orientation corresponding to $\alpha_0 = 0^\circ$. Because of the symmetry of the flow, the disk maintains the $\alpha = 0^\circ$ orientation until contact with the bubble. This gives the disk an almost identical behavior to that of a

similar-radius sphere, and so results for a disk with this orientation were also taken to be the expected movement of a sphere under similar flow conditions.

Similar trends for this orientation were seen when using the equations for intermediate flow as shown in Fig. 5.14. In both cases, $-U_{rc}$ decreases as r_c/R_b increases although in the intermediate flow the rate of $-U_{rc}$ decrease is faster. The decrease in $-U_{rc}$ with decreasing disk size is also greater in intermediate flow.

Figures 5.15 and 5.16 compare the potential flow and intermediate flow cases for an initial disk orientation of $\alpha_0 = 90^\circ$, $\beta_0 = 0^\circ$. Both show a decrease in $-U_{rc}$ as r_c/R_b increases for the larger disk sizes. For smaller disks in potential flow, a minimum in $-U_{rc}$ is observed, which corresponds to where the contact point shifts from the front edge of the disk to the back edge. Thus, at the minimum point, the disk is contacting the bubble along the disk side.

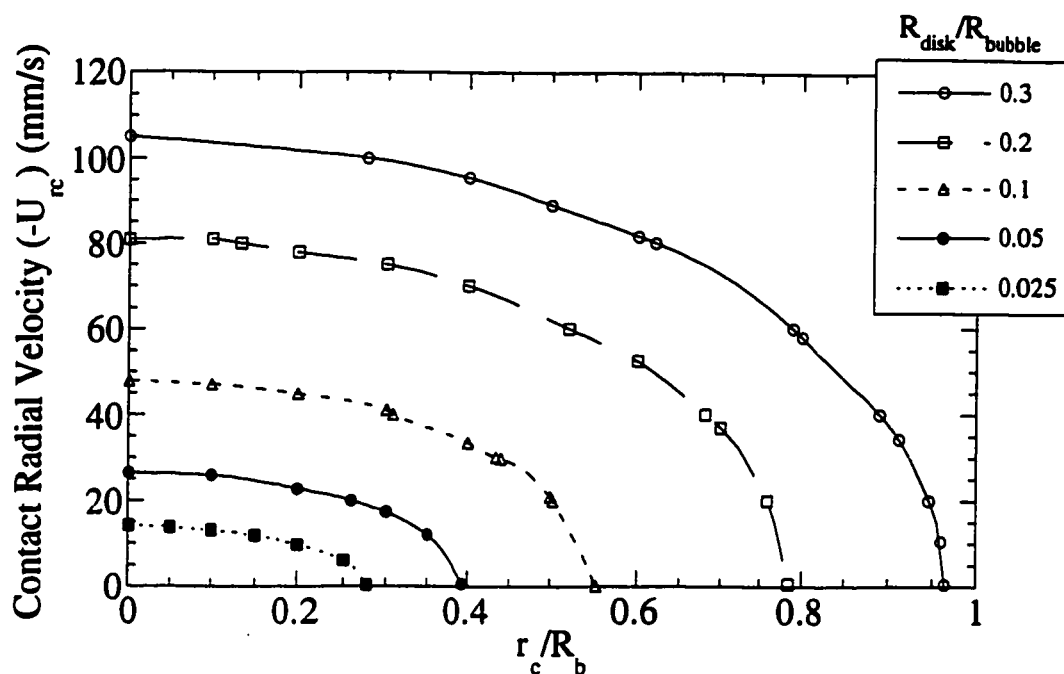


Figure 5.13 Contact radial velocity of a disk in potential flow with an initial orientation of $\alpha_0 = 0^\circ$ and an undisturbed fluid velocity of 200 mm/s.

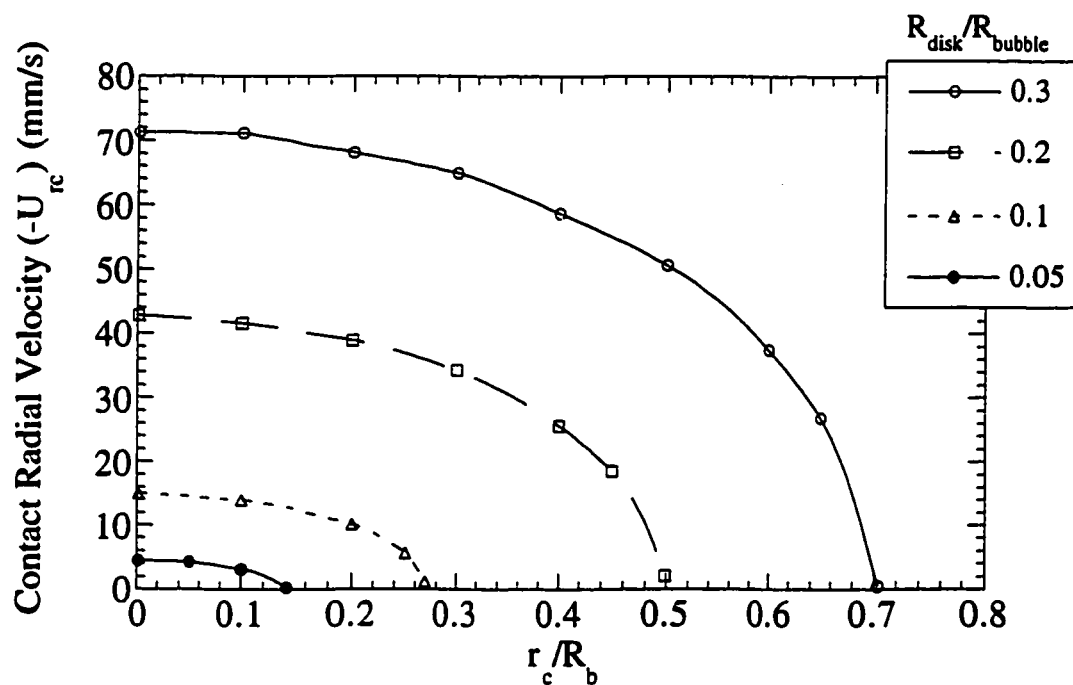


Figure 5.14 Contact radial velocity of a disk in intermediate flow with an initial orientation of $\alpha_0 = 0^\circ$ and an undisturbed fluid velocity of 200 mm/s.

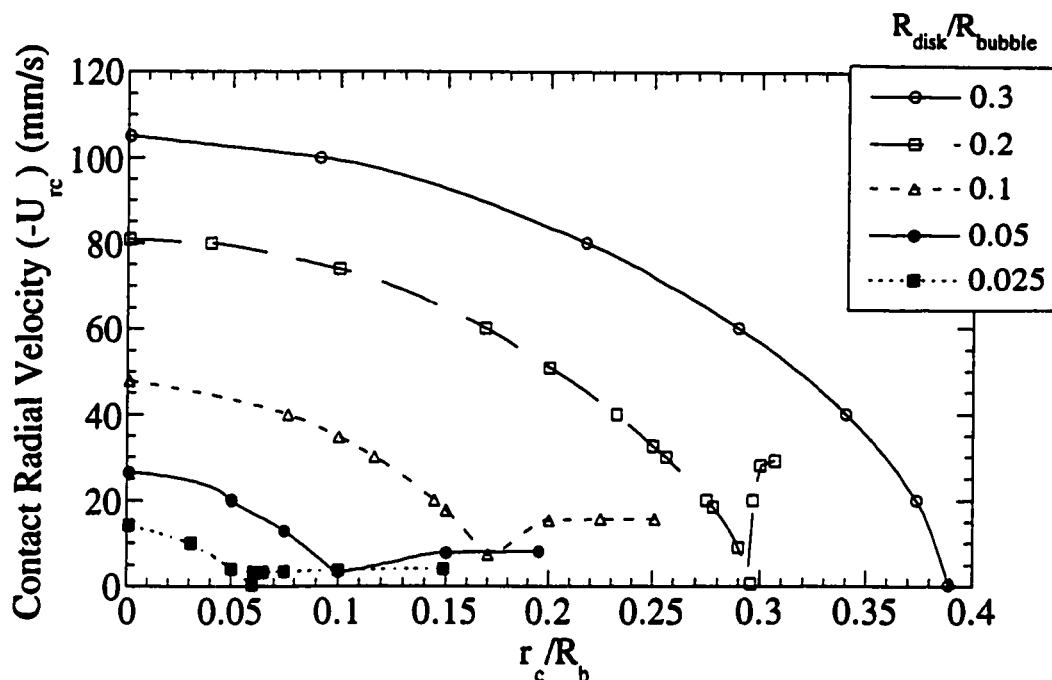


Figure 5.15 Contact radial velocity of a disk in potential flow with an initial orientation of $\alpha_0 = 90^\circ$, $\beta_0 = 0^\circ$, and an undisturbed fluid velocity of 200 mm/s.

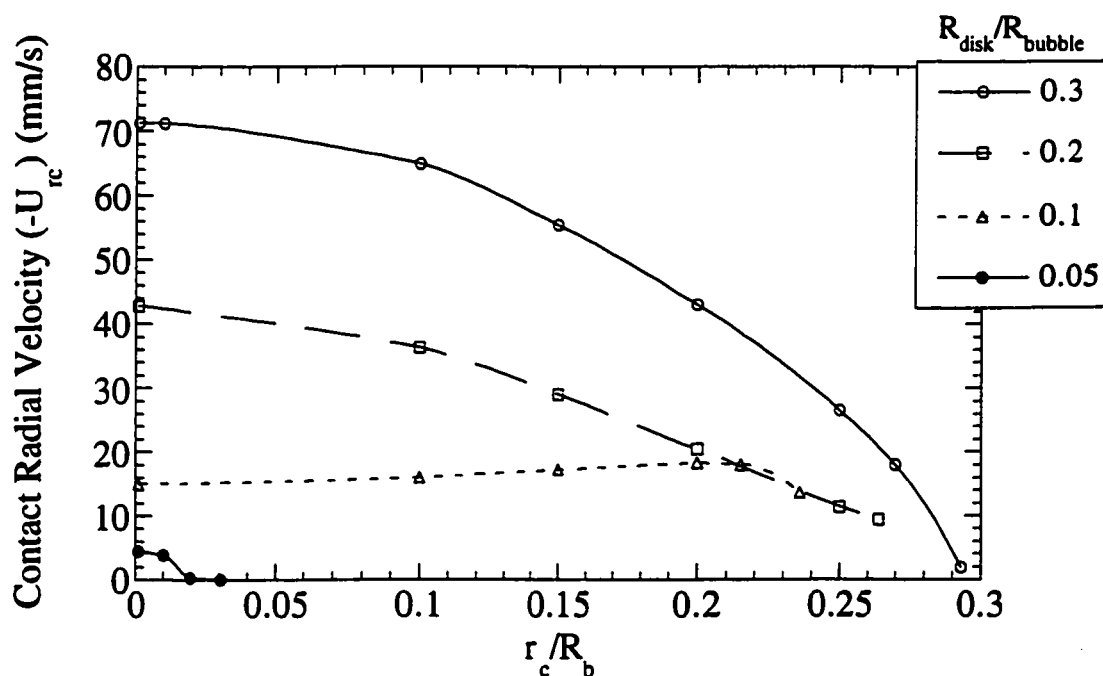


Figure 5.16 Contact radial velocity of a disk in intermediate flow with an initial orientation of $\alpha_0 = 90^\circ$, $\beta_0 = 0^\circ$, and an undisturbed fluid velocity of 200 mm/s.

Figures 5.17 and 5.18 compare the potential flow and intermediate flow cases for an initial disk orientation of $\alpha_o = 90^\circ$, $\beta_o = 90^\circ$. They follow similar trends, but the contact radial velocity predicted for intermediate flow at this orientation is an order of magnitude less than that predicted for potential flow. Although the contact radial velocity is very low, it is difficult to say whether the adhesion efficiency will be close to 100% for the intermediate flow case. This is because almost all collisions at this orientation in intermediate flow are against the disk side rather than at the disk edge. This will result in a larger drainage area which may increase the induction time and interfere with flotation.

Other orientations tend to be a combination of what was seen for the three primary orientations. For example, Fig. 5.19 shows a disk with an initial orientation of $\alpha_o = 40.368^\circ$, $\beta_o = 45^\circ$ in potential flow.

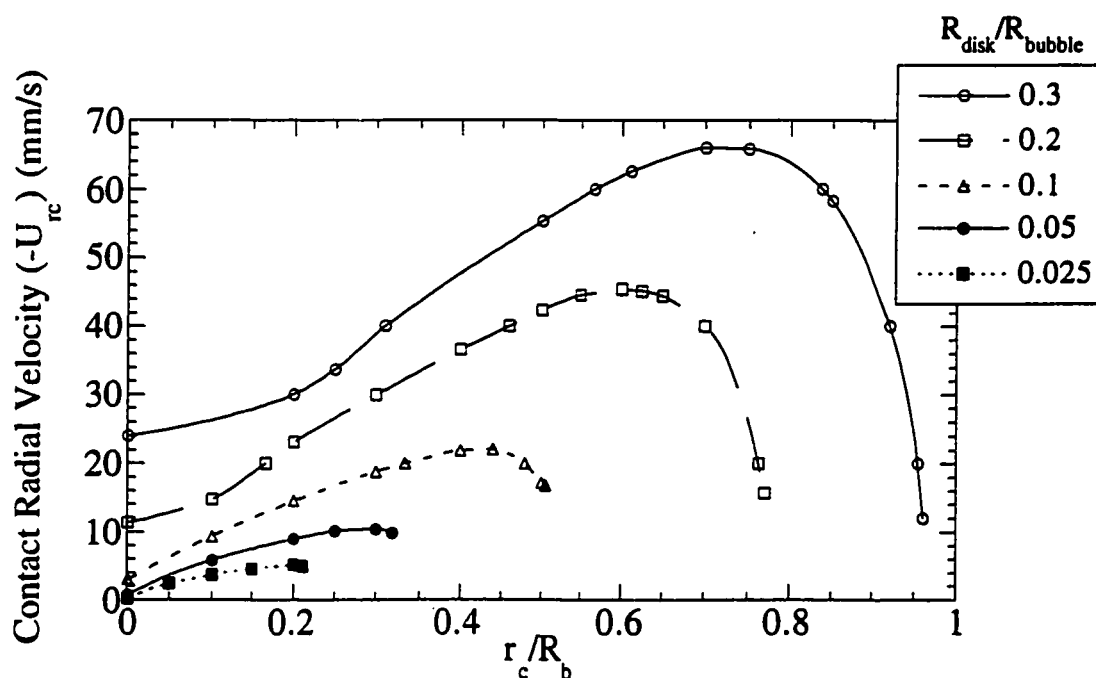


Figure 5.17 Contact radial velocity of a disk in potential flow with an initial orientation of $\alpha_o = 90^\circ$, $\beta_o = 90^\circ$, and an undisturbed fluid velocity of 200 mm/s.

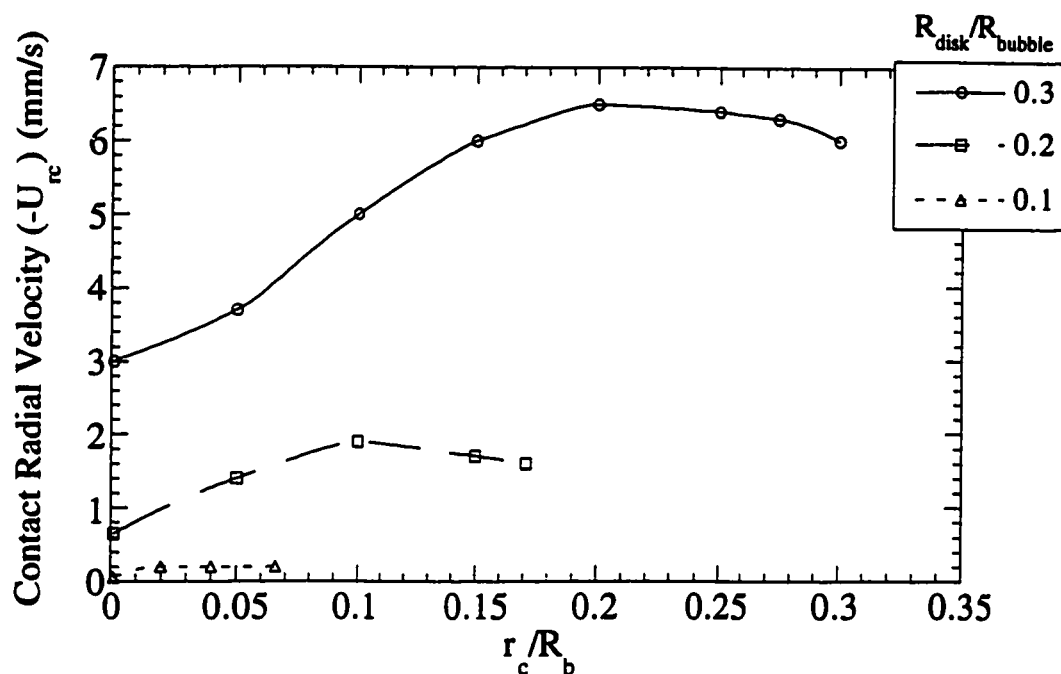


Figure 5.18 Contact radial velocity of a disk in intermediate flow with an initial orientation of $\alpha_0 = 90^\circ$, $\beta_0 = 90^\circ$, and an undisturbed fluid velocity of 200 mm/s.

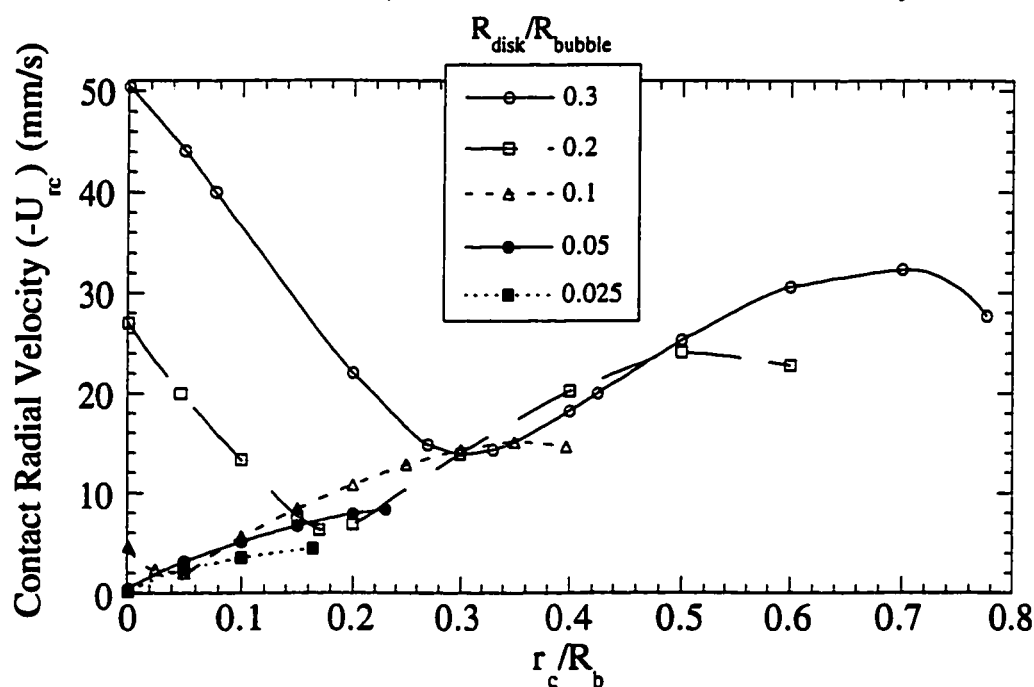


Figure 5.19 Contact radial velocity of a disk in potential flow with an initial orientation of $\alpha_0 = 40.368^\circ$, $\beta_0 = 45^\circ$, and an undisturbed fluid velocity of 200 mm/s.

As noted above, it can be assumed that the radial contact velocity of a sphere will be described by Fig. 5.13 for potential flow. Using the results of this graph, a collision efficiency for a given range of contact radial velocities can be calculated. For example, the sphere collision efficiency for an r_c/R_b ratio of 0.1 that will result in a contact radial velocity between 20 and 40 mm/s would be:

$$E_c = \left(\frac{r_c}{R_b} \right)_{\text{at } -U_{rc}=20}^2 - \left(\frac{r_c}{R_b} \right)_{\text{at } -U_{rc}=40}^2 = 0.153 \quad (5.33)$$

Calculations were performed for a variety of points and the results are plotted in Fig. 5.20. As expected, larger spheres are seen to have a higher probability of colliding with the bubble at higher contact radial velocities.

A similar graph was constructed for a disk by averaging the collision efficiency for a given $-U_{rc}$ range over a large number of equally spaced orientations. The result for potential flow is shown in Fig. 5.21.

The exact contact radial velocity required for adhesion is not known, but it is known from experimental observation that higher velocities result in no attachment. Consider the 300 μm -radius, 15 μm -width disk that earlier was found to have a much higher collision efficiency than a similar-size, 100 μm -radius sphere when approaching a 1 mm-radius bubble. The collision efficiency numbers for different $-U_{rc}$ ranges are summarized in Table 5.1. If we assume that only particles with a $-U_{rc}$ below an arbitrary value will result in attachment, then the disk will always have a lower attachment efficiency than the sphere. For example, if it is assumed that only particles that collide with a $-U_{rc}$ value of less than 40 mm/s will attach to the bubble, then the attachment efficiency will be:

$$E_a = \frac{(E_c)_{0 < -U_{rc} < 20} + (E_c)_{20 < -U_{rc} < 40}}{E_{c \text{ total}}} \quad (5.34)$$

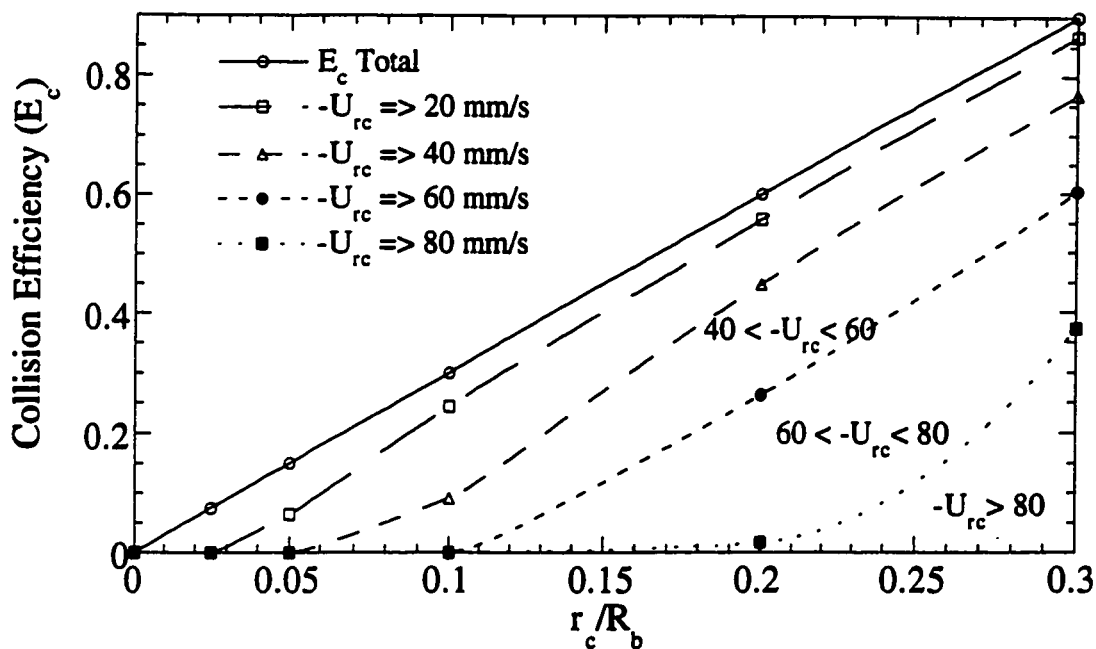


Figure 5.20 Sphere collision efficiencies in potential flow for different ranges of contact radial velocities. Undisturbed fluid velocity = 200 mm/s.

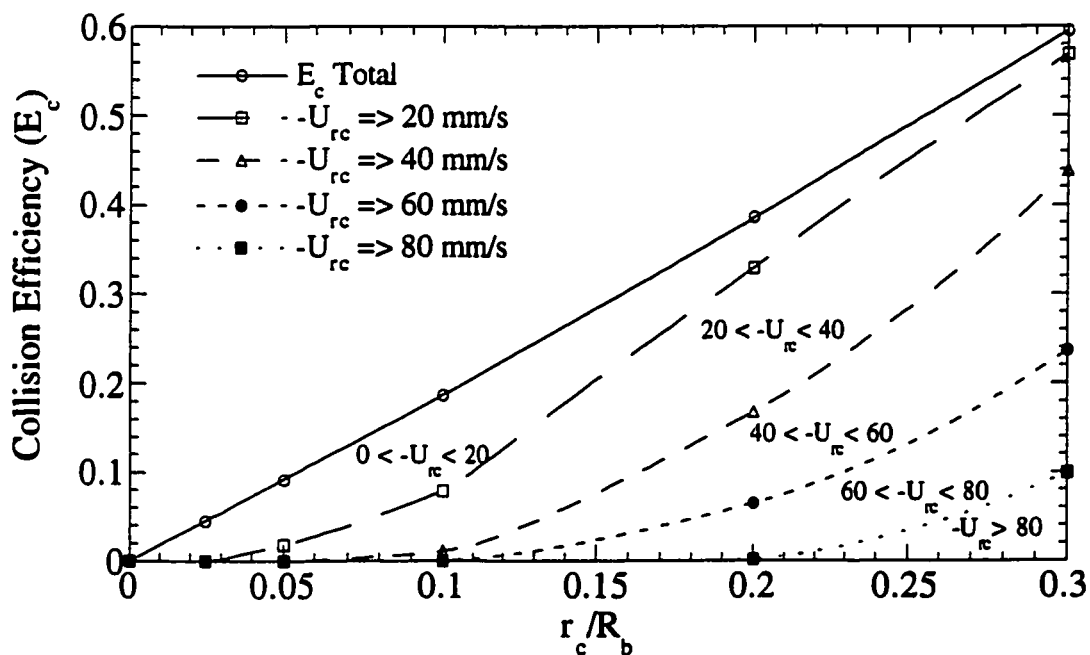


Figure 5.21 Disk collision efficiencies in potential flow for different ranges of contact radial velocities. Undisturbed fluid velocity = 200 mm/s.

Table 5.1 Collision efficiencies at different contact radial velocity ranges in potential flow for a similar size disk and sphere.

	Sphere - $r_c/R_b = 0.1$	Disk - $r_c/R_b = 0.3$
$0 \text{ mm/s} < -U_{rc} < 20 \text{ mm/s}$	0.056	0.025
$20 \text{ mm/s} < -U_{rc} < 40 \text{ mm/s}$	0.153	0.132
$40 \text{ mm/s} < -U_{rc} < 60 \text{ mm/s}$	0.091	0.201
$60 \text{ mm/s} < -U_{rc} < 80 \text{ mm/s}$	0	0.138
$-U_{rc} > 80 \text{ mm/s}$	0	0.099
E_c Total	0.300	0.595

This results in an attachment efficiency of 0.70 for the sphere, but only 0.26 for the disk. The total collection efficiency for the sphere, $E = E_c E_a$, will be 0.21, one-third greater than the collection efficiency of 0.16 for the disk.

For smaller disks, differences in attachment efficiency between disks and spheres decrease and collision efficiency becomes the predominant step. This leads to smaller differences in flotation behavior, as has been experimentally observed.

This approach towards attachment efficiency ignores the effect of the contact tangential velocity, which should also favor attachment of spheres over disks. It also ignores effects from the size of the contact area between the particle and bubble, which should favor attachment of disks over spheres. However, the effect from the size of the contact area is of lesser magnitude than the effect from the contact radial velocity, as observed experimentally in Chapter 4.

5.5 Conclusions

The hydrodynamic model predicted that disks, or flat, plate-shaped particles in general, behave differently in flotation than more spherically-shaped particles because of

the large effect that orientation has on the particle/bubble interactions. Large disk-to-bubble radius ratios (> 0.1) were found always to yield greater collision efficiencies than those for equivalent spherical particles, where an equivalent sphere was defined as one with the same volume as a disk computed on the basis of an aspect ratio of 40 (a typical value for experimental runs). This was in qualitative agreement with the experimental observations reported earlier. Smaller disk sizes may result in lower collision efficiencies than equivalent spheres depending upon the flow assumed to exist around the bubble. Potential flow predicted that even very small disks will have a higher collision efficiency than equivalent spheres. However, the intermediate flow prediction, which found that disks only have a higher collision efficiency when the disk-to-bubble radius ratio is greater than 0.14, may be more realistic.

The opposite trend was seen for attachment efficiency. Large disks were found to always have a much lower probability of attachment than equivalent spheres due to the higher tendency of disks to bounce off the bubble surface after collision, as was also observed in experimental observations. For smaller disks, differences in attachment efficiency and flotation behavior between disks and spheres decreased and collision efficiency became the predominant step. The decrease in E_a for large disks was greater than the increase in E_c leading to a decrease in the overall collection efficiency for disks vs. spheres, in agreement with experiment.

As disk size becomes very small with respect to bubble size, it is expected that the approach of this work will be less applicable as viscous and lubrication forces become dominant. For very small disk particles, a different approach such as Stokesian dynamics may be more useful.^{24, 33}

CHAPTER 6

Summary, Conclusions and Future Work

6.1 Summary and Conclusions

The objective of this research was to investigate fundamentally the reasons why toners are difficult to remove from repulped slurries by flotation. The study was limited to an investigation of toner electrostatic properties, an experimental study on the effect of particle shape on flotation, and a model study of the effect of particle shape and size on flotation. The preceding experiments and modelling support the following conclusions:

- Electrostatic properties of toner particles, as measured by the zeta potential, do not play a major role in toner flotation. This is because the toner surface is already hydrophobic before the addition of surfactants. The potential at the surface of a hydrophobic solid is primarily controlled by the aqueous phase and any contributions by the solid phase are generally due to charged hydrophilic sites. Because toner surfaces have few charged hydrophilic sites, zeta potential has little correlation with floatability.
- Disk-shaped toner particles have lower flotation rates than comparable size spheres. The reason for this, as observed using high-speed cinematography, is that disks either collide edge-on with a bubble, bouncing off due to the short contact time, or they rotate to the side and fail to attach due to the large liquid drainage area separating the disk and bubble surfaces.
- Disks, or flat, plate-shaped particles in general, behave differently in flotation than more spherically-shaped particles because of the large effect that orientation has on the particle/bubble interactions. Initial disk orientation will strongly affect both the

probability of particle/bubble collision (collision efficiency) and the probability of particle/bubble attachment after collision (attachment efficiency).

- Assuming a random initial orientation, collision efficiencies for disks with large disk-to-bubble radius ratios (> 0.1) are always greater than those for equivalent spherical particles, where an equivalent sphere is defined as one with the same volume as a disk computed on the basis of a diameter-to-thickness aspect ratio of 40. This was qualitatively confirmed in experimental observations. Smaller disk sizes may result in lower collision efficiencies than equivalent spheres depending upon the flow assumed to exist around the bubble. For example, potential flow predicts that even very small disks will have a higher collision efficiency than equivalent spheres. However, using an empirical stream function for intermediate Reynolds numbers more realistically predicts that disks only have a higher collision efficiency when the disk-to-bubble radius ratio is greater than 0.14.
- Attachment efficiency exhibits a trend opposite to that described above. Assuming a random initial orientation, large disks always have a much lower probability of attachment than equivalent spheres due to the higher tendency of disks to bounce off the bubble surface after collision, as was also observed in experimental observations.
- The decrease in attachment efficiency for large disks is greater than the increase in collision efficiency so that the overall collection efficiency for disks is less than for spheres, in agreement with flotation experiments.

- Finally, for smaller disks, differences in attachment efficiency and flotation behavior between disks and spheres decreases, and collision efficiency becomes the controlling step.

In a practical sense, this research implies that just as much attention needs to be given to the size and shape of toner particles exiting the pulping stage as is now given to the effect of collector surfactants on toner hydrophobicity in the flotation stage. This also has application to flotation in general. Whenever particles of a flat or oblate shape prove unexpectedly difficult to recover by flotation, it may be the result of their topology.

6.2 Recommendations for Future Work

Although the model developed in this work qualitatively agrees with experimental results for large disks, the assumptions of the model become invalid as disk size decreases. As disk size becomes very small with respect to bubble size, it is expected that the approach of this work will be less applicable as viscous and lubrication forces become dominant. For very small disk particles, a different approach, such as Stokesian dynamics, might be useful in observing how shape and size affect flotation.

Also, the adverse effects of particle shape may be partly compensated by changing the surface chemistry of the system and thereby increasing the attachment efficiency. The attachment efficiency is dependent upon the stability of the thin-film separating the particle and bubble. How soon this film will drain and rupture depends upon the attractive and repulsive forces existing between the particle and bubble surfaces at small distances. These forces can now be measured using the atomic force microscope (AFM) and measurement on the forces acting between a toner particle and an air-water interface in different solution chemistries could be beneficial towards predicting flotation performance.

List Of References

1. Carr, W. F., "New trends in deinking technology - removing difficult inks from wastepaper", *Tappi Journal* **74**(2):127 (1991).
2. Quick, T. H. and K. T. Hodgson, "Xerography deinking - a fundamental approach", *Tappi Journal* **69**(3):102 (1986).
3. Shrinath, A., J. T. Szewczak and I. J. Bowen, "A review of ink-removal techniques in current deinking technology", *Tappi Journal* **74**(7):85 (1991).
4. Gaudin, A. M., Flotation, McGraw Hill, New York, (1957).
5. Sutherland, K. L. and I. W. Wark, Principles of Flotation, Australasian Institute of Mining and Metallurgy, Melbourne, (1955).
6. Ortner, H. E., Flotation Deinking, TAPPI Press, Atlanta, (1981).
7. Larsson, A., P. Stenius and L. Ödberg, "Surface chemistry in flotation deinking Part 1. The floatability of model ink particles", *Svensk Papperstidning* **1984**(18):R158 (1984).
8. Ferguson, L. D., "Deinking chemistry: part 1", *Tappi Journal* **75**(7):75 (1992).
9. Johansson, B., M. Wickman and G. Ström, "The mechanism of offset ink particles agglomeration in a calcium-fatty acid collector system", 3rd Research Forum on Recycling, p. 51 (1995).
10. Seldin, I., "Xerographic copy recycling", 1985 TAPPI Pulping Conference Proceedings, p. 303 (1985).
11. Borchardt, J. K., J. H. Rask, G. A. York and K. Cathie, "Microscopic analysis of toner-printed paper after pulping", *Progress in Paper Recycling* **4**(4):16 (1995).
12. Borchardt, J. K., J. H. Rask, J. D. Miller and Q. Yu, "Toner ink particle morphology in air-sparged hydrocyclone flotation deinking", *Progress in Paper Recycling* **5**(2):29 (1996).
13. Leja, J., Surface Chemistry of Froth Flotation, Plenum Press, New York, (1982).
14. Epple, M. and J. C. Berg, "The effect of adsorbed surfactants on the electrostatic properties and wettability of a photocopy toner", *Progress in Paper Recycling* **3**(2):52 (1994).
15. Sutherland, K. L., "Physical chemistry of flotation", *Journal of Physical Chemistry* **52**:394 (1948).

16. Derjaguin, B. V. and S. S. Dukhin, "Theory of flotation of small and medium-size particles", *Bulletin of the Institute of Mining and Metallurgy* **70**:221 (1961).
17. Schulze, H. J., *Physico-chemical Elementary Processes in Flotation*, Elsevier, Amsterdam, (1984).
18. Schulze, H. J., "Hydrodynamics of bubble-mineral particle collisions", *Mineral Processing and Extractive Metallurgy Review* **5**:43 (1989).
19. Reay, D. and G. A. Ratcliff, "Removal of fine particles from water by dispersed air flotation: effects of bubble size and particle size on collection efficiency", *Canadian Journal of Chemical Engineering* **51**:178 (1973).
20. Weber, M. E. and D. Paddock, "Interceptional and gravitational collision efficiencies for single collectors at intermediate reynolds numbers", *Journal of Colloid and Interface Science* **94**(2):328 (1983).
21. Jiang, Z. W. and P. N. Holtham, "Theoretical model of collision between particles and bubbles in flotation", *Transactions of the Institute of Mining and Metallurgy* **95**:C187 (1986).
22. Yoon, R. and G. H. Luttrell, "The effect of bubble size on fine particle flotation", *Mineral Processing and Extractive Metallurgy Review* **5**:101 (1989).
23. Schimmoller, B. K., G. H. Luttrell and R. Yoon, "A combined hydrodynamic-surface force model for bubble-particle collection", In: XVIII International Mineral Processing Congress, (ed.), The Australasian Institute of Mining and Metallurgy, Sydney, Australia, p. 751 (1993).
24. Pan, R., F. G. Paulsen, D. A. Johnson, D. W. Bousfield and E. V. Thompson, "A global model for predicting flotation efficiency: Part I. Model results and experimental studies", *Tappi Journal* **79**(4):177 (1996).
25. Flint, L. R. and W. J. Howarth, "The collision efficiency of small particles with spherical air bubbles", *Chemical Engineering Science* **26**:1155 (1971).
26. Nguyen-Van, A. and S. Kmet', "Collision efficiency for fine mineral particles with single bubble in a countercurrent flow regime", *International Journal of Mineral Processing* **35**:205 (1992).
27. Nguyen-Van, G., "The collision between fine particles and single air bubbles in flotation", *Journal of Colloid and Interface Science* **162**:123 (1994).
28. Seeley, L. E., R. L. Hummel and J. W. Smith, "Experimental velocity profiles in laminar flow around spheres at intermediate Reynolds numbers", *Journal of Fluid Mechanics* **68**(3):591 (1975).
29. Schulze, H. J., "The fundamentals of flotation deinking in comparison to mineral flotation", 1991 Recycling Forum, p. 161 (1991).

30. Pan, R., D. W. Bousfield and E. V. Thompson, "Modelling particle-bubble dynamics and adhesion in air bubble/solid particle/liquid systems", *Proceedings TAPPI Pulping Conference*, p. 941 (1992).
31. Pan, R., F. G. Paulsen, D. A. Johnson, D. W. Bousfield and E. V. Thompson, "A global model for predicting flotation efficiencies: Model results and experimental studies", *TAPPI 1993 Pulping Conference Proceedings*, p. 1155 (1993).
32. Paulsen, F. G., R. Pan, D. W. Bousfield and E. V. Thompson, "The dynamics of bubble/particle approach and attachment during flotation and the influence of short-range nonhydrodynamic forces on disjoining film rupture", *Proceedings Second Research Forum on Recycling*, p. 1 (1993).
33. Brady, J. F. and G. Bossis, "Stokesian dynamics", *Annual Review of Fluid Mechanics* **20**:111 (1988).
34. Rulev, N. N., S. S. Dukhin and A. G. Chaplygin, "Efficiency of particle capture by bubble in flotation with multiple inertial reflections", *Kolloidnyi Zhurnal* **49**(5):939 (1987).
35. Sven-Nilsson, I., *Kolloid Z.* **69**:230 (1934).
36. Dobby, G. S. and J. A. Finch, "A model of particle sliding time for flotation size bubbles", *Journal of Colloid and Interface Science* **109**(2):493 (1986).
37. Dobby, G. S. and J. A. Finch, "Particle size dependence in flotation derived from a fundamental model of the capture process", *International Journal of Mineral Processing* **21**:241 (1987).
38. Nguyen Van, A., "On the sliding time in flotation", *International Journal of Mineral Processing* **37**:1 (1993).
39. Hewitt, D., D. Fornasiero and J. Ralston, "Bubble-particle attachment", *Journal of the Chemical Society Faraday Transactions* **91**(13):1997 (1995).
40. Li, D., J. A. Fitzpatrick and J. C. Slaterry, "Rate of collection of particles by flotation", *Industrial and Engineering Chemistry Research* **29**(6):955 (1990).
41. Schulze, H. J., "Flotation as a heterocoagulation process: Possibilities of calculating the probability of flotation", *In: Coagulation and Flocculation: Theory and Applications*, B. Dobias (ed.), Marcel Dekker, New York, p. 321 (1993).
42. Fisher, L. R., E. E. Mitchell, D. Hewitt, J. Ralston and J. Wolfe, "The drainage of a thin aqueous film between a solid surface and an approaching gas bubble", *Colloids and Surfaces* **52**:163 (1991).
43. Yoon, R.-H. and J. L. Yordan, "Induction time measurements for the quartz-amine flotation system", *Journal of Colloid and Interface Science* **141**(2):374 (1991).
44. Ralston, J., "Thin films and froth flotation", *Advanced Colloid and Interface Science* **19**:1 (1983).

45. Arbiter, N. and C. C. Harris, "Flotation kinetics", *In: Froth Flotation, 50th Anniversary Volume*, D. W. Fuerstenau (ed.), American Inst. Mining, Metallurgical and Petroleum Engineers Inc., New York, p. 215 (1962).
46. Scheludko, A., "Thin liquid films", *Advanced Colloid and Interface Science* **1**(4):391 (1967).
47. Lucassen-Reynders, E. H. and J. Lucassen, "Thin films, contact angles, wetting", *In: The Scientific Basis of Flotation*, K. J. Ives (ed.), Martinus Nijhoff Publishers, The Hague, p. 79 (1984).
48. Derjaguin, B. V., *Theory of Stability of Colloids and Thin Films*, Consultants Bureau, New York, (1989).
49. Pugh, R. J. and E. Manev, "The study of thin aqueous films as models for froths and flotation", *In: Innovations in Flotation Technology*, P. Mavros and K. A. Matis (ed.), Kluwer Academic Publishers, Dordrecht, p. 1 (1992).
50. Lu, S., "Hydrophobic interaction in flocculation and flotation 3. Role of hydrophobic interaction in particle-bubble attachment", *Colloids and Surfaces* **57**:73 (1991).
51. Pashley, R. M., "Interparticulate forces", *In: Colloid Chemistry in Mineral Processing*, J. S. Laskowski and J. Ralston (ed.), Elsevier, Amsterdam, p. 97 (1992).
52. Derjaguin, B. V. and M. Kussakov, *Acta Physicochim. U.R.S.S.* **10**(1):26 (1939).
53. Platikanov, D., "Experimental investigation on the "dimpling" of thin liquid films.", *Journal of Physical Chemistry* **68**:3619 (1964).
54. Blake, T. D. and J. A. Kitchener, "Stability of aqueous films on hydrophobic methylated silica", *Journal of the Chemical Society Faraday Transactions* **68**:1435 (1972).
55. Yoon, R. and J. L. Yordan, "The critical rupture thickness of thin water films on hydrophobic surfaces", *Journal of Colloid and Interface Science* **146**(2):565 (1991).
56. Schulze, H. J. and J. O. Bizer, "Stability of thin liquid films on Langmuir-Blodgett layers on silica surfaces", *Colloids and Surfaces* **24**:209 (1987).
57. Paulsen, F. G., R. Pan, D. W. Bousfield and E. V. Thompson, "The dynamics of bubble/particle attachment and the application of two disjoining film rupture models to flotation I. Nondraining Model", *Journal of Colloid and Interface Science* **178**(2):400 (1996).
58. Anfruns, J. F. and J. A. Kitchener, "Rate of capture of small particles in flotation", *Transactions of the Institution of Mining and Metallurgy Section C* **86**:C9 (1977).
59. Nutt, C. W., "Froth flotation: The adhesion of solid particles to flat interfaces and bubbles", *Chemical Engineering Science* **12**:133 (1960).

60. Baichenko, A. A. and A. V. Listovnichii, "Rim of an apolar reagent on the surface of a particle being floatedd", *Kolloidnyi Zhurnal* **51**(1):123 (1989).
61. Huh, C. and S. G. Mason, "The flotation of axisymmetric particles at horizontal liquid interfaces.", *Journal of Colloid and Interface Science* **47**:271 (1974).
62. Princen, H., "The equilibrium shape of interfaces", *In: Surface and Colloid Science*, E. Matjjevic (ed.), John Wiley & Sons, New York, p. 1 (1969).
63. Nishkov, I. and R. J. Pugh, "Selective bubble-particle detachment forces and flotation for the galena/quartz system", *In: Processing of Complex Ores*, (ed.), p. 87 (1989).
64. Janczuk, B., "Detachment force of air bubble from the solid surface (sulfur or graphite) in water", *Journal of Colloid and Interface Science* **93**(2):411 (1983).
65. Janczuk, B. and Bialopiotrowicz, "Adhesion of air bubbles to teflon surfaces in water", *Journal of Colloid and Interface Science* **128**(1):1 (1989).
66. Stratton, R. A., "The surface chemistry off flotation of stickies and laser printed inks", 1991 Recycling Forum, p. 161 (1991).
67. Laskowski, J. S., "Frothers and flotation froth", *Mineral Processing and Extractive Metallurgy Review* **12**:61 (1993).
68. Wrobel, S. A., "Flotation frothers, their action, composition, properties, and structure", *In: Recent Developments in Mineral Dressing*, (ed.), Inst. Min. Met., London, p. 431 (1958).
69. Wrobel, S. A., "Power and stability of flotation frothers", *Mine and Quarry* **19**:363 (1953).
70. Klimpel, R. R. and R. D. Hansen, "Frothers", *In: Reagents in Mineral Technology*, P. Somasundaran and B. M. Moudgil (ed.), Marcel Dekker, Inc., New York, p. 385 (1988).
71. Klimpel, R. R. and S. Isherwood, "Some industrial implications of changing frother chemical structure", *International Journal of Mineral Processing* **33**:369 (1991).
72. Klimpel, R. R., "Some results of various new chemical reagents for modifying coal flotation performance", *Coal Preparation* **10**:159 (1992).
73. Trahar, W. J., "A rational interpretation of the role of particle size in flotation", *International Journal of Mineral Processing* **8**:289 (1981).
74. Crawford, R. and J. Ralston, "The influence of particle size and contact angle in mineral flotation", *International Journal of Mineral Processing* **23**:1 (1988).
75. Scheludko, A., B. V. Toshev and D. T. Bojadjiev, "Attachment of particles to a liquid surface (capillary theory of flotation)", *Journal of the Chemical Society Faraday Transactions I* **72**:2815 (1976).

76. Johnson, D. A. and E. V. Thompson, "Fiber and toner detachment during repulping of mixed office waste containing photocopied and laser-printed paper", *Tappi Journal* 78(2):41 (1995).
77. Hunter, R. J., *Zeta Potential in Colloid Science*, Academic Press, London, (1981).
78. Kydros, K. A. and K. A. Matis, "Flotation of iron sulfide minerals: electrokinetic aspects", *In: Flotation Science and Engineering*, K. A. Matis (ed.), Mercel Dekker, New York, p. 127 (1995).
79. Berg, J. C., "The use and limitations of wetting measurements in the prediction of adhesive performance", *In: Composite systems from natural and synthetic polymers*, L. Salmén, A. d. Ruvo, J. C. Seferis and E. B. Stark (ed.), Elsevier, Amsterdam, p. 23 (1986).
80. Fuerstenau, D. W., P. H. Metzger and G. D. Seele, "How to use this modified Hallimond tube for better flotation testing", *Engineering and Mining Journal* 158(3):93 (1957).
81. Snyder, B. A., D. C. Schmidt and J. C. Berg, "Characterization and flotation studies of electrostatic inks", *Progress in Paper Recycling* 3(1):17 (1993).
82. Johnson, R. E., Jr. and R. H. Dettre, "Wettability and contact angles", *In: Surface and Colloid Science*, E. Matijevic' (ed.), Wiley-Interscience, New York, p. 85 (1969).
83. Harris, C. C., "How much flotation research really pays off?", *Mining Magazine* 126:439 (1972).
84. Arbiter, N., Y. Fujii, B. Hansen and A. Raja, "Surface properties of hydrophobic solids", *In: Advances in Interfacial Phenomena of Particulate/Solution/Gas Systems; Applications to Flotation Research*, P. Somasundaran and R. B. Grieve (ed.), AIChE, New York, p. 176 (1975).
85. Epple, M., D. C. Schmidt and J. C. Berg, "The effect of froth stability and wettability on the flotation of a xerographic toner", *Colloid & Polymer Science* 272(10):1264 (1994).
86. Schmidt, D. C. and J. C. Berg, "The effect of particle shape on the flotation of toner particles", *Progress in Paper Recycling* 5(2):67 (1996).
87. Ralston, J., "The influence of particle size and contact angle in flotation", *In: Colloid Chemistry in Mineral Processing*, J. S. Laskowski and J. Ralston (ed.), Elsevier, Amsterdam, p. 203 (1992).
88. McCool, M. A. and L. Silveri, "Removal of Specks and Non-dispersed Ink from a Deinking Furnish", *Proceedings TAPPI Pulping Conference*, p. 33 (1987).
89. Spedden, H. R. and W. S. Hannan, "Attachment of mineral particles to air bubbles in flotation", *Mineral Technology* 12:T. P. 2354 (1948).

90. Whelan, P. F. and D. J. Brown, "Particle-bubble attachment in froth flotation", *Transactions of the Institute of Mining and Metallurgy* **65**:181 (1956).
91. Schulze, H. J. and G. Gottschalk, "Investigations of the hydrodynamic interaction between a gas bubble and mineral particles in flotation", *In: Mineral Processing*, J. Laskowski (ed.), Elsevier, Amsterdam, p. 63 (1981).
92. Batchelder, R. F. and C. C. Li, "High speed photographic investigation of coal flotation", *In: Advances in Fine Particles Processing*, J. Hanna and Y. A. Attia (ed.), Elsevier, New York, p. 335 (1990).
93. Schmidt, D. C. and J. C. Berg, "A preliminary hydrodynamic analysis of the flotation of disk-shaped toner particles", *Progress in Paper Recycling* :(submitted for publication) (1996).
94. Jameson, G. J., "Physics and hydrodynamics of bubbles", *In: The Scientific Basis of Flotation*, K. J. Ives (ed.), Martinus Nijhoff Publishers, The Hague, p. 53 (1984).
95. Michael, D. H. and P. W. Norey, "Particle collision efficiencies for a sphere", *Journal of Fluid Mechanics* **37**(3):565 (1969).
96. Jeffery, G. B., "The motion of ellipsoidal particles immersed in a viscous fluid", *Proceeding of the Royal Society of London A*. **102**:161 (1923).
97. van de Ven, T. G. M., *Colloidal Hydrodynamics*, Academic Press, London, (1989).
98. Chapra, S. C. and R. P. Canale, *Numerical Methods for Engineers*, McGraw-Hill, New York, (1988).
99. Goren, S. L. and M. E. O'Neill, "On the hydrodynamic resistance to a particle of a dilute suspension when in the neighborhood of a large obstacle", *Chemical Engineering Science* **26**:325 (1971).
100. Emory, S. F. and J. C. Berg, "Surface tension effects on particle collection efficiency", *Industrial and Engineering Chemistry Fundamentals* **17**(3):225 (1978).
101. Clift, R., J. R. Grace and M. E. Weber, *Bubbles, Drops, and Particles*, Academic Press, New York, (1978).

APPENDIX A

Fortran Code of Model

A.1 Introduction

The computer model consists of three different computer programs. The first program, HMODP, solves the equations of Chapter 5 to calculate the trajectory and changes in orientation of a disk of given size, initial orientation, and initial position as it approaches a bubble. The second program, COLMOD, determines the critical initial displacement distance from the bubble centerline at which a disk of a given size and initial orientation will just make contact with the bubble. Finally, VRCMOD calculates the initial displacement distance from the bubble centerline at which a disk of given size and initial orientation will collide with the bubble with a given contact radial velocity.

The equations of Chapter 5 are solved in all three programs in the following manner:

- Equations (5.13) - (5.15) and (5.19) - (5.24) are solved in subroutine VARBLS.
- The integrals in equations (5.16) - (5.18) are numerically solved using Romberg integration and Simpson's rule in subroutines WDTN, RIWDR, and WDR.
- The integrals in equations (5.25) - (5.27) are numerically solved using Romberg integration and Simpson's rule in subroutines UDTN, RIUDR, and UDR.
- The differential equations (5.28) - (5.32) are numerically solved using the 4th order Runge-Kutta method in subroutines RK4C and RINTEG.

A.2 HMODP Program

A.2.1 Fortran Code

```

PROGRAM    HMODP
C
C This program determines the movement and orientation of a disk as it
C approaches and flows around a bubble. It is a simple hydrodynamic model
C which uses the potential flow equations for flow around a sphere to
C approximate the flow around the bubble. The assumption of particle density
C neutrality is made. Flow is in the negative y direction. The bubble is
C centered at the origin. The center of the disk in x, y, z coordinates is
C Ox, Oy, and Oz. The orientation of the disk is described by two angles.
C Alpha is the angle between the z-axis and a line drawn perpendicular
C to the disk at the disk center. Beta is the angle between the x-axis
C and the projection of the perpendicular line is the x-y plane.
C
      INTEGER QUITPR,TRUE,FALSE,PCOUNT,PRINTI,CONTCT,CONTYP
      DOUBLE PRECISION T,Y,H,RDISK,RBUB,VINF,A,Y1,Y2,PI,MISBUB,SEPMIN,
      &                XP,YP,THETA
      DIMENSION Y(5)
C
      OPEN(UNIT=1,FILE='hin',STATUS='OLD')
      OPEN(UNIT=2,FILE='hout',STATUS='NEW')
C
C Initialized variables NEQ (number of equations), T (time in seconds),
C CONTCT (tracks whether contact between particle and bubble has been
C made), CONTYP (type of contact between particle and bubble - 0 is miss,
C 1 is contact on edge, 2 is contact on side, 3 is when the max. number of
C iterations, MAXSTP, has been exceeded), QUITPR (flag for when to end
C program), ISTEP (# of iterations), PCOUNT (print counter), and PI.
C
      NEQ = 5
      T = 0d0
      FALSE = 0
      TRUE = 1
      CONTCT = FALSE
      CONTYP = 0
      QUITPR = FALSE
      ISTEP = 0
      PCOUNT = 0
      SEPMIN = 10.0D0
      PI = 3.141592653589793D0
C
C Call datain subroutine to input data: alpha (Y(1)), beta (Y(2)), Ox
C (Y(3)), Oy (Y(4)), Oz (Y(5)), disk radius (RDISK), bubble radius (RBUB),
C the velocity of the undisturbed flow (VINF), the step size (H), the
C maximum number of iterations (MAXSTP), and the interval at which to
C output the data (PRINTI).
C
      CALL DATAIN (Y,RDISK,RBUB,VINF,H,MAXSTP,PRINTI)
C
C The disk is assumed to miss bubble if disk center drops below the bubble
C center.
      MISBUB = 0.0D0
C
C Calculate new position and orientation at each timestep by calling a
C fourth-order runha-kutta subroutine. Update timestep. Repeat until
C either QUITPR is true or ISTEP exceeds MAXSTP.
C

```

```

10  CONTINUE
    CALL RR4C (NEQ,T,Y,H,RDISK,RBUB,VINF)
    T = T + H
C
C Check if disk has made contact with bubble and calculate minimum
C separation distance (SEPMIN)
C
    CALL CHKCON (Y,RDISK,RBUB,CONTCT,CONTYP,A,SEPMIN,XP,YP)
C
C If contact with bubble has been made or Oy is less than zero then quit
C program.
C
    IF (CONTCT.EQ.TRUE) QUITPR = TRUE
    IF (Y(4).LE.MISBUB) QUITPR = TRUE
C
C Advance iterations step counter (ISTEP) and print counter (PCOUNT) by 1.
C If PCOUNT is greater than PRINTI, write disk orientation and position to
C output file.
    ISTEP = ISTEP + 1
    PCOUNT = PCOUNT + 1
    IF (PCOUNT.GE.PRINTI) THEN
        Y1 = Y(1)*180.0D0/PI
        Y2 = Y(2)*180.0D0/PI
        WRITE(2,100) T,Y1,Y2,(Y(I),I=3,5)
        PCOUNT = 0
    ENDIF
    IF ((QUITPR.EQ.FALSE).AND.(ISTEP.LT.MAXSTP)) GOTO 10
C
    IF (ISTEP.GE.MAXSTP) CONTYP = 3
C
C Call subroutine to print out final results.
C
    CALL DATOUT (T,Y,CONTCT,CONTYP,ISTEP,MAXSTP,A,SEPMIN,XP,YP,
    & RDISK,RBUB,VINF,THETA)
C
100  FORMAT (1X,E12.5,F10.5,F10.5,F10.5,F10.5,F10.5)
C
    END

```

```

    SUBROUTINE CHKCON (Y,RDISK,RBUB,CONTCT,CONTYP,A,SEPMIN,XP,YP)
C This subroutine checks if the disk has made contact with the bubble.
C If contact has been made, it determines whether the contact is on the
C side or the edge. Subroutine also keeps track of the minimum
C separation distance between the bubble and disk (SEPMIN) and returns the
C values of XP and YP which are used later in the datout subroutine to
C determine exact point of contact.
C
    INTEGER QUITPR,TRUE,FALSE,CONTCT,CONTYP
    DOUBLE PRECISION Y,RDISK,RBUB,A,KX,KY,K,SEPMIN,SEP,XP,YP
    DIMENSION Y(5)
C
    FALSE = 0
    TRUE = 1
C These equation determine the radial distance, A, at which the distance
C between the disk and the bubble surface is at a minimum.
C
    KX = DCOS(Y(1))*DCOS(Y(2))*Y(3)
    & + DCOS(Y(1))*DSIN(Y(2))*Y(4) - DSIN(Y(1))*Y(5)

```

```

      KY = DCOS(Y(2))*Y(4) - DSIN(Y(2))*Y(3)
      K = DSQRT(KX**2 + KY**2)
      A = K
C
C The equations above allow for an infinitely large disk, so if A is
C greater than the actual disk radius, then A become RDISK.
C
      IF (A.GT.RDISK) A=RDISK
      XP = -KX*A/K
      YP = -KY*A/K
C
C R is the distance between a point on A and the bubble center. If R is
C less than the bubble radius, then a disk/bubble collision has taken
C place. If this is true and A is less than the bubble radius, then the
C contact has taken place along the disk side, rather than the disk edge.
C
      R = SQRT(A*A - 2*A*K + Y(3)**2 + Y(4)**2 + Y(5)**2)
      SEP = R - RBUB
      IF (SEP.LT.SEPMIN) SEPMIN = SEP
      IF (R.LE.RBUB) THEN
        CONTCT = TRUE
        IF (A.LT.RDISK) THEN
          CONTYP = 2
        ELSE
          CONTYP = 1
        ENDIF
      ENDIF
C
      RETURN
      END

```

```

      SUBROUTINE DATAIN(Y,RDISK, RBUB,VINF,H,MAXSTP,PRINTI)
C This subroutine inputs starting disk position and orientation (Y), disk
C radius (RDISK), bubble radius (RBUB), the velocity at infinity (VINF),
C the step size for the runga-kutta method (H), the maximum number of
C iterations that will be performed before the program stops (MAXSTP), and
C the interval at which data will be written to out data file (PRINTI).
C Initial data is also written to the output file.
C
      INTEGER PRINTI
      CHARACTER*12 LABEL(11)
      CHARACTER*55 TITLE
      DOUBLE PRECISION Y,RDISK, RBUB,VINF,H,PI
      DIMENSION Y(5)
C
      READ(1,5) TITLE
5     FORMAT (A55)
      READ(1,*) (LABEL(I),I=1,5)
      READ(1,*) (Y(I),I=1,5)
      READ(1,*)
      READ(1,*) (LABEL(I),I=6,11)
      READ(1,*) RDISK, RBUB,VINF,H,MAXSTP,PRINTI
C
      WRITE(2,*) TITLE
      WRITE(2,*) '          Initial Data'
      WRITE(2,10) LABEL(1),Y(1),LABEL(6),RDISK
      WRITE(2,10) LABEL(2),Y(2),LABEL(7),RBUB
      WRITE(2,10) LABEL(3),Y(3),LABEL(8),VINF

```

```

WRITE(2,20) LABEL(4),Y(4),LABEL(9),H
WRITE(2,30) LABEL(5),Y(5),LABEL(10),MAXSTP
WRITE(2,40) LABEL(11),PRINTI
WRITE(2,*)
WRITE(2,50)
WRITE(2,60)

C
PI = 3.141592653589793D0
Y(1) = Y(1)/180.0D0*PI
Y(2) = Y(2)/180.0D0*PI

C
10  FORMAT (1X,A6,' ':',F10.5,4X,A,' ':',F10.5)
20  FORMAT (1X,A6,' ':',F10.5,4X,A,' ':',E12.5)
30  FORMAT (1X,A6,' ':',F10.5,4X,A,' ':',I7)
40  FORMAT (1X,22X,A,' ':',I4)
50  FORMAT (6X,'Time',7X,'Alpha',5X,'Beta',7X,'Ox',8X,'Oy',8X,'Oz')
60  FORMAT (3X,'(seconds)',3X,'(degrees)',1X,'(degrees)',3X,'(mm)',6X,
&      '(mm)',6X,'(mm)')

C
RETURN
END

```

```

SUBROUTINE DATOUT(T,Y,CONTCT,CONTYP,ISTEP,MAXSTP,A,SEPMIN,
& XP,YP,RDISK,RBUB,VINF,THETA)
C This subroutine writes to the output file the final disk position and
C orientation and whether the disk contacted the bubble. Contact
C information is determined by the value of CONTYP. It also computes
C and writes the disk velocities, the velocity of the point of the disk
C contacting the bubble, and the angle between the plane containing the
C disk and the plane tangent to the bubble at the point of contact
C (THETA).
C
INTEGER CONTCT,CONTYP
DOUBLE PRECISION T,Y,PI,SEPMIN,A,XP,YP,Y1,Y2,RDISK,RBUB,VINF,
& WX,WY,WZ,UX,UY,UZ,XC,YC,ZC,XD,YD,ZD,TOP,BOT,THETA,UTH,UR,
& UXC,UYC,UZC,UTHC,URC,TH,THC,PHI,PHIC,UPHI,UPHIC
DIMENSION Y(5)

C
PI = 3.141592653589793D0

C
C Convert angles from radians to degrees.
Y1 = Y(1)*180.0D0/PI
Y2 = Y(2)*180.0D0/PI

C
WRITE(2,*)
WRITE(2,*) ' Final Disk Position'
WRITE(2,10) T,Y1,Y2,(Y(I),I=3,5)
WRITE(2,*)
WRITE(2,20) ISTEP
WRITE(2,25) SEPMIN
WRITE(2,*)

C
IF (CONTYP.EQ.0) WRITE(2,30)
IF (CONTYP.EQ.1) WRITE(2,40)
IF (CONTYP.EQ.2) WRITE(2,50) A
IF (CONTYP.EQ.3) WRITE(2,60) MAXSTP

C
IF (CONTYP.EQ.1.OR.CONTYP.EQ.2) THEN

```

```

C Calculate the point at which the bubble and disk contact (XC, YC, and
C ZC) from values of XP and YP (values of X and Y in particle fixed
C coordinates, calculated in subroutine chkcon) and alpha (Y(1)), beta,
C (Y(2)), Ox (Y(3)), Oy (Y(4)), and Oz (Y(5)).
      XC = DCOS(Y(1))*DCOS(Y(2))*XP - DSIN(Y(2))*YP + Y(3)
      YC = DCOS(Y(1))*DSIN(Y(2))*XP + DCOS(Y(2))*YP + Y(4)
      ZC = -DSIN(Y(1))*XP + Y(5)
C
C Calculate coordinates of a unit vector normal to the disk (XD,YD,ZD).
      XD = DSIN(Y(1))*DCOS(Y(2))
      YD = DSIN(Y(1))*DSIN(Y(2))
      ZD = DCOS(Y(1))
C
C The incident angle of collision (THETA) is the dot product of the disk
C vector and the vector to the point of collision (which vector defines a
C plane tangent to the bubble at the point of contact).
      TOP = XC*XD + YC*YD + ZC*ZD
      TOP = DABS(TOP)
      BOT = DSQRT(XC**2 + YC**2 + ZC**2)
      THETA = DACOS(TOP/BOT)
      THETA = THETA*180.0D0/PI
C
C Subroutine RINTEG2 calculates translational (UX, UY, UZ) and angular
C velocities (WX, WY, WZ) of the disk at the time of contact.
      CALL RINTEG2 (Y,RDISK,RBUB,VINF,WX,WY,WZ,UX,UY,UZ)
C
C Calculate the disk velocity in the R and theta directions (UR and UTH).
      TH = DATAN( DSQRT(Y(3)**2 + Y(5)**2) / Y(4) )
      PHI = DATAN(Y(5)/Y(3))
      IF (PHI.LT.0.0D0.AND.Y(3).LT.0.0D0) PHI = PHI + PI
      UTH = -DSIN(TH)*UY + DCOS(TH)*(SIN(PHI)*UZ + COS(PHI)*UX)
      UR = DCOS(TH)*UY + DSIN(TH)*(SIN(PHI)*UZ + COS(PHI)*UX)
      UPHI = -DSIN(PHI)*UX + DCOS(PHI)*UZ
C
C Calculate the velocity of the edge or side of disk contacting the bubble
C (UXC, UYC, UZC) including the velocity in the R and theta directions
C (URC, UTHC).
      UXC = UX + WY*(ZC - Y(5)) - WZ*(YC - Y(4))
      UYC = UY + WZ*(XC - Y(3)) - WX*(ZC - Y(5))
      UZC = UZ + WX*(YC - Y(4)) - WY*(XC - Y(3))
      THC = DATAN( DSQRT(XC**2 + ZC**2) / YC )
      PHIC = DATAN(ZC/XC)
      IF (PHIC.LT.0.0D0.AND.XC.LT.0.0D0) PHIC = PHIC + PI
      UTHC = -DSIN(THC)*UYC + DCOS(THC)*(SIN(PHIC)*UZC +
&          COS(PHIC)*UXC)
      URC = DCOS(THC)*UYC + DSIN(THC)*(SIN(PHIC)*UZC +
&          COS(PHIC)*UXC)
      UPHIC = -DSIN(PHIC)*UXC + DCOS(PHIC)*UZC
C
C Write information to file
      WRITE(2,110) THETA
      WRITE(2,*)
      WRITE(2,100) XC, YC, ZC
      WRITE(2,120) UX, UY, UZ
      WRITE(2,130) WX, WY, WZ
      WRITE(2,140) UTH, UR, UPHI
      WRITE(2,150) UXC, UYC, UZC
      WRITE(2,160) UTHC, URC, UPHIC
C
      ENDIF
C

```



```

10  FORMAT (1X,E12.5,F10.5,F10.5,F10.5,F10.5,F10.5)
20  FORMAT (1X,'Number of iterations = ',I6)
25  FORMAT (1X,'Minimum separation distance: ',F9.6)
30  FORMAT (1X,'Disk has missed contacting bubble.')
40  FORMAT (1X,'Disk has contacted bubble on the disk edge.')
50  FORMAT (1X,'Disk has contacted bubble on the disk side.  A = ',
    & F10.5)
60  FORMAT (1X,'Maximum number of iterations exceeded! Max. steps = ',
    & I6)
100 FORMAT (' Contact Point      x:',F10.5,'      y:',F10.5,'      z:',
    & F10.5)
110 FORMAT (' Incident angle of disk with bubble surface:',F10.5)
120 FORMAT (' Disk Velocity   Ux:',F10.5,'      Uy:',F10.5,'      Uz:',
    & F10.5)
130 FORMAT (' Angular Vel.    Wx:',F10.5,'      Wy:',F10.5,'      Wz:',
    & F10.5)
140 FORMAT (' Disk Velocity   Uth:',F10.5,'      Ur:',F10.5,'      Uphi:',
    & F10.5)
150 FORMAT (' Point Vel.      Uxc:',F10.5,'      Uyc:',F10.5,'      Uzc:',
    & F10.5)
160 FORMAT (' Point Vel.      Uthc:',F10.5,'      Urc:',F10.5,'      Uphic:',
    & F10.5)
C
    RETURN
    END

```

```

      SUBROUTINE RINTEG (Y,RDISK,RBUB,VINF,F)
C
C This subroutine calls the subroutines WDTN and UDTN to solve the double
C integrals which define the rotational velocities (wx, wy, wz) and the
C translational velocities (Ux, Uy, and Uz) of the disk. The change of
C alpha and beta with respect to time are dependent upon WX, WY, and WZ as
C shown below in the definition of F(1) and F(2).
C
      DOUBLE PRECISION Y,RDISK,RBUB,VINF,F,WX,WY,WZ,UX,UY,UZ
      CHARACTER*2 EQN
      DIMENSION Y(5), F(5)
C
      EQN = 'WX'
      CALL WDTN (Y,RDISK,RBUB,VINF,WX,EQN)
      EQN = 'WY'
      CALL WDTN (Y,RDISK,RBUB,VINF,WY,EQN)
      EQN = 'WZ'
      CALL WDTN (Y,RDISK,RBUB,VINF,WZ,EQN)
C
      EQN = 'UX'
      CALL UDTN (Y,RDISK,RBUB,VINF,WX,WY,WZ,UX,EQN)
      EQN = 'UY'
      CALL UDTN (Y,RDISK,RBUB,VINF,WX,WY,WZ,UY,EQN)
      EQN = 'UZ'
      CALL UDTN (Y,RDISK,RBUB,VINF,WX,WY,WZ,UZ,EQN)
C
      F(1) = WY*DCOS(Y(2)) - WX*DSIN(Y(2))
C
      IF (DABS(DTAN(Y(1)))>.LT.(1.0D-2)) THEN
        IF (DTAN(Y(1))>.LT.(0.0D0)) THEN
          F(2) = WZ + (WX*DCOS(Y(2)) + WY*DSIN(Y(2))) / 1.0D-2
        ELSE

```

```

      F(2) = WZ - (WX*DCOS(Y(2)) + WY*DSIN(Y(2))) / 1.0D-2
    ENDIF
  ELSE
    F(2) = WZ - (WX*DCOS(Y(2)) + WY*DSIN(Y(2))) / DTAN(Y(1))
  ENDIF
C
  F(3) = UX
  F(4) = UY
  F(5) = UZ
C
  RETURN
END

```

```

      SUBROUTINE RINTEG2 (Y,RDISK,RBUB,VINF,WX,WY,WZ,UX,UY,UZ)
C
C This subroutine calls the subroutines WDTN and UDTN to solve the double
C integrals which define the rotational velocities (wx, wy, wz) and the
C translational velocities (Ux, Uy, and Uz) of the disk.
C
      DOUBLE PRECISION Y,RDISK,RBUB,VINF,WX,WY,WZ,UX,UY,UZ
      CHARACTER*2 EQN
      DIMENSION Y(5)
C
      EQN = 'WX'
      CALL WDTN (Y,RDISK,RBUB,VINF,WX,EQN)
      EQN = 'WY'
      CALL WDTN (Y,RDISK,RBUB,VINF,WY,EQN)
      EQN = 'WZ'
      CALL WDTN (Y,RDISK,RBUB,VINF,WZ,EQN)
C
      EQN = 'UX'
      CALL UDTN (Y,RDISK,RBUB,VINF,WX,WY,WZ,UX,EQN)
      EQN = 'UY'
      CALL UDTN (Y,RDISK,RBUB,VINF,WX,WY,WZ,UY,EQN)
      EQN = 'UZ'
      CALL UDTN (Y,RDISK,RBUB,VINF,WX,WY,WZ,UZ,EQN)
C
      RETURN
END

```

```

      SUBROUTINE RIUDR (Y,TH,RDISK,RBUB,VINF,WX,WY,WZ,UTH,EQN)
C
C This subroutine uses Romberg integration to calculate the integral in
C Ux, Uy, or Uz with respect to dr (thus theta (TH) is held constant) to
C within a given error value (ERRMAX). The integral being solved (wx,
C Uy, or Uz) is defined by the string value of EQN. The integration
C depends upon the values of theta (TH), alpha (Y(1)), beta (Y(2)), Ox
C (Y(3)), Oy (Y(4)), Oz (Y(5)), disk radius (RDISK), bubble radius
C (RBUB), and the velocity of the undisturbed flow (VINF).
C
      DOUBLE PRECISION Y,TH,RDISK,RBUB,VINF,WX,WY,WZ,UR,UTH,G,ERROR,ERRMAX
      CHARACTER*2 EQN
      DIMENSION Y(5),G(6,6)
C
C Set iteration number (I), number of steps (N) to 1, maximum number of

```

```

C iterations (MAXIT) and the maximum allowed error (ERRMAX).
  I=0
  N=1
  MAXIT=5
  ERRMAX = 1.0D-6
C
C Subroutine udr calculates the value of the integral (UR) using the
C trapazoidal rule for a given number of steps (N).
  CALL UDR (N,Y,TH,RDISK,RBUB,VINF,WX,WY,WZ,UR,EQN)
C
C Romberg integration takes two estimates of the integral and
C calculates a third, more accurate estimate. We begun by taking two
C calculations of the integral with different step sizes, G(1,1) and G(2,1),
C and calculate a third value, G(2,1). We continue to do this for a larger
C number step sizes in an iterative process until the calculated error is
C within an acceptable value.
C
  G(1,1) = UR
C
10  CONTINUE
    I = I+1
    N = 2**I
    CALL UDR (N,Y,TH,RDISK,RBUB,VINF,WX,WY,WZ,UR,EQN)
    G(I+1,1) = UR
C
    DO 20 K=2,I+1
      J = 2+I-K
      G(J,K) = (4**(K-1)*G(J+1,K-1) - G(J,K-1))/(4**(K-1) - 1)
20  CONTINUE
C
C Calculate error and compare to maximum allow error.
  ERROR = ABS((G(J,I+1) - G(J,I))/G(J,I+1))
  IF ((ERROR.GT.ERRMAX).AND.(I.LT.MAXIT)) GOTO 10
C
C If ERROR has not dropped below ERRMAX within the allowed number of
C iterations, assume Romberg integration will not converge and assign UTH
C as the last value obtained with the trapezoidal rule in subroutine UDR.
C Otherwise, set UTH to the integraion estimate form the Romberg method.
  IF (ERROR.GT.ERRMAX) THEN
    UTH = UR
  ELSE
    UTH = G(J,I+1)
  ENDIF
C
  RETURN
  END

```

```

SUBROUTINE RIWDR (Y,TH,RDISK,RBUB,VINF,WTH,EQN)
C
C This subroutine uses Romberg integration to calculate the integral in
C wx, wy, or wz with respect to dr (thus theta (TH) is held constant) to
C within a given error value (ERRMAX). The integral being solved (wx,
C wy, or wz) is defined by the string value of EQN. The integration
C depends upon the values of theta (TH), alpha (Y(1)), beta (Y(2)), Ox
C (Y(3)), Oy (Y(4)), Oz (Y(5)), disk radius (RDISK), bubble radius
C (RBUB), and the velocity of the undisturbed flow (VINF).
C
  DOUBLE PRECISION Y,TH,RDISK,RBUB,VINF,WR,WTH,G,ERROR,ERRMAX

```

```

      CHARACTER*2 EQN
      DIMENSION Y(5),G(6,6)
C
C Set iteration number (I), number of steps (N) to 1, maximum number of
C iterations (MAXIT) and the maximum allowed error (ERRMAX).
      I=0
      N=1
      MAXIT=5
      ERRMAX = 1.0D-6
C
C Subroutine wdr calculates the value of the integral (WR) using the
C trapezoidal rule for a given number of steps (N).
      CALL WDR (N,Y,TH,RDISK,RBUB,VINF,WR,EQN)
C
C Romberg integration takes two estimates of the integral and
C calculates a third, more accurate estimate. We begun by taking two
C calculations of the integral with different step sizes, G(1,1) and G(2,1),
C and calculate a third value, G(2,1). We continue to do this for a larger
C number step sizes in an iterative process until the calculated error is
C within an acceptable value.
C
      G(1,1) = WR
C
C 10 CONTINUE
      I = I+1
      N = 2**I
      CALL WDR (N,Y,TH,RDISK,RBUB,VINF,WR,EQN)
      G(I+1,1) = WR
C
      DO 20 K=2,I+1
        J = 2+I-K
        G(J,K) = (4**(K-1)*G(J+1,K-1) - G(J,K-1))/(4**(K-1) - 1)
C
      20 CONTINUE
C
C Calculate error and compare to maximum allow error.
      ERROR = ABS((G(J,I+1) - G(J,I))/G(J,I+1))
      IF ((ERROR.GT.ERRMAX).AND.(I.LT.MAXIT)) GOTO 10
C
C If ERROR has not dropped below ERRMAX within the allowed number of
C iterations, assume Romberg integration will not converge and assign WTH
C as the last value obtained with the trapezoidal rule in subroutine WDR.
C Otherwise, set WTH to the integraion estimate form the Romberg method.
      IF (ERROR.GT.ERRMAX) THEN
        WTH = WR
      ELSE
        WTH = G(J,I+1)
      ENDIF
C
      RETURN
      END

```

```

      SUBROUTINE RK4C (NEQ,T,Y,H,RDISK,RBUB,VINF)
C This subroutine solves the differential equations by using the 4th
C order Runge-Kutta method. RINTEG subroutine is called to solve the double
C integrals. The variables used in the integrations include alpha (Y(1)),
C beta (Y(2)), Ox (Y(3)), Oy (Y(4)), Oz (Y(5)), disk radius (RDISK),
C bubble radius (RBUB), and the velocity of the undisturbed flow (VINF).

```

C H is the step size, T is the independent variable time, and K1 - K4 are
C variables used in the Runge-Kutta method.

```

C
      DOUBLE PRECISION T,TN,Y,YN,H,RDISK,RBUB,VINF,K1,K2,K3,K4
      DIMENSION Y(NEQ),YN(NEQ),K1(NEQ),K2(NEQ),K3(NEQ),K4(NEQ)
C
C Calculate K1 for all equations.
      DO 10 I=1,NEQ
        YN(I) = Y(I)
10    CONTINUE
      TN = T
      CALL RINTEG (YN,RDISK,RBUB,VINF,K1)
C
C Calculate K2 for all equations.
      DO 20 I=1,NEQ
        YN(I) = Y(I) + 0.5D0*H*K1(I)
20    CONTINUE
      TN = T + 0.5D0*H
      CALL RINTEG (YN,RDISK,RBUB,VINF,K2)
C
C Calculate K3 for all equations.
      DO 30 I=1,NEQ
        YN(I) = Y(I) + 0.5D0*H*K2(I)
30    CONTINUE
      TN = T + 0.5D0*H
      CALL RINTEG (YN,RDISK,RBUB,VINF,K3)
C
C Calculate K4 for all equations.
      DO 40 I=1,NEQ
        YN(I) = Y(I) + H*K3(I)
40    CONTINUE
      TN = T + H
      CALL RINTEG (YN,RDISK,RBUB,VINF,K4)
C
C Update the value of Y at time (T+H)
      DO 50 I=1,NEQ
        Y(I) = Y(I) + H/6.0D0 * (K1(I)+2.0D0*K2(I)+2.0D0*K3(I)+K4(I))
50    CONTINUE
C
      RETURN
      END

```

SUBROUTINE UDR (N,Y,TH,RDISK,RBUB,VINF,WX,WY,WZ,UR,EQN)

```

C
C This subroutine uses the trapezoidal rule to solve the integral for
C disk translational velocities (Ux, Uy, or Uz) with respect to dr at a
C constant theta (TH) for a given number of steps (N). The integral being
C solved (Ux, Uy, or Uz) is defined by the string value of EQN. The
C integration depends upon the number of steps, N, and the values of
C theta (TH), alpha (Y(1)), beta (Y(2)), Ox (Y(3)), Oy (Y(4)), Oz (Y(5)),
C disk radius (RDISK), bubble radius (RBUB), the velocity of the
C undisturbed flow (VINF), and the x, y, and z components of the disk
C angular velocity (WX, WY, WZ).
C
      DOUBLE PRECISION A,B,H,R,Y,TH,RDISK,RBUB,VINF,WX,WY,WZ,RX,RY,RZ,
      & VX,VY,VZ,UR,SUM,F
      CHARACTER*2 EQN
      DIMENSION Y(5)

```

```

C
C Set integration limits, A and B, to 0.0 and RDISK respectively
C
    A = 0.0D0
    B = RDISK
C
C H is the step size used in the integration
C
    H=(B-A)/N
    R=A
    CALL VARBLs (Y,TH,R,RBUB,VINF,RX,RY,RZ,VX,VY,VZ)
C
C F is the value of the function within the integral for a given value of R.
C The equation used to determine F depend upon the string value of EQN
C where EQN will be either 'UX', 'UY', or 'UZ'.
C
    IF (EQN.EQ.'UX') THEN
        F = (VX - (WY*RZ - WZ*RY)) * R
    ELSEIF (EQN.EQ.'UY') THEN
        F = (VY - (WZ*RX - WX*RZ)) * R
    ELSEIF (EQN.EQ.'UZ') THEN
        F = (VZ - (WX*RY - WY*RX)) * R
    ELSE
        PRINT*, 'EQN not defined correctly in subroutine udr!'
        STOP
    ENDIF
C
    SUM = F
C
    DO 10 I=1, N-1
        R = R+H
        CALL VARBLs (Y,TH,R,RBUB,VINF,RX,RY,RZ,VX,VY,VZ)
C
        IF (EQN.EQ.'UX') THEN
            F = (VX - (WY*RZ - WZ*RY)) * R
        ELSEIF (EQN.EQ.'UY') THEN
            F = (VY - (WZ*RX - WX*RZ)) * R
        ELSEIF (EQN.EQ.'UZ') THEN
            F = (VZ - (WX*RY - WY*RX)) * R
        ENDIF
C
        SUM = SUM + 2.0D0*F
10  CONTINUE
C
    R=B
    CALL VARBLs (Y,TH,R,RBUB,VINF,RX,RY,RZ,VX,VY,VZ)
C
    IF (EQN.EQ.'UX') THEN
        F = (VX - (WY*RZ - WZ*RY)) * R
    ELSEIF (EQN.EQ.'UY') THEN
        F = (VY - (WZ*RX - WX*RZ)) * R
    ELSEIF (EQN.EQ.'UZ') THEN
        F = (VZ - (WX*RY - WY*RX)) * R
    ENDIF
C
    SUM = SUM + F
C
    UR = (B-A) * SUM/(2*N)
C
    RETURN
END

```

```

      SUBROUTINE UDTH (Y,RDISK,RBUB,VINF,WX,WY,WZ,U,EQN)
C
C This subroutine uses Simpson's rule to solve the integral for
C disk translational velocities (Ux, Uy, or Uz) for a given number of steps
C (N) with respect to theta (TH). (Solving the second integral with
C respect to r is done in the later subroutine udr). The integral being
C solved (Ux, Uy, or Uz) is defined by the string value of EQN. The
C integration depends upon the number of steps, N, and the values of
C alpha (Y(1)), beta (Y(2)), Ox (Y(3)), Oy (Y(4)), Oz (Y(5)), disk radius
C (RDISK), bubble radius (RBUB), the velocity of the undisturbed flow
C (VINF), and the X, y, and z components of the disk angular velocity
C (WX, WY, WZ).
C
      DOUBLE PRECISION A,B,H,Y,TH,RDISK,RBUB,VINF,WX,WY,WZ,U,SUM,UTH,PI
      CHARACTER*2 EQN
      DIMENSION Y(5)
C
C Set integration limits, A and B, to 0.0 and 2*pi respectively
C
      PI = 3.141592653589793D0
      A = 0.0D0
      B = 2.0D0*PI
      N = 32
C
C H is the step size used in the integration
C
      H = (B-A)/N
      TH = A
      CALL RIUDR (Y,TH,RDISK,RBUB,VINF,WX,WY,WZ,UTH,EQN)
      SUM = UTH
C
      TH = A + H
C
      DO 10 I=1, N-1, 2
        TH = TH + 2.0D0*H
        CALL RIUDR (Y,TH,RDISK,RBUB,VINF,WX,WY,WZ,UTH,EQN)
        SUM = SUM + 4.0D0*UTH
10    CONTINUE
C
      TH = A
C
      DO 20 I=1, N-2, 2
        TH = TH + 2.0D0*H
        CALL RIUDR (Y,TH,RDISK,RBUB,VINF,WX,WY,WZ,UTH,EQN)
        SUM = SUM + 2.0D0*UTH
20    CONTINUE
C
      TH = B
      CALL RIUDR (Y,TH,RDISK,RBUB,VINF,WX,WY,WZ,UTH,EQN)
      SUM = SUM + UTH
C
      U = 1.0D0/(PI*RDISK**2) * (B-A) * SUM/(3*N)
C
      RETURN
      END

```

```

      SUBROUTINE VARBL5 (Y,TH,R,RBUB,VINF,RX,RY,RZ,VX,VY,VZ)
C
C This subroutine calculates the value of rx, ry, rz, Vx, Vy, and Vz from
C the variables theta (TH), alpha (Y(1)), beta (Y(2)), Ox (Y(3)), Oy
C (Y(4)), Oz (Y(5)), r (R), bubble radius (RBUB), and the velocity of
C undisturbed flow (VINF).
      DOUBLE PRECISION Y,TH,R,RBUB,VINF,RX,RY,RZ,VX,VY,VZ,XX,YY,ZZ,BOT
      DIMENSION Y(5)
C
C Calculate rx, ry, rz, the three components of the position vector which
C points from the disk origin to the point defined by r (R) and theta
C (TH). Since rx, ry, and rz are in space-fixed coordinates and r and
C theta are in particle-fixed coordinates, the two disk rotation
C angles, alpha (Y(1)) and beta (Y(2)), are also required.
C
      RX= R*DCOS(TH)*DCOS(Y(1))*DCOS(Y(2)) - R*DSIN(TH)*DSIN(Y(2))
      RY= R*DCOS(TH)*DCOS(Y(1))*DSIN(Y(2)) + R*DSIN(TH)*DCOS(Y(2))
      RZ=-R*DCOS(TH)*DSIN(Y(1))
C
C Calculate fluid velocities Vx, Vy, Vz by using the equations for
C potential flow around a sphere.
C
      XX = RX+Y(3)
      YY = RY+Y(4)
      ZZ = RZ+Y(5)
      BOT= 2.0D0 * (XX**2+YY**2+ZZ**2)**2.5D0
C
      VX = 3.0D0 * VINF * RBUB**3 * XX * YY / BOT
      VY =-VINF * (1.0D0 - RBUB**3 * (2.0D0*YY**2 - XX**2 - ZZ**2)/BOT)
      VZ = 3.0D0 * VINF * RBUB**3 * ZZ * YY /BOT
C
      RETURN
      END

```

```

      SUBROUTINE WDR (N,Y,TH,RDISK,RBUB,VINF,WR,EQN)
C
C This subroutine uses the trapazoidal rule to solve the integral for
C disk rotational velocities (wx, wy, or wz) with respect to dr at a
C constant theta (TH) for a given number of steps (N). The integral being
C solved (wx, wy, or wz) is defined by the string value of EQN. The
C integration depends upon the number of steps, N, and the values of
C theta (TH), alpha (Y(1)), beta (Y(2)), Ox (Y(3)), Oy (Y(4)), Oz (Y(5)),
C disk radius (RDISK), bubble radius (RBUB), and the velocity of the
C undisturbed flow (VINF).
C
      DOUBLE PRECISION A,B,H,R,Y,TH,RDISK,RBUB,VINF,RX,RY,RZ,VX,VY,VZ,WR,
& SUM,F
      CHARACTER*2 EQN
      DIMENSION Y(5)
C
C Set integration limits, A and B, to 0.0 and RDISK respectively
C
      A = 0.0D0
      B = RDISK
C
C H is the step size used in the integration
C
      H=(B-A)/N

```



```

      R=A
      CALL VARBL5 (Y,TH,R,RBUB,VINF,RX,RY,RZ,VX,VY,VZ)
C
C F is the value of the function within the integral for a given value of R.
C The equation used to determine F depend upon the string value of EQN
C where EQN will be either 'WX', 'WY', or 'WZ'.
C
      IF (EQN.EQ.'WX') THEN
        F = (RY*VZ - RZ*VY) * R
      ELSEIF (EQN.EQ.'WY') THEN
        F = (RZ*VX - RX*VZ) * R
      ELSEIF (EQN.EQ.'WZ') THEN
        F = (RX*VY - RY*VX) * R
      ELSE
        PRINT*,'EQN not defined correctly in subroutine wdr!'
        STOP
      ENDIF
C
      SUM = F
C
      DO 10 I=1, N-1
        R = R+H
        CALL VARBL5 (Y,TH,R,RBUB,VINF,RX,RY,RZ,VX,VY,VZ)
C
        IF (EQN.EQ.'WX') THEN
          F = (RY*VZ - RZ*VY) * R
        ELSEIF (EQN.EQ.'WY') THEN
          F = (RZ*VX - RX*VZ) * R
        ELSEIF (EQN.EQ.'WZ') THEN
          F = (RX*VY - RY*VX) * R
        ENDIF
C
        SUM = SUM + 2.0D0*F
10    CONTINUE
C
      R=B
      CALL VARBL5 (Y,TH,R,RBUB,VINF,RX,RY,RZ,VX,VY,VZ)
C
      IF (EQN.EQ.'WX') THEN
        F = (RY*VZ - RZ*VY) * R
      ELSEIF (EQN.EQ.'WY') THEN
        F = (RZ*VX - RX*VZ) * R
      ELSEIF (EQN.EQ.'WZ') THEN
        F = (RX*VY - RY*VX) * R
      ENDIF
C
      SUM = SUM + F
C
      WR = (B-A) * SUM/(2*N)
C
      RETURN
      END

```

```

      SUBROUTINE WDR (Y,RDISK,RBUB,VINF,W,EQN)
C
C This subroutine uses Simpson's rule to solve the integral for
C disk rotational velocities (wx, wy, or wz) for a given number of steps
C (N) with respect to theta (TH). (Solving the second integral with
C respect to r is done in the later subroutine wdr). The integral being
C solved (wx, wy, or wz) is defined by the string value of EQN. The
C integration depends upon the number of steps, N, and the values of
C alpha (Y(1)), beta (Y(2)), Ox (Y(3)), Oy (Y(4)), Oz (Y(5)), disk radius
C (RDISK), bubble radius (RBUB), and the velocity of the undisturbed flow
C (VINF).
C
      DOUBLE PRECISION A,B,H,Y,TH,RDISK,RBUB,VINF,W,SUM,WTH,PI
      CHARACTER*2 EQN
      DIMENSION Y(5)
C
C Set integration limits, A and B, to 0.0 and 2*pi respectively
C
      PI = 3.141592653589793D0
      A = 0.0D0
      B = 2.0D0*PI
      N = 32
C
C H is the step size used in the integration
C
      H = (B-A)/N
      TH = A
      CALL RIWDR (Y,TH,RDISK,RBUB,VINF,WTH,EQN)
      SUM = WTH
C
      TH = A + H
C
      DO 10 I=1, N-1, 2
        TH = TH + 2.0D0*H
        CALL RIWDR (Y,TH,RDISK,RBUB,VINF,WTH,EQN)
        SUM = SUM + 4.0D0*WTH
      10 CONTINUE
C
      TH = A
C
      DO 20 I=1, N-2, 2
        TH = TH + 2.0D0*H
        CALL RIWDR (Y,TH,RDISK,RBUB,VINF,WTH,EQN)
        SUM = SUM + 2.0D0*WTH
      20 CONTINUE
C
      TH = B
      CALL RIWDR (Y,TH,RDISK,RBUB,VINF,WTH,EQN)
      SUM = SUM + WTH
C
      W = 2.0D0/(PI*RDISK**4) * (B-A)*SUM/(3*N)
C
      RETURN
      END

```

A.2.2 Sample Input File

The following is the input file HIN used with HMODP to calculate the disk trajectory for the disk in potential flow shown in Fig. 5.5:

```
Hmodp run. Sample disk in potential flow.
alpha      beta      Ox      Oy      Oz
90.0       0.0       0.28     3.000    0.000

Disk-radius  Bub-radius V-infinity  H      Max-steps  Print-int
.20         1.00      200.     0.00005   2500      20
```

A.2.3 Sample Output File

The output file HOUT after running HMODP with the input file above:

```
Hmodp run. Sample disk in potential flow.
Initial Data
alpha : 90.00000 Disk-radius : .20000
beta : .00000 Bub-radius : 1.00000
Ox : .28000 V-infinity : 200.00000
Oy : 3.00000 H : .50000E-04
Oz : .00000 Max-steps : 2500
Print-int : 20

Time Alpha Beta Ox Oy Oz
(seconds) (degrees) (degrees) (mm) (mm) (mm)
.10000E-02 90.00000 .04589 .28117 2.80799 .00000
.20000E-02 90.00000 .11089 .28271 2.61775 .00000
.30000E-02 90.00000 .20510 .28478 2.42981 .00000
.40000E-02 90.00000 .34516 .28760 2.24491 .00000
.50000E-02 90.00000 .55924 .29155 2.06404 .00000
.60000E-02 90.00000 .89628 .29717 1.88855 .00000
.70000E-02 90.00000 1.44334 .30537 1.72026 .00000
.80000E-02 90.00000 2.35672 .31760 1.56147 .00000
.90000E-02 90.00000 3.91220 .33612 1.41480 .00000
.10000E-01 90.00000 6.55714 .36436 1.28241 .00000
.11000E-01 90.00000 10.84577 .40697 1.16446 .00000
.12000E-01 90.00000 16.92854 .46919 1.05676 .00000

Final Disk Position
.12550E-01 90.00000 20.65198 .51328 .99846 .00000

Number of iterations = 251
Minimum separation distance: -.000462

Disk has contacted bubble on the disk edge.
Incident angle of disk with bubble surface: 33.60954

Contact Point x: .58382 y: .81132 z: .00000
Disk Velocity Ux: 86.86842 Uy: -107.28297 Uz: .00000
Angular Vel. Wx: .00000 Wy: .00000 Wz: 116.68822
Disk Velocity Uth: 126.30709 Ur: -55.69809 Uphi: .00000
Point Vel. Uxc: 108.70639 Uyc: -99.05200 Uzc: .00000
Point Vel. Uthc: 146.09098 Urc: -16.90572 Uphic: .00000
```

A.3 COLMOD Program

A.3.1 Fortran Code

```

      PROGRAM COLMOD
C This program uses the secant method and the hmodp subroutine to
C determine the initial Ox position at which the disk just barely hits
C bubble surface. See the hmodp subroutine for a description of how it
C works as well as definition of variables.
      INTEGER PRINTI
      DOUBLE PRECISION Y,YI,H,RDISK,RBUB,VINF,SEPMIN,THETA
      DIMENSION Y(5),YI(5)
      CHARACTER*12 LABEL(11)
      CHARACTER*55 TITLE

C
      OPEN(UNIT=1,FILE='cin',STATUS='OLD')
      OPEN(UNIT=2,FILE='hout',STATUS='NEW')
      OPEN(UNIT=3,FILE='cout',STATUS='NEW')

C
C Call subroutine CDATIN to input data
      CALL CDATIN(Y,RDISK,RBUB,VINF,H,MAXSTP,PRINTI,LABEL,SEPMAX,NMAX,
&               TITLE,X1)

C
C Set initial values of Y
      DO 10 I=1,5
         YI(I) = Y(I)
10    CONTINUE

C
C Write title info to hout file
      WRITE(2,*) TITLE
      WRITE(2,*)
      WRITE(2,*) 'Individual runs:'
      WRITE(2,*)

C
C Set initial value of X2 for secant method equation. calculate minimum
C separation distance (SEPMIN) for that value by calling HMODP subroutine.
C Set initial value of S2 as SEPMIN
      X2 = YI(3)
      CALL HMODP (Y,RDISK,RBUB,VINF,H,MAXSTP,PRINTI,LABEL,SEPMIN,THETA)
      S2 = SEPMIN

C
C Reset Y to initial values
      DO 20 I=1,5
         Y(I) = YI(I)
20    CONTINUE

C Set Y(3) to X1 and find SEPMIN. Set initial value of S1.
      Y(3) = X1
      CALL HMODP (Y,RDISK,RBUB,VINF,H,MAXSTP,PRINTI,LABEL,SEPMIN,THETA)
      S1 = SEPMIN

C
C Set NSTEP to 2 (NSTEP is how many time HMODP has been called)
      NSTEP = 2

C
C Beginning of loop. Calculate new value of Y(3) (XNEW) using Secant
C method. Reset Y values and set Y(3) to XNEW. Calculate SEPMIN. If
C SEPMIN is less than SEPMAX, repeat loop.
30    CONTINUE
         XNEW = X2 - (S2 * (X1 - X2))/(S1 - S2)

C

```

```

DO 40 I=1,5
  Y(I) = YI(I)
40 CONTINUE
C
  Y(3) = XNEW
  CALL HMODP (Y,RDISK,RBUB,VINF,H,MAXSTP,PRINTI,LABEL,SEPMIN,
    &          THETA)
C
  X1 = X2
  X2 = XNEW
  S1 = S2
  S2 = SEPMIN
  NSTEP = NSTEP + 1
  IF ((ABS(SEPMIN).GT.SEPMAX).AND.(NSTEP.LT.NMAX)) GOTO 30
C
C Write results to file cout
  WRITE(3,100) XNEW
  WRITE(3,110) SEPMIN
  WRITE(3,120) NSTEP
C
100 FORMAT (1x,'Critical value of Ox:',F8.5)
110 FORMAT (1x,'Separation distance: ',F9.6)
120 FORMAT (1x,'Number of iterations: ',I2)
C
  END

```

```

SUBROUTINE CDATIN(Y,RDISK,RBUB,VINF,H,MAXSTP,PRINTI,LABEL,SEPMAX,
  &               NMAX,TITLE,X1)
C This subroutine inputs starting disk position and orientation (Y), disk
C radius (RDISK), bubble radius (RBUB), the velocity at infinity (VINF),
C the step size for the runga-kutta method (H), the maximum number of
C iterations that will be performed before the program stops (MAXSTP), and
C the interval at which data will be written to out data file (PRINTI).
C Initial data is also written to the output file.
C
  INTEGER PRINTI
  CHARACTER*12 LABEL(11)
  CHARACTER*14 LABEL2,LABEL3,LABEL4
  CHARACTER*55 TITLE
  DOUBLE PRECISION Y,RDISK,RBUB,VINF,H,PI
  DIMENSION Y(5)
C
  READ(1,5) TITLE
5  FORMAT (A55)
  READ(1,*) (LABEL(I),I=1,5)
  READ(1,*) (Y(I),I=1,5)
  READ(1,*)
  READ(1,*) (LABEL(I),I=6,11)
  READ(1,*) RDISK,RBUB,VINF,H,MAXSTP,PRINTI
  READ(1,*)
  READ(1,*) LABEL2,LABEL3,LABEL4
  READ(1,*) NMAX,SEPMAX,X1
C
  WRITE(3,*) TITLE
  WRITE(3,*)
  WRITE(3,*) '          Initial Data'
  WRITE(3,10) LABEL(1),Y(1),LABEL(6),RDISK

```

```

WRITE(3,10) LABEL(2),Y(2),LABEL(7),RBUB
WRITE(3,10) LABEL(3),Y(3),LABEL(8),VINP
WRITE(3,20) LABEL(4),Y(4),LABEL(9),H
WRITE(3,30) LABEL(5),Y(5),LABEL(10),MAXSTP
WRITE(3,40) LABEL(11),PRINTI
WRITE(3,50) LABEL2,NMAX,LABEL3,SEPMAX
WRITE(3,60) LABEL4,X1
WRITE(3,*)

```

```

C
10  FORMAT (1X,A6,' ':',F10.5,4X,A,' ':',F10.5)
20  FORMAT (1X,A6,' ':',F10.5,4X,A,' ':',E12.5)
30  FORMAT (1X,A6,' ':',F10.5,4X,A,' ':',I7)
40  FORMAT (1X,22X,A,' ':',I4)
50  FORMAT (1X,A12,' ':',I4,4X,A,' ':',F9.6)
60  FORMAT (1X,A12,' ':',F8.4)

```

```

C
RETURN
END

```

```

SUBROUTINE DATAIN(Y,RDISK,RBUB,VINF,H,MAXSTP,PRINTI,LABEL)
C This subroutine prints starting disk position and orientation (Y), disk
C radius (RDISK), bubble radius (RBUB), the velocity at infinity (VINF),
C the step size for the runga-kutta method (H), the maximum number of
C iterations that will be performed before the program stops (MAXSTP), and
C the interval at which data will be written to out data file (PRINTI).
C Initial data is written to the output file hout.

```

```

C
INTEGER PRINTI
CHARACTER*12 LABEL(11)
DOUBLE PRECISION Y,RDISK,RBUB,VINF,H,PI
DIMENSION Y(5)

C
WRITE(2,*) ' Initial Data'
WRITE(2,10) LABEL(1),Y(1),LABEL(6),RDISK
WRITE(2,10) LABEL(2),Y(2),LABEL(7),RBUB
WRITE(2,10) LABEL(3),Y(3),LABEL(8),VINF
WRITE(2,20) LABEL(4),Y(4),LABEL(9),H
WRITE(2,30) LABEL(5),Y(5),LABEL(10),MAXSTP
WRITE(2,40) LABEL(11),PRINTI
WRITE(2,*)
WRITE(2,50)
WRITE(2,60)

```

```

C
PI = 3.141592653589793D0
Y(1) = Y(1)/180.0D0*PI
Y(2) = Y(2)/180.0D0*PI

C
10  FORMAT (1X,A6,' ':',F10.5,4X,A,' ':',F10.5)
20  FORMAT (1X,A6,' ':',F10.5,4X,A,' ':',E12.5)
30  FORMAT (1X,A6,' ':',F10.5,4X,A,' ':',I7)
40  FORMAT (1X,22X,A,' ':',I4)
50  FORMAT (6X,'Time',7X,'Alpha',5X,'Beta',7X,'Ox',8X,'Oy',8X,'Oz')
60  FORMAT (3X,'(seconds)',3X,'(degrees)',1X,'(degrees)',3X,'(mm)',6X,
&      '(mm)',6X,'(mm)')

```

```

C
RETURN
END

```

```

      SUBROUTINE DATOUT(T,Y,CONTCT,CONTYP,ISTEP,MAXSTP,A,SEPMIN,XP,YP,
& RDISK,RBUB,VINF,THETA)
C This subroutine writes to the output file the final disk position and
C orientation and whether the disk contacted the bubble. Contact
C information is determined by the value of CONTYP. It also computes
C and writes the disk velocities, the velocity of the point of the disk
C contacting the bubble, and the angle between the plane containing the
C disk and the plane tangent to the bubble at the point of contact
C (THETA).
C
      INTEGER CONTCT,CONTYP
      DOUBLE PRECISION T,Y,PI,SEPMIN,A,XP,YP,Y1,Y2,RDISK,RBUB,VINF,
& WX,WY,WZ,UX,UY,UZ,XC,YC,ZC,XD,YD,ZD,TOP,BOT,THETA,UTH,UR,
& UXC,UYC,UZC,UTHC,URC,TH,THC,PHI,PHIC,UPHI,UPHIC
      DIMENSION Y(5)

C
      PI = 3.141592653589793D0

C
C Convert angles from radians to degrees.
      Y1 = Y(1)*180.0D0/PI
      Y2 = Y(2)*180.0D0/PI

C
      WRITE(2,*)
      WRITE(2,*) '                Final Disk Position'
      WRITE(2,10) T,Y1,Y2,(Y(I),I=3,5)
      WRITE(2,*)
      WRITE(2,20) ISTEP
      WRITE(2,25) SEPMIN
      WRITE(2,*)

C
      IF (CONTYP.EQ.0) WRITE(2,30)
      IF (CONTYP.EQ.1) WRITE(2,40)
      IF (CONTYP.EQ.2) WRITE(2,50) A
      IF (CONTYP.EQ.3) THEN
        WRITE(2,60) MAXSTP
        STOP
      ENDIF

C
      IF (CONTYP.EQ.1.OR.CONTYP.EQ.2) THEN
C Calculate the point at which the bubble and disk contact (XC, YC, and
C ZC) from values of XP and YP (values of X and Y in particle fixed
C coordinates, calculated in subroutine chkcon) and alpha (Y(1)), beta,
C (Y(2)), Ox (Y(3)), Oy (Y(4)), and Oz (Y(5)).
        XC = DCOS(Y(1))*DCOS(Y(2))*XP - DSIN(Y(2))*YP + Y(3)
        YC = DCOS(Y(1))*DSIN(Y(2))*XP + DCOS(Y(2))*YP + Y(4)
        ZC = -DSIN(Y(1))*XP + Y(5)

C
C Calculate coordinates of a unit vector normal to the disk (XD,YD,ZD).
        XD = DSIN(Y(1))*DCOS(Y(2))
        YD = DSIN(Y(1))*DSIN(Y(2))
        ZD = DCOS(Y(1))

C
C The incident angle of collision (THETA) is the dot product of the disk
C vector and the vector to the point of collision (which vector defines a
C plane tangent to the bubble at the point of contact).
        TOP = XC*XD + YC*YD + ZC*ZD
        TOP = DABS(TOP)
        BOT = DSQRT(XC**2 + YC**2 + ZC**2)
        THETA = DACOS(TOP/BOT)
        THETA = THETA*180.0D0/PI
C

```

```

C Subroutine RINTEG2 calculates translational (UX, UY, UZ) and angular
C velocities (WX, WY, WZ) of the disk at the time of contact.
      CALL RINTEG2 (Y,RDISK,RBUB,VINF,WX,WY,WZ,UX,UY,UZ)
C
C Calculate the disk velocity in the R and theta directions (UR and UTH).
      TH = DATAN( DSQRT(Y(3)**2 + Y(5)**2) / Y(4) )
      PHI = DATAN(Y(5)/Y(3))
      IF (PHI.LT.0.0D0.AND.Y(3).LT.0.0D0) PHI = PHI + PI
      UTH = -DSIN(TH)*UY + DCOS(TH)*(SIN(PHI)*UZ + COS(PHI)*UX)
      UR = DCOS(TH)*UY + DSIN(TH)*(SIN(PHI)*UZ + COS(PHI)*UX)
      UPHI = -DSIN(PHI)*UX +DCOS(PHI)*UZ
C
C Calculate the velocity of the edge or side of disk contacting the bubble
C (UXC, UYC, UZC) including the velocity in the R and theta directions
C (URC, UTHC).
      UXC = UX + WY*(ZC - Y(5)) - WZ*(YC - Y(4))
      UYC = UY + WZ*(XC - Y(3)) - WX*(ZC - Y(5))
      UZC = UZ + WX*(YC - Y(4)) - WY*(XC - Y(3))
      THC = DATAN( DSQRT(XC**2 + ZC**2) / YC )
      PHIC = DATAN(ZC/XC)
      IF (PHIC.LT.0.0D0.AND.XC.LT.0.0D0) PHIC = PHIC + PI
      UTHC = -DSIN(THC)*UYC + DCOS(THC)*(SIN(PHIC)*UZC +
&          COS(PHIC)*UXC)
      URC = DCOS(THC)*UYC + DSIN(THC)*(SIN(PHIC)*UZC +
&          COS(PHIC)*UXC)
      UPHIC = -DSIN(PHIC)*UXC +DCOS(PHIC)*UZC
C
C Write information to file
      WRITE(2,110) THETA
      WRITE(2,*)
      WRITE(2,100) XC, YC, ZC
      WRITE(2,120) UX, UY, UZ
      WRITE(2,130) WX, WY, WZ
      WRITE(2,140) UTH, UR, UPHI
      WRITE(2,150) UXC, UYC, UZC
      WRITE(2,160) UTHC, URC, UPHIC
C
      ENDIF
C
      WRITE(2,*)
      WRITE(2,*) '-----'
C
10  FORMAT (1X,E12.5,F10.5,F10.5,F10.5,F10.5,F10.5)
20  FORMAT (1X,'Number of iterations = ',I6)
25  FORMAT (1X,'Minimum separation distance: ',F9.6)
30  FORMAT (1X,'Disk has missed contacting bubble.')
40  FORMAT (1X,'Disk has contacted bubble on the disk edge.')
50  FORMAT (1X,'Disk has contacted bubble on the disk side.  A = ',
& F10.5)
60  FORMAT (1X,'Maximum number of iterations exceeded! Max. steps = ',
& I6)
100 FORMAT (' Contact Point      x:',F10.5,'      y:',F10.5,'      z:',
& F10.5)
110 FORMAT (' Incident angle of disk with bubble surface:',F10.5)
120 FORMAT (' Disk Velocity  Ux:',F10.5,'      Uy:',F10.5,'      Uz:',
& F10.5)
130 FORMAT (' Angular Vel.   Wx:',F10.5,'      Wy:',F10.5,'      Wz:',
& F10.5)
140 FORMAT (' Disk Velocity  Uth:',F10.5,'      Ur:',F10.5,'      Uphi:',
& F10.5)
150 FORMAT (' Point Vel.     Uxc:',F10.5,'      Uyc:',F10.5,'      Uzc:',

```



```

      & F10.5)
160   FORMAT (' Point Vel.    Uthc:',F10.5,'    Urc:',F10.5,' Uphic:',
      & F10.5)

```

```

C
      RETURN
      END

```

```

      SUBROUTINE HMODP(Y,RDISK,RBUB,VINF,H,MAXSTP,PRINTI,LABEL,
      & SEPMIN,THETA)

```

```

C
C This subroutine determines the movement and orientation of a disk as it
C approaches and flows around a bubble. It is a simple hydrodynamic model
C which uses the potential flow equations for flow around a sphere to
C approximate the flow around the bubble. The assumption of particle density
C neutrality is made. Flow is in the negative y direction. The bubble
C center of axis origin. The center of the disk in x, y, z coordinates is
C Ox, Oy, and Oz. The orientation of the disk is described by two angles.
C Alpha is the angle between the z-axis and a line drawn perpendicular
C to the disk at the disk center. Beta is the angle between the x-axis
C and the projection of the perpendicular line is the x-y plane.
C

```

```

      CHARACTER*12 LABEL(11)
      INTEGER QUITPR,TRUE,FALSE,PCOUNT,PRINTI,CONTCT,CONTYP
      DOUBLE PRECISION T,Y,H,RDISK,RBUB,VINF,A,Y1,Y2,PI,MISBUB,SEPMIN,
      & XP,YP,THETA
      DIMENSION Y(5)

```

```

C
C Initialized variables NEQ (number of equations), T (time in seconds),
C CONTCT (tracks whether contact between particle and bubble has been
C made), CONTYP (type of contact between particle and bubble - 0 is miss,
C 1 is contact on edge, 2 is contact on side, 3 is when the max. number of
C iterations, MAXSTP, has been exceeded), QUITPR (flag for when to end
C program), ISTEP (# of iterations), PCOUNT (print counter), and PI.
C

```

```

      NEQ = 5
      T = 0d0
      FALSE = 0
      TRUE = 1
      CONTCT = FALSE
      CONTYP = 0
      QUITPR = FALSE
      ISTEP = 0
      PCOUNT = 0
      SEPMIN = 10.0D0
      PI = 3.141592653589793D0

```

```

C
C Call datain subroutine to input data: alpha (Y(1)), beta (Y(2), Ox
C (Y(3)), Oy (Y(4)), Oz (Y(5)), disk radius (RDISK), bubble radius (RBUB),
C the velocity of the undisturbed flow (VINF), the step size (H), the
C maximum number of iterations (MAXSTP), and the interval at which to
C output the data (PRINTI).
C

```

```

      CALL DATAIN (Y,RDISK,RBUB,VINF,H,MAXSTP,PRINTI,LABEL)

```

```

C
C The disk is assumed to miss bubble if disk center drops below the bubble
C center.

```

```

      MISBUB = 0.0D0

```

```

C

```

```

C Calculate new position and orientation at each timestep by calling a
C fourth-order runge-kutta subroutine. Update timestep. Repeat until
C either QUITPR is true or ISTEP exceeds MAXSTP.
C
10    CONTINUE
      CALL RK4C (NEQ,T,Y,H,RDISK,RBUB,VINF)
      T = T + H
C
C Check if disk has made contact with bubble and calculate minimum
C separation distance (SEPMIN)
C
      CALL CHKCON (Y,RDISK,RBUB,CONTCT,CONTYP,A,SEPMIN,XP,YP)
C
C If Oy is less than zero then quit program.
C
      IF (Y(4).LE.MISBUB) QUITPR = TRUE
C
C Advance iterations step counter (ISTEP) and print counter (PCOUNT) by 1.
C If PCOUNT is greater than PRINTI, write disk orientation and position to
C output file.
      ISTEP = ISTEP + 1
      PCOUNT = PCOUNT + 1
      IF (PCOUNT.GE.PRINTI) THEN
        Y1 = Y(1)*180.0D0/PI
        Y2 = Y(2)*180.0D0/PI
        WRITE(2,100) T,Y1,Y2,(Y(I),I=3,5)
        PCOUNT = 0
      ENDIF
      IF ((QUITPR.EQ.FALSE).AND.(ISTEP.LT.MAXSTP)) GOTO 10
C
      IF (ISTEP.GE.MAXSTP) CONTYP = 3
C
C Call subroutine to print out final results.
C
      CALL DATOUT (T,Y,CONTCT,CONTYP,ISTEP,MAXSTP,A,SEPMIN,XP,YP,
& RDISK,RBUB,VINF,THETA)
C
100  FORMAT (1X,E12.5,F10.5,F10.5,F10.5,F10.5,F10.5)
C
      RETURN
      END

```

The following subroutines of COLMOD are identical to those in the HMODP program and can be found in Section A.2.1: CHKCON, RINTEG, RINTEG2, RIUDR, RIWDR, RK4C, UDR, UDRH, VARBL, WDR, and WDRH.

A.3.2 Sample Input File

The sample input file CIN:

Colmod directory. Sample Colmod Run 9/20/96

alpha	beta	Ox	Oy	Oz
90.0	0.0	0.25	3.000	0.000

Disk-radius	Bub-radius	V-infinity	H	Max-steps	Print-int
.200	1.00	200.	0.00005	800	20

N-Maximum	Max-Separation	2nd-Ox-guess
8	0.0002	0.40

A.3.3 Sample Output File

The output file COUT after running COLMOD with the above input file:

Colmod directory. Sample Colmod Run 9/20/96

Initial Data

alpha :	90.00000	Disk-radius :	.20000
beta :	.00000	Bub-radius :	1.00000
Ox :	.25000	V-infinity :	200.00000
Oy :	3.00000	H :	.50000E-04
Oz :	.00000	Max-steps :	800
		Print-int :	20
N-Maximum :	8	Max-Separation:	.000200
2nd-Ox-guess:	.4000		

Critical value of Ox: .30750
 Separation distance: -.000108
 Number of iterations: 3

The output file HOUT after running COLMOD with the above input file:

Colmod directory. Sample Colmod Run 9/20/96

Individual runs:

Initial Data

alpha :	90.00000	Disk-radius :	.20000
beta :	.00000	Bub-radius :	1.00000
Ox :	.25000	V-infinity :	200.00000
Oy :	3.00000	H :	.50000E-04
Oz :	.00000	Max-steps :	800
		Print-int :	20

Time (seconds)	Alpha (degrees)	Beta (degrees)	Ox (mm)	Oy (mm)	Oz (mm)
.10000E-02	90.00000	.04126	.25105	2.80803	.00000
.20000E-02	90.00000	.09978	.25243	2.61786	.00000
.30000E-02	90.00000	.18472	.25429	2.43001	.00000
.40000E-02	90.00000	.31123	.25683	2.24525	.00000
.50000E-02	90.00000	.50504	.26038	2.06458	.00000
.60000E-02	90.00000	.81115	.26546	1.88940	.00000

.70000E-02	50.00000	1.31020	.27287	1.72160	.00000
.80000E-02	90.00000	2.14877	.28396	1.56361	.00000
.90000E-02	90.00000	3.59087	.30082	1.41825	.00000
.10000E-01	90.00000	6.08209	.32666	1.28804	.00000
.11000E-01	90.00000	10.23079	.36597	1.17369	.00000
.12000E-01	90.00000	16.38354	.42398	1.07176	.00000
.13000E-01	90.00000	23.54811	.50507	.97299	.00000
.14000E-01	90.00000	29.02415	.61036	.86278	.00000
.15000E-01	90.00000	30.34061	.73492	.72298	.00000
.16000E-01	90.00000	26.97910	.86294	.53538	.00000
.17000E-01	90.00000	20.17509	.96498	.29194	.00000
.18000E-01	90.00000	12.34614	1.00720	.00790	.00000

Final Disk Position

.18050E-01	90.00000	11.98394	1.00731	-.00673	.00000
------------	----------	----------	---------	---------	--------

Number of iterations = 361

Minimum separation distance: -.017933

Disk has contacted bubble on the disk edge.

Incident angle of disk with bubble surface: .91656

Contact Point	x:	.96579	y:	.18891	z:	.00000
Disk Velocity	Ux:	.35523	Uy:	-292.72599	Uz:	.00000
Angular Vel.	Wx:	.00000	Wy:	.00000	Wz:	-125.40980
Disk Velocity	Uth:	-292.71708	Urc:	-2.31160	Uphi:	.00000
Point Vel.	Uxc:	24.89055	Uyc:	-287.51804	Uzc:	.00000
Point Vel.	Uthc:	286.94889	Urc:	-30.76524	Uphic:	.00000

Initial Data

alpha :	90.00000	Disk-radius :	.20000
beta :	.00000	Sub-radius :	1.00000
Ox :	.40000	V-infinity :	200.00000
Oy :	3.00000	H :	.50000E-04
Oz :	.00000	Max-steps :	800
		Print-int :	20

Time (seconds)	Alpha (degrees)	Beta (degrees)	Ox (mm)	Oy (mm)	Oz (mm)
.10000E-02	90.00000	.06320	.40163	2.80776	.00000
.20000E-02	90.00000	.15222	.40378	2.61720	.00000
.30000E-02	90.00000	.28032	.40663	2.42881	.00000
.40000E-02	90.00000	.46903	.41052	2.24324	.00000
.50000E-02	90.00000	.75405	.41591	2.06137	.00000
.60000E-02	90.00000	1.19577	.42353	1.88435	.00000
.70000E-02	90.00000	1.89731	.43453	1.71368	.00000
.80000E-02	90.00000	3.03289	.45069	1.55109	.00000
.90000E-02	90.00000	4.87990	.47471	1.39826	.00000
.10000E-01	90.00000	7.80515	.51040	1.25593	.00000
.11000E-01	90.00000	12.04607	.56246	1.12219	.00000
.12000E-01	90.00000	17.10052	.63499	.99044	.00000
.13000E-01	90.00000	21.22233	.72878	.84839	.00000
.14000E-01	90.00000	22.28055	.83750	.67972	.00000
.15000E-01	90.00000	19.39365	.94382	.46948	.00000
.16000E-01	90.00000	13.45015	1.01982	.21462	.00000

Final Disk Position

.16800E-01	90.00000	7.94971	1.04020	-.00980	.00000
------------	----------	---------	---------	---------	--------

Number of iterations = 336

Minimum separation distance: .028845

Disk has missed contacting bubble.

Initial Data

alpha : 90.00000 Disk-radius : .20000
 beta : .00000 Bub-radius : 1.00000
 Ox : .30750 V-infinity : 200.00000
 Oy : 3.00000 H : .50000E-04
 Oz : .00000 Max-steps : 800
 Print-int : 20

Time (seconds)	Alpha (degrees)	Beta (degrees)	Ox (mm)	Oy (mm)	Oz (mm)
.10000E-02	90.00000	.05003	.30878	2.80794	.00000
.20000E-02	90.00000	.12082	.31047	2.61764	.00000
.30000E-02	90.00000	.22327	.31272	2.42961	.00000
.40000E-02	90.00000	.37531	.31580	2.24457	.00000
.50000E-02	90.00000	.60713	.32009	2.06350	.00000
.60000E-02	90.00000	.97095	.32620	1.88770	.00000
.70000E-02	90.00000	1.55887	.33510	1.71892	.00000
.80000E-02	90.00000	2.53422	.34832	1.55934	.00000
.90000E-02	90.00000	4.17933	.36827	1.41137	.00000
.10000E-01	90.00000	6.93409	.39852	1.27685	.00000
.11000E-01	90.00000	11.28972	.44383	1.15545	.00000
.12000E-01	90.00000	17.22125	.50931	1.04230	.00000
.13000E-01	90.00000	23.25534	.59819	.92660	.00000
.14000E-01	90.00000	26.76703	.70895	.79235	.00000
.15000E-01	90.00000	25.98125	.83137	.62111	.00000
.16000E-01	90.00000	21.07015	.94248	.39915	.00000
.17000E-01	90.00000	13.78837	1.00974	.13012	.00000

Final Disk Position

.17500E-01 90.00000 10.10516 1.01814 -.01400 .00000

Number of iterations = 350

Minimum separation distance: -.000108

Disk has contacted bubble on the disk side. A = .19242

Incident angle of disk with bubble surface: .00000

Contact Point x: .98438 y: .17544 z: .00000
 Disk Velocity Ux: -1.84227 Uy: -289.78192 Uz: .00000
 Angular Vel. Wx: .00000 Wy: .00000 Wz: -122.08323
 Disk Velocity Uth: -289.77985 Ur: -2.14302 Uph: .00000
 Point Vel. Uxc: 21.28511 Uyc: -285.66015 Uzc: .00000
 Point Vel. Uthc: 284.96340 Urc: -29.16569 Uphc: .00000

A.4 VRCMOD Program

A.4.1 Fortran Code

```

      PROGRAM VRCMOD
C This program uses the false-position method and the hmodp subroutine to
C determine the initial Ox position at which the the point of the disk in
C contact with the bubble when the disk and bubble first make contact has
C a given radial velocity (RVEL). See the hmodp subroutine for a
C description of how it works as well as definition of variables.
      INTEGER PRINTI
      DOUBLE PRECISION Y,YI,H,RDISK,RBUB,VINF,SEPMIN,URC,UTHC,THETA,
&      S,SN,SP,XN,XP,XNEW,RVEL,SEPMAX
      DIMENSION Y(5),YI(5)
      CHARACTER*12 LABEL(11)
      CHARACTER*55 TITLE
C
      OPEN(UNIT=1,FILE='vrin',STATUS='OLD')
      OPEN(UNIT=2,FILE='hout',STATUS='NEW')
      OPEN(UNIT=3,FILE='vrout',STATUS='NEW')
C
C Call subroutine ADATIN to input data
      CALL ADATIN(Y,RDISK,RBUB,VINF,H,MAXSTP,PRINTI,LABEL,SEPMAX,NMAX,
&      TITLE,XP,RVEL)
C
C Set initial values of Y
      DO 10 I=1,5
        YI(I) = Y(I)
10    CONTINUE
C
C Write title info to hout file
      WRITE(2,*) TITLE
      WRITE(2,*)
      WRITE(2,*) 'Individual runs:'
      WRITE(2,*)
C
C Set initial value of x-negative (XN) for false-position equation,
C calculate contact point radial velocity (URC) for XN value by calling
C HMODP subroutine. Set initial value of SN as URC minus desired radial
C velocity (RVEL).
C
      XN = YI(3)
      CALL HMODP (Y,RDISK,RBUB,VINF,H,MAXSTP,PRINTI,LABEL,SEPMIN,URC,
& UTHC,THETA)
      IF (SEPMIN.GT.0.0D0) THEN
        SN = -RVEL - 10.0D0
      ELSE
        SN = URC - RVEL
      ENDIF
C
      IF (SN.GT.0.0D0) THEN
        WRITE(3,*) 'Initial guess is too large!'
        WRITE(3,*) 'Simulation stopped!'
        WRITE(3,*) ' URC = ',URC
        WRITE(3,*) ' RVEL = ',RVEL
        STOP
      ENDIF
C
C Reset Y to initial values
      DO 20 I=1,5

```

```

        Y(I) = YI(I)
20    CONTINUE
C Set Y(3) to XP and find URC. Set initial value of SP.
    Y(3) = XP
    CALL HMODP (Y,RDISK,RBUB,VINF,H,MAXSTP,PRINTI,LABEL,SEPMIN,URC,
&    UTHC,THETA)
    SP = URC - RVEL
    IF (SP.LT.0.0D0) THEN
        WRITE(3,*) 'XP guess is too small!'
        WRITE(3,*) 'Simulation stopped!'
        WRITE(3,*) ' URC = ',URC
        WRITE(3,*) 'RVEL = ',RVEL
        STOP
    ENDIF
C
C Set NSTEP to 2 (NSTEP is how many time HMODP has been called)
    NSTEP = 2
C
C Beginning of loop. Calculate new value of Y(3) (XNEW) using
C false-position method. Reset Y values and set Y(3) to XNEW. Calculate
C URC. If URC minus RVEL (also called S) is less than SEPMAX, repeat
C loop.
C
30    CONTINUE
        XNEW = XP - (SP * (XN - XP))/(SN - SP)
C
        DO 40 I=1,5
            Y(I) = YI(I)
40    CONTINUE
C
        Y(3) = XNEW
        CALL HMODP (Y,RDISK,RBUB,VINF,H,MAXSTP,PRINTI,LABEL,SEPMIN,
&    URC,UTHC,THETA)
        S = URC - RVEL
C
        IF (S.GT.0.0D0) THEN
            SP = S
            XP = XNEW
        ELSE
            SN = S
            XN = XNEW
        ENDIF
        NSTEP = NSTEP + 1
        IF ((ABS(S).GT.SEPMAX).AND.(NSTEP.LT.NMAX)) GOTO 30
C
C Write results to file cout
    WRITE(3,100) XNEW
    WRITE(3,110) URC
    WRITE(3,120) RVEL
    WRITE(3,130) UTHC
    WRITE(3,140) THETA
    WRITE(3,150) NSTEP
C
100  FORMAT (1X,'Critical value of Ox: ',F8.5)
110  FORMAT (1X,'Contact point radial velocity: ',F10.4)
120  FORMAT (1X,'Desired radial velocity: ',F10.4)
130  FORMAT (1X,'Contact point angular velocity: ',F10.4)
140  FORMAT (1X,'Incident disk/bubble angle: ',F9.4)
150  FORMAT (1X,'Number of iterations: ',I2)
C

```

END

```

      SUBROUTINE ADATIN(Y,RDISK,RBUB,VINF,H,MAXSTP,PRINTI,LABEL,SEPMAX,
&      NMAX,TITLE,XP,RVEL)
C This subroutine inputs starting disk position and orientation (Y), disk
C radius (RDISK), bubble radius (RBUB), the velocity at infinity (VINF),
C the step size for the runga-kutta method (H), the maximum number of
C iterations that will be performed in subroutine HMODP before the
C program stops (MAXSTP), the interval at which data will be written to
C out data file (PRINTI), the maximum difference allowed between actual
C angle and desired angle (SEPMAX), the maximum number of iteration for
C the main angmod program (NMAX), a data title (TITLE), the second initial
C guess for x (XP), and the desired disk contact point radial
C velocity (RVEL). Initial data is also written to the output file.
C
      INTEGER PRINTI
      CHARACTER*12 LABEL(11)
      CHARACTER*14 LABEL2(4)
      CHARACTER*55 TITLE
      DOUBLE PRECISION Y,RDISK,RBUB,VINF,H,PI,SEPMAX,XP,RVEL
      DIMENSION Y(5)
C
      READ(1,5) TITLE
5      FORMAT (A55)
      READ(1,*) (LABEL(I),I=1,5)
      READ(1,*) (Y(I),I=1,5)
      READ(1,*)
      READ(1,*) (LABEL(I),I=6,11)
      READ(1,*) RDISK,RBUB,VINF,H,MAXSTP,PRINTI
      READ(1,*)
      READ(1,*) (LABEL2(I),I=1,4)
      READ(1,*) NMAX,SEPMAX,XP,RVEL
C
      WRITE(3,*) TITLE
      WRITE(3,*)
      WRITE(3,*) '              Initial Data'
      WRITE(3,10) LABEL(1),Y(1),LABEL(6),RDISK
      WRITE(3,10) LABEL(2),Y(2),LABEL(7),RBUB
      WRITE(3,10) LABEL(3),Y(3),LABEL(8),VINF
      WRITE(3,20) LABEL(4),Y(4),LABEL(9),H
      WRITE(3,30) LABEL(5),Y(5),LABEL(10),MAXSTP
      WRITE(3,40) LABEL(11),PRINTI
      WRITE(3,50) LABEL2(1),NMAX,LABEL2(2),SEPMAX
      WRITE(3,60) LABEL2(3),XP,LABEL2(4),RVEL
      WRITE(3,*)
C
10      FORMAT (1X,A6,' : ',F10.5,4X,A,' : ',F10.5)
20      FORMAT (1X,A6,' : ',F10.5,4X,A,' : ',E12.5)
30      FORMAT (1X,A6,' : ',F10.5,4X,A,' : ',I7)
40      FORMAT (1X,22X,A,' : ',I4)
50      FORMAT (1X,A12,' : ',I4,4X,A,' : ',F9.6)
60      FORMAT (1X,A12,' : ',F8.5,4X,A,' : ',F10.4)
C
      RETURN
      END

```

```

      SUBROUTINE DATOUT(T,Y,CONTCT,CONTYP,ISTEP,MAXSTP,A,SEPMIN,XP,YP,
& RDISK,RBUB,VINF,URC,UTHC,THETA)
C This subroutine writes to the output file the final disk position and
C orientation and whether the disk contacted the bubble. Contact
C information is determined by the value of CONTYP. It also computes
C and writes the disk velocities, the velocity of the point of the disk
C contacting the bubble, and the angle between the plane containing the
C disk and the plane tangent to the bubble at the point of contact
C (THETA).
C
      INTEGER CONTCT,CONTYP
      DOUBLE PRECISION T,Y,PI,SEPMIN,A,XP,YP,Y1,Y2,RDISK,RBUB,VINF,
& WX,WY,WZ,UX,UY,UZ,XC,YC,ZC,XD,YD,ZD, TOP,BOT,THETA,UTH,UR,
& UXC,UYC,UZC,UTHC,URC,TH,THC,PHI,PHIC,UPHI,UPHIC
      DIMENSION Y(5)

C
      PI = 3.141592653589793D0
C
C Convert angles from radians to degrees.
      Y1 = Y(1)*180.0D0/PI
      Y2 = Y(2)*180.0D0/PI
C
      WRITE(2,*)
      WRITE(2,*) '                Final Disk Position'
      WRITE(2,10) T,Y1,Y2,(Y(I),I=3,5)
      WRITE(2,*)
      WRITE(2,20) ISTEP
      WRITE(2,25) SEPMIN
      WRITE(2,*)
C
      IF (CONTYP.EQ.0) WRITE(2,30)
      IF (CONTYP.EQ.1) WRITE(2,40)
      IF (CONTYP.EQ.2) WRITE(2,50) A
      IF (CONTYP.EQ.3) THEN
        WRITE(2,60) MAXSTP
        STOP
      ENDIF
C
      IF (CONTYP.EQ.1.OR.CONTYP.EQ.2) THEN
C Calculate the point at which the bubble and disk contact (XC, YC, and
C ZC) from values of XP and YP (values of X and Y in particle fixed
C coordinates, calculated in subroutine chkcon) and alpha (Y(1)), beta,
C (Y(2)), Ox (Y(3)), Oy (Y(4)), and Oz (Y(5)).
        XC = DCOS(Y(1))*DCOS(Y(2))*XP - DSIN(Y(2))*YP + Y(3)
        YC = DCOS(Y(1))*DSIN(Y(2))*XP + DCOS(Y(2))*YP + Y(4)
        ZC = -DSIN(Y(1))*XP + Y(5)
C
C Calculate coordinates of a unit vector normal to the disk (XD,YD,ZD).
        XD = DSIN(Y(1))*DCOS(Y(2))
        YD = DSIN(Y(1))*DSIN(Y(2))
        ZD = DCOS(Y(1))
C
C The incident angle of collision (THETA) is the dot product of the disk
C vector and the vector to the point of collision (which vector defines a
C plane tangent to the bubble at the point of contact).
        TOP = XC*XD + YC*YD + ZC*ZD
        TOP = DABS(TOP)
        BOT = DSQRT(XC**2 + YC**2 + ZC**2)
        THETA = DACOS(TOP/BOT)
        THETA = THETA*180.0D0/PI

```

```

C
C Subroutine RINTEG2 calculates translational (UX, UY, UZ) and angular
C velocities (WX, WY, WZ) of the disk at the time of contact.
      CALL RINTEG2 (Y,RDISK,RBUB,VINF,WX,WY,WZ,UX,UY,UZ)
C
C Calculate the disk velocity in the R and theta directions (UR and UTH).
      TH = DATAN( DSQRT(Y(3)**2 + Y(5)**2) / Y(4) )
      PHI = DATAN(Y(5)/Y(3))
      IF (PHI.LT.0.0D0.AND.Y(3).LT.0.0D0) PHI = PHI + PI
      UTH = -DSIN(TH)*UY + DCOS(TH)*(SIN(PHI)*UZ + COS(PHI)*UX)
      UR = DCOS(TH)*UY + DSIN(TH)*(SIN(PHI)*UZ + COS(PHI)*UX)
      UPHI = -DSIN(PHI)*UX +DCOS(PHI)*UZ
C
C Calculate the velocity of the edge or side of disk contacting the bubble
C (UXC, UYC, UZC) including the velocity in the R and theta directions
C (URC, UTHC).
      UXC = UX + WY*(ZC - Y(5)) - WZ*(YC - Y(4))
      UYC = UY + WZ*(XC - Y(3)) - WX*(ZC - Y(5))
      UZC = UZ + WX*(YC - Y(4)) - WY*(XC - Y(3))
      THC = DATAN( DSQRT(XC**2 + ZC**2) / YC )
      PHIC = DATAN(ZC/XC)
      IF (PHIC.LT.0.0D0.AND.XC.LT.0.0D0) PHIC = PHIC + PI
      UTHC = -DSIN(THC)*UYC + DCOS(THC)*(SIN(PHIC)*UZC +
& COS(PHIC)*UXC)
      URC = DCOS(THC)*UYC + DSIN(THC)*(SIN(PHIC)*UZC +
& COS(PHIC)*UXC)
      UPHIC = -DSIN(PHIC)*UXC +DCOS(PHIC)*UZC
C
C Write information to file
      WRITE(2,110) THETA
      WRITE(2,*)
      WRITE(2,100) XC, YC, ZC
      WRITE(2,120) UX, UY, UZ
      WRITE(2,130) WX, WY, WZ
      WRITE(2,140) UTH, UR, UPHI
      WRITE(2,150) UXC, UYC, UZC
      WRITE(2,160) UTHC, URC, UPHIC
C
      ENDIF
C
      WRITE(2,*)
      WRITE(2,*) '-----'
C
10  FORMAT (1X,E12.5,F10.5,F10.5,F10.5,F10.5,F10.5)
20  FORMAT (1X,'Number of iterations = ',I6)
25  FORMAT (1X,'Minimum separation distance: ',F9.6)
30  FORMAT (1X,'Disk has missed contacting bubble.')
40  FORMAT (1X,'Disk has contacted bubble on the disk edge.')
50  FORMAT (1X,'Disk has contacted bubble on the disk side. A = ',
& F10.5)
60  FORMAT (1X,'Maximum number of iterations exceeded! Max. steps = ',
& I6)
100 FORMAT (' Contact Point      x:',F10.5,'      y:',F10.5,'      z:',
& F10.5)
110 FORMAT (' Incident angle of disk with bubble surface:',F10.5)
120 FORMAT (' Disk Velocity      Ux:',F10.5,'      Uy:',F10.5,'      Uz:',
& F10.5)
130 FORMAT (' Angular Vel.      Wx:',F10.5,'      Wy:',F10.5,'      Wz:',
& F10.5)
140 FORMAT (' Disk Velocity      Uth:',F10.5,'      Ur:',F10.5,'      Uphi:',
& F10.5)

```

```

150  FORMAT (' Point Vel.      Uxc:',F10.5,'   Uyc:',F10.5,'   Uzc:',
& F10.5)
160  FORMAT (' Point Vel.      Uthc:',F10.5,'   Urc:',F10.5,' Uphic:',
& F10.5)
C
      RETURN
      END

```

```

      SUBROUTINE HMODP(Y,RDISK,RBUB,VINF,H,MAXSTP,PRINTI,LABEL,
& SEPMIN,URC,UTHC,THETA)
C
C This subroutine determines the movement and orientation of a disk as it
C approaches and flows around a bubble. It is a simple hydrodynamic model
C which uses the potential flow equations for flow around a sphere to
C approximate the flow around the bubble. The assumption of particle density
C neutrality is made. Flow is in the negative y direction. The bubble
C center of axis origin. The center of the disk in x, y, z coordinates is
C Ox, Oy, and Oz. The orientation of the disk is described by two angles.
C Alpha is the angle between the z-axis and a line drawn perpendicular
C to the disk at the disk center. Beta is the angle between the x-axis
C and the projection of the perpendicular line is the x-y plane.
C
      CHARACTER*12 LABEL(11)
      INTEGER QUITPR,TRUE,FALSE,PCOUNT,PRINTI,CONTCT,CONTYP
      DOUBLE PRECISION T,Y,H,RDISK,RBUB,VINF,A,Y1,Y2,PI,MISBUB,SEPMIN,
& XP,YP,URC,UTHC,THETA
      DIMENSION Y(5)
C
C Initialized variables NEQ (number of equations), T (time in seconds),
C CONTCT (tracks whether contact between particle and bubble has been
C made), CONTYP (type of contact between particle and bubble - 0 is miss,
C 1 is contact on edge, 2 is contact on side, 3 is when the max. number of
C iterations, MAXSTP, has been exceeded), QUITPR (flag for when to end
C program), ISTEP (# of iterations), PCOUNT (print counter), and PI.
C
      NEQ = 5
      T = 0d0
      FALSE = 0
      TRUE = 1
      CONTCT = FALSE
      CONTYP = 0
      QUITPR = FALSE
      ISTEP = 0
      PCOUNT = 0
      SEPMIN = 10.0D0
      PI = 3.141592653589793D0
C
C Call datain subroutine to input data: alpha (Y(1)), beta (Y(2)), Ox
C (Y(3)), Oy (Y(4)), Oz (Y(5)), disk radius (RDISK), bubble radius (RBUB),
C the velocity of the undisturbed flow (VINF), the step size (H), the
C maximum number of iterations (MAXSTP), and the interval at which to
C output the data (PRINTI).
C
      CALL DATAIN (Y,RDISK,RBUB,VINF,H,MAXSTP,PRINTI,LABEL)
C
C The disk is assumed to miss bubble if disk center drops below the bubble
C center.
      MISBUB = 0.0D0

```

```

C
C Calculate new position and orientation at each timestep by calling a
C fourth-order runge-kutta subroutine. Update timestep. Repeat until
C either QUITPR is true or ISTEP exceeds MAXSTP.
C
10  CONTINUE
      CALL RK4C (NEQ,T,Y,H,RDISK,RBUB,VINF)
      T = T + H
C
C Check if disk has made contact with bubble and calculate minimum
C separation distance (SEPMIN)
C
      CALL CHKCON (Y,RDISK,RBUB,CONTCT,CONTYP,A,SEPMIN,XP,YP)
C
C If Oy is less than zero then quit program.
C
      IF (Y(4).LE.MISBUB) QUITPR = TRUE
      IF (CONTCT.EQ.TRUE) QUITPR = TRUE
C
C Advance iterations step counter (ISTEP) and print counter (PCOUNT) by 1.
C If PCOUNT is greater than PRINTI, write disk orientation and position to
C output file.
      ISTEP = ISTEP + 1
      PCOUNT = PCOUNT + 1
      IF (PCOUNT.GE.PRINTI) THEN
        Y1 = Y(1)*180.0D0/PI
        Y2 = Y(2)*180.0D0/PI
        WRITE(2,100) T,Y1,Y2,(Y(I),I=3,5)
        PCOUNT = 0
      ENDIF
      IF ((QUITPR.EQ.FALSE).AND.(ISTEP.LT.MAXSTP)) GOTO 10
C
      IF (ISTEP.GE.MAXSTP) CONTYP = 3
C
C Call subroutine to print out final results.
C
      CALL DATOUT (T,Y,CONTCT,CONTYP,ISTEP,MAXSTP,A,SEPMIN,XP,YP,
        & RDISK,RBUB,VINF,URC,UTHC,THETA)
C
100  FORMAT (1X,E12.5,F10.5,F10.5,F10.5,F10.5,F10.5)
C
      RETURN
      END

```

The following subroutines of COLMOD are identical to those in the HMODP program and can be found in Section A.2.1: CHKCON, RINTEG, RINTEG2, RIUDR, RIWDR, RK4C, UDR, UDTH, VARBLs, WDR, and WDTN. The subroutine DATAIN in VRCMOD is identical to DATAIN in COLMOD and can be found in Section A.3.1.

A.4.2 Sample Input File

A sample input file for VRIN:

```
vrcmod run in vrcmod directory. 6/10/96
alpha      beta      Ox      Oy      Oz
90.        0.        0.10    3.000   0.000

Disk-radius  Bub-radius V-infinity  H      Max-steps  Print-int
.300        1.00      200.      0.00005  2500      20

N-Maximum    Max-Difference  2nd-Ox-guess  R-Velocity
8            0.25          0.38         -50.
```

A.4.3 Sample Output File

The output file VROUT after running VRCMOD with the above input file:

```
vrcmod run in vrcmod directory. 6/10/96

Initial Data
alpha : 90.00000  Disk-radius : .30000
beta : .00000    Bub-radius : 1.00000
Ox : .10000     V-infinity : 200.00000
Oy : 3.00000    H : .50000E-04
Oz : .00000     Max-steps : 2500
Print-int : 20
N-Maximum : 8    Max-Difference: .250000
2nd-Ox-guess: .38000  R-Velocity : -50.0000

Critical value of Ox: .31512
Contact point radial velocity: -49.8856
Desired radial velocity: -50.0000
Number of iterations: 6
```

The output file HOUT is identical in format to HOUT from the COLMOD program, found in section A.4.3.

A.5 Modification of Programs for Intermediate Flow

When using the assumption of intermediate Reynolds number flow rather than potential flow, the only change made in all three programs is the definition of the fluid flow velocities, V_x , V_y , and V_z , within the subroutine VARBLS. The modified subroutine is given below.

```

      SUBROUTINE VARBL5 (Y,TH,R,RBUB,VINF,RX,RY,RZ,VX,VY,VZ)
C
C This subroutine calculates the value of rx, ry, rz, vx, vy, and vz from
C the variables theta (TH), alpha (Y(1)), beta (Y(2)), Ox (Y(3)), Oy
C (Y(4)), Oz (Y(5)), r (R), bubble radius (RBUB), and the velocity of
C undisturbed flow (VINF).
      DOUBLE PRECISION Y,TH,R,RBUB,VINF,RX,RY,RZ,VX,VY,VZ,XX,YY,ZZ,
      & REY,RR
      DIMENSION Y(5)
      REY = 100D0
C
C Calculate rx, ry, rz, the three components of the position vector which
C points from the disk origin to the point defined by r (R) and theta
C (TH). Since rx, ry, and rz are in space-fixed coordinates and r and
C theta are in particle-fixed coordinates, the two disk rotation
C angles, alpha (Y(1)) and beta (Y(2)), are also required.
C
      RX= R*DCOS(TH)*DCOS(Y(1))*DCOS(Y(2)) - R*DSIN(TH)*DSIN(Y(2))
      RY= R*DCOS(TH)*DCOS(Y(1))*DSIN(Y(2)) + R*DSIN(TH)*DCOS(Y(2))
      RZ=-R*DCOS(TH)*DSIN(Y(1))
C
C Calculate fluid velocities Vx, Vy, Vz by using the equations for
C intermediate flow around a sphere.
C
      XX = RX+Y(3)
      YY = RY+Y(4)
      ZZ = RZ+Y(5)
      RF = (XX**2 + YY**2 + ZZ**2)**0.5D0
C
      VX = VINF*XX*YY*(3D0/4D0*RBUB/RR**3*(1D0 - (RBUB/RR)**2) -
      & REY**0.72D0/15D0 * (4D0*RBUB**4/RR**6 -
      & 3D0*RBUB**3/RR**5 - 2D0*RBUB**2/RR**4 + RBUB/RR**3))
C
      VY =-VINF*(1D0 - 3D0/4D0*RBUB/RR**3*(YY**2 + RR**2) +
      & RBUB**3/4D0/RR**5*(3D0*YY**2 - RR**2) +
      & REY**0.72D0/15D0 * (2D0*RBUB**4/RR**6*(2D0*YY**2 - RR**2)
      & - RBUB**3/RR**5*(3D0*YY**2 - RR**2) +
      & RBUB/RR**3*(YY**2 + RR**2) - 2D0*RBUB**2/RR**4*YY**2))
C
      VZ = VINF*ZZ*YY*(3D0/4D0*RBUB/RR**3*(1D0 - (RBUB/RR)**2) -
      & REY**0.72D0/15D0 * (4D0*RBUB**4/RR**6 -
      & 3D0*RBUB**3/RR**5 - 2D0*RBUB**2/RR**4 + RBUB/RR**3))
C
      RETURN
      END

```

Vita

Dale Charles Schmidt was born on September 22, 1965, in Midland, Michigan. He graduated from H. H. Dow High School in June of 1984, and enrolled at Brigham Young University in Provo, Utah the following Fall. He interrupted his education from 1985 to 1987 to serve as a missionary for the Church of Jesus Christ of Latter-Day Saints at Frankfurt, Germany. He graduated from Brigham Young University with a B.S. degree in Chemical Engineering in December of 1990. After working eight months at Wiltec Inc. in Provo, Utah, he began his graduate studies at the Department of Chemical Engineering at the University of Washington in Seattle, Washington. He graduated with a Ph.D. in Chemical Engineering in October of 1996, and will begin working for Dow Chemical Co., back in Midland, Michigan, the following December.